From Molecular Vibrations to Bonding, Chemical Reactions, and Reaction Mechanism

Dieter Cremer* and Elfi Kraka

Department of Chemistry, Southern Methodist University, 3215 Daniel Ave, Dallas, Texas 75275-0314, USA

Abstract: The vibrational motions of a molecule in its equilibrium or during a chemical reaction provide a wealth of information about its structure, stability, and reactivity. This information is hidden in measured vibrational frequencies and intensities, however can be unraveled by utilizing quantum chemical tools and applying the *Cal-X* methods in form *Vib-Cal-X*. *Vib-Cal-X* uses the measured frequencies, complements them to a complete set of 3N-L values (N number of atoms; L number of translations and rotations), derives experimentally based force constants, and converts them into local mode stretching, bending, and torsional force constants associated with the internal coordinates describing the geometry of the molecule. This is done by utilizing the adiabatic vibrational mode concept, which is based on a decomposition of delocalized normal vibrational modes into adiabatic internal coordinate modes (AICoMs) needed to describe bonding or changes in bonding. AICoM force constants relate to the intrinsic bond dissociation energy (IBDE) of a bond and, accordingly, are excellent descriptors for bond order and bond strength. It is shown that bond dissociation energies, bond lengths, or bond densities are not directly related to the bond strength because they also depend on other quantities than just the bond strength: the bond dissociation energy on the stabilization energies of the fragments, the bond length on the compressibility limit distance between the atoms, the bond stretching frequency on the atom masses, etc. The bond stretching force constants however lead directly to bond order and bond strength as has been demonstrated for the bonds in typical organic molecules. Using this insight, the generalized vibrational frequencies of reacting molecules are used to obtain insight into the chemical processes of bond breaking and forming. An elementary chemical reaction based on these processes is characterized by a curved reaction path. Path curvature is a prerequisite for chemical change and directly related to the changes in the stretching force constants as they respond to the bond polarizing power of a reaction partner. The features of the path curvature can be used to partition the reaction path and by this the reaction mechanism in terms of reaction phases. A reaction phase is characterized by an elementary structural change of the reaction complex leading to a chemically meaningful transient structure that can convert into a real transition state or intermediate upon changing the environmental conditions or the electronic structure (substituents, etc.) of the reaction complex. A unified approach to the study of reaction mechanism (URVA: Unified Reaction Valley Approach) is discussed that is based extensively on the analysis of vibrational modes and that is aimed at detailed understanding of chemical reactions with the goal of controlling them.

Key Words: Cal-X methods, vibrational frequency, bond strength, chemical bond, adiabatic internal Coordinate mode (AICoM), unified reaction valley approach (URVA), reaction path curvature, reaction path.

1. COLLABORATION BETWEEN EXPERIMENT AND THEORY: THE *CAL-X METHODS*

In the last four decades quantum chemistry has become a valuable and indispensable tool of chemistry that is peer to any spectroscopic or analytic tool of chemical research [1-3]. Quantum chemical calculations can be utilized in three different ways. First, they can lead to chemical information not amenable to experiment (possibility I). This possibility is exploited whenever principle reasons hinder chemical experiments, because they are too costly, time consuming, or too dangerous. Secondly, quantum chemistry is also often used to complement, confirm, or correct experimental results (possibility II). Nowadays, this is done on a routine basis and there are many experimentalists who take advantage of this possibility without considering themselves as being quantum chemists. The third possibility (possibility III) is based on a combination of experimental and computational tools with the objective of extracting additional chemical information from experimental measurements, especially information that is hidden in experimental results obtained from spectroscopy, structure analysis, and other chemo-physical measurements. Possibility III of utilizing quantum chemistry has been less frequently exploited although a number of examples can be found in the literature (see below). Unfortunately, different and sometimes misleading terms have been used in connection with this approach. Therefore, we will use in this article a terminology that clearly distinguishes this use of quantum chemistry from possibilities I and II. We will speak of the *Cal-X* combination methods, which use *Cal*culations to obtain important additional information from e*X*periment, for example measured NMR chemical shifts and spin-spin coupling constants to determine the geometry of molecules in solution (*NMR-Cal-X* combination method), measured vibrational frequencies to determine molecular structure and stability (*Vib-Cal-X* combination method), measured infrared intensities to determine atomic charges (*Vib-Cal-X*), etc.

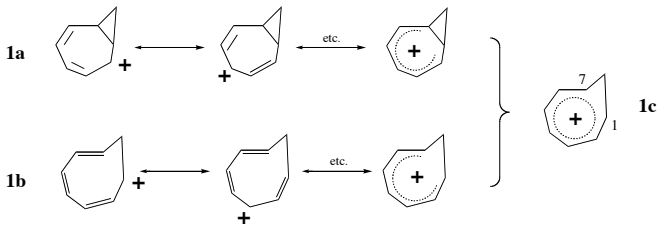

An example for an NMR-X approach concerning the structure of the homotropenylium cation (Scheme **1**) in solution is shortly described here [4-6]. Early investigations had provided rather

*Address correspondence to this author at the Department of Chemistry, Southern Methodist University, 3215 Daniel Ave, Dallas, Texas 75275-0314, USA; Tel: (214) 768-1300; E-mail: dcremer@smu.edu

1385-2728/10 $55.00+.00

confusing descriptions of the equilibrium geometry of this cation [7-11]. Some investigations described the molecule as possessing a rather short C1C7 bond of 1.6 Å typical of a bicyclic structure (**1a**) whereas others suggested a long C1C7 interaction distance of 2.4 Å typical of a monocyclic cation (**1b**). These observations had to be considered critically because the structural information of substituted homotropenylium cations referred to the solid state, which did not provide a reliable basis for predicting the solution phase structure of the cation. A direct structure determination of the homotropenylium cation in solution would have provided a direct answer to the question of its electronic nature, however was not possible because of principle reasons. In this situation, the dependence of NMR chemical shifts on the molecular geometry was exploited computationally to determine the geometry of the cation and its electronic nature in solution [4]. For a series of fifteen 1,7-distances increasing from 1.44 to 2.54 Å the geometry of the cation was optimized and the ^{13}C NMR chemical shifts were calculated with the IGLO (individual gauge for localized orbitals) method [12-14]. The minimum of the mean deviation of calculated and solution phase measured NMR chemical shifts determined the molecular geometry as possessing a 1,7-distance of 1,97 Å in solution (**1c**, Scheme 1), which confirmed homoaromatic character (delocalization of a 6π electron system bridging the methylene group through-space corresponding to a non-classical carbocation structure) [4]. This finding could later be confirmed by high level ab initio calculations performed at the MP4 level of theory [4,6,15]. Similar studies were carried out in the sense of this early example of an NMR-Cal-X approach to determine the geometry of donor-acceptor complexes (BH_3NH_3, [5] $F_3SiONMe_2$ [16]), silyl cations in solution, [17-21] carbo cations [4,5,22-24] or carbonyl oxides [25] where some of this work is summarized in two review articles [6,15].

The key feature of the NMR-Cal-X approach (originally coined NMR/ab initio/IGLO or NMR/DFT/IGLO according to the quantum chemical methods used [4-6,16-25]) is the dependence of NMR chemical shifts on molecular geometry, i.e. the measured NMR chemical shift values carry beside magnetic and electronic structure information on a molecule also hidden geometric information. If there is a large variation of the molecular geometry in dependence of the environment, the changes in the chemical shifts will be large enough to be unraveled with the help of the quantum chemical calculations. This is the essence of the Cal-X methods in general, which have the advantage to operate with measured rather than computed values because the latter provide for these methods just auxiliary quantities. Therefore, the question of calculational accuracy is of minor concern. For example, the problem of directly calculating the 1,7-distance of the homotropenylium cation with highly correlated ab initio methods such as coupled cluster with triple excitations (e.g., CCSD(T) [26]) was avoided at a time when these calculations were too costly. All what was needed in the case described above was a reasonable description of the ^{13}C chemical shifts with the moderately costly but sufficiently reliable HF/IGLO method [14].

In this review article, the use of molecular vibrations in the sense of a Cal-X method are discussed. The normal vibrational modes of a molecule are investigated by infrared and/or Raman spectroscopy and the information obtained from measured vibrational spectra is provided in form of normal mode frequencies and intensities [27-30]. Depending on its geometry, conformation, and electronic structure, each molecule has typical vibrational spectra, which are used to identify and characterize new chemical compounds [29]. In this connection, experimental work is strongly supported by quantum chemistry. If a given new compound is formed in a mixture of different compounds, its identification, for example by infrared spectroscopy, may be problematic. The quantum chemical calculation of the infrared spectrum in question clarifies which infrared bands at what frequencies with what intensities can be expected thus facilitating the identification. The combination of experiment and quantum chemical calculations has been utilized numerous times, especially in connection with the matrix isolation spectroscopy [31] of labile compounds such as biradicals, [32-38] carbenes, [39,40] carbonyl oxides or dioxiranes [41-43]. A highlight of this work was the first identification and characterization of m-benzyne in the matrix by Sander and co-workers using the CCSD(T) calculations of the biradical by Kraka [33]. This however can be considered as a standard complementation of experimental work by quantum chemical calculations, which as such has little to do with the *Vib-Cal-X* (calculation of *Vib*rational spectra to obtain additional information from e*X*perimental spectra) approach discussed in Section 2.

Vib-Cal-X is based on the fact that the vibrational spectra of a molecule contain detailed, although hidden, information on bonding, geometry, charge distribution, and stability [44-49]. In so far, vibrational spectroscopy should lead to the most complete characterization of molecules, which in reality is far from being accomplished. Most experimental work on medium-seized and larger molecules uses vibrational spectra just for the rapid identification of the functional groups of a molecule or a fingerprint-type comparison of different molecules. In this review, we will describe and summarize research that makes it possible to fully exploit the information content of measured vibrational spectra utilizing quantum chemistry in form of the Vib-Cal-X approach. Vib-Cal-X is based on the adiabatic mode concept of Cremer and co-workers [50-54] and we will sketch the contents of the latter in Section 2. In Section 3, we will apply Vib-Cal-X to describe the bond strength of typical organic bonds. This will imply some basic considerations on the nature of the chemical bond and how this is best characterized utilizing experimental quantities. Section 4 will lead from vibrating molecules to chemical reactions. The physical connection between the force constant of a vibrating bond, its changes under the impact of a reaction partner, and the curving of the reaction path is drawn. The path curvature will be the basis for the dissection of the reaction mechanism into reaction phases. In Section 5, it will be discussed how the various phases can be described using the properties of the reaction complex. Important results, conclusions, and outlook of the mechanistic analysis based on the vibrations of the reaction complex will be presented in the last section.

2. THE *VIB-CAL-X* METHOD AND THE ADIABATIC MODE CONCEPT

Modern vibrational spectroscopy has shifted its focus more in the direction of macromolecules, polymers, materials, and living matter using advanced techniques such as imaging, 2D correlation spectroscopy or Operando spectroscopy [29,30]. Vib-Cal-X, however, refers to the part of vibrational spectroscopy that aims at the characterization of isolated, small to medium-seized molecules ($N \leq 100$ atoms) and that has already been considered as becoming superfluous [55] because rivalling analytical methods such as NMR or mass spectrometry lead to much more detailed information on molecular composition and structure. In so far this article aims at triggering a renaissance of traditional vibrational spectroscopy carried by the combination of spectroscopic and computational

work in the form of Vib-Cal-X. On the quantum chemical side, there is no need to expedite and improve the computational techniques used to calculate vibrational spectra, for example by developing an easier and more accurate way of determining anharmonic corrections to harmonic vibrational frequencies either by explicitly calculating cubic and quartic force constants [56-58] or implicitly obtaining correct normal mode frequencies with ab initio molecular dynamics calculations [59-61]. (For a review on the calculation of vibrational frequencies, see Ref. [62].) It is an advantage of the Vib-Cal-X method that it is based exclusively on measured normal mode frequencies whereas calculated frequencies are only used as an analysis tool, which does not require high accuracy. This makes it possible to apply Vib-Cal-X to many interesting molecules using standard calculational techniques at moderate costs. The unraveling of structural and stability information from the vibrational data and a detailed insight into the electronic structure of a target molecule is the reward of applying traditional vibrational spectroscopy and its analytical tool Vib-Cal-X.

For the purpose of attaining the objectives of Vib-Cal-X, three prerequisites have to be fulfilled: 1) Vibrational frequencies depend both on the electronic structure of a molecule and the vibrating mass, which leads to different values in the case of isotopomers and makes a comparison of different bond types with regard to their properties difficult. Therefore it is desirable to obtain from measured vibrational frequencies the corresponding vibrational force constants which depend exclusively on the electronic nature of the chemical bonds of a molecule. The problem to be solved is how to obtain force constants from measured vibrational frequencies. - 2) Often the complete set of N_{vib}=3N−L (N: number of atoms of a molecule; L: number of translational and rotational motions) cannot be determined in the experiment. In this situation, a way has to be found to complement the experimental frequencies in a reliable manner so that added frequencies are largely independent of the way they have been generated. - 3) Vibrational normal modes are in many cases delocalized modes that include a larger number of atoms of the molecules. If one wants to describe the bonds of a molecule with the help of its vibrational modes, these have to be converted in some way into localized bond stretching vibrations that do no longer couple to other vibrational modes of the molecule. In the following we will present the solutions to these three problems.

2.1. Obtaining Vibrational Force Constants from Measured Vibrational Frequencies

Vibrational frequencies are derived from the vibrational eigenvalues λ of the standard vibrational equation [49, 63, 64]

$$\mathbf{FD = G^{-1}D\Lambda} \tag{2.1}$$

where **F** is the force constant matrix and **D** contains the normal mode vectors $\mathbf{d}_\mu$ (μ=1,…,N_{vib}) given as column vectors. Both matrices are expressed in terms of internal coordinates. Matrix **G** is the Wilson matrix [27] (kinetic energy of the vibrating molecule) and matrix **Λ** is a diagonal matrix with the vibrational eigenvalues $\lambda_\mu = 4\pi^2 c^2 \omega_\mu^2$ on the diagonal where ω_μ is the (harmonic) vibrational frequency of mode μ and c the speed of light. The number of vibrations N_{vib} determines the size of the four square matrices involved.

From Eq. (2.1) it is obvious that the vibrational eigenvalues λ_μ and by this the vibrational frequencies ω_μ are connected to the force constants via the vibrational eigenvectors collected in **D**. These are not available from experiment. The Wilson **G** matrix, however is easily determined from the mass matrix **M** and the **B** matrix

$$\mathbf{G = B\,M^{-1}B^{\dagger}} \tag{2.2}$$

with

$$B_{ni} = \left(\frac{\partial q_n(\mathbf{X})}{\partial x_i} \right)_{\mathbf{x}=\mathbf{x}_e} \tag{2.3}$$

and q_n being an internal coordinate. Once **G** and a reasonable approximation of matrix **D** are known, one can use first order perturbation theory to derive from calculated force constants the corresponding analogues associated with the measured vibrational frequencies ω_μ^{exp}. For this purpose, the differences between experimental and calculated frequencies, $\omega_\mu^{exp} - \omega_\mu^{cal}$, and correspondingly $\lambda_\mu^{exp} - \lambda_\mu^{cal}$ are used to set up a correction matrix **ΔΛ** associated with a correction matrix **ΔF**. Furthermore, one assumes that the perturbation **ΔΛ** leaves **D** unchanged so that the new vibrational Eq. (2.4) has to be solved:

$$\mathbf{D(F_0 + \Delta F)D^{\dagger} = \Lambda + \Delta\Lambda} \tag{2.4}$$

It holds that

$$\mathbf{D^{\dagger}\,F_0 D = \Lambda} \tag{2.5}$$

because the normal mode eigenvectors collected in matrix **D** are normalized with regard to **G**, i.e. $\mathbf{DD^{\dagger}=G}$. The corresponding equation for the first order correction is given by Eq. (2.6)

$$\mathbf{D^{\dagger}\Delta F D = \Delta\Lambda} \tag{2.6}$$

which leads to

$$\mathbf{\Delta F = (D^{-1})^{\dagger}\Delta\Lambda (D)^{-1} = G^{-1}D\Delta\Lambda D^{\dagger}G^{-1}} \tag{2.7}$$

and an experimental force constant matrix

$$\mathbf{F^{exp} = F_0 + \Delta F} \tag{2.8}$$

corresponding to the measured vibrational frequencies ω_μ^{exp}. Force constants are not measurable quantities (frequencies are) and therefore it is not problematic that the force constants of Eq. (2.8) are harmonic. They absorb the anharmonicities (described by cubic and quartic force constants [56]) needed in theory to calculate normal mode frequencies corresponding to the measured ones. It is appropriate to speak in this case of effective force constants leading directly to the correct vibrational frequencies measured by infrared or Raman spectroscopy.

2.2. Complementing Measured Vibrational Frequencies to a Complete Set

In the case that the set of N_{vib} vibrational normal modes is not complete, frequencies, which have not been experimentally observed, can be taken from calculated spectra after appropriate scaling. Calculated vibrational frequencies are mostly based on the harmonic approximation, which yields frequency values that are too large by 5 - 15 %, especially in the case of vibrational modes dominated by bond stretching motions (less problematic are the frequencies of the framework deformation modes). Apart from these deficiencies one has to consider that calculated vibrational frequencies are inaccurate because of the use of an incomplete basis set or electron correlation errors of the method employed. For

molecules with heavy atoms relativistic errors may also play a role. A priori one cannot expect that a single scaling factor can account for the different error sources, however in reality the harmonic approximation causes by far the largest deviation from experimental frequency values provided a reliable quantum chemical method with a sufficiently large basis set is used. In the last 25 years, scaled quantum mechanical force fields, [65] direct scaling of force constants, [66] frequency scaling, [67] the effective scaling frequency factor method based on the diagonal coefficients of the potential energy distribution (PED) matrix, [68,69] or the wavenumber-linear scaling method [70,71] have been used to adjust calculated harmonic frequencies to experimental normal mode frequencies. Also, a numerical procedure has been suggested to derive force field scaling factors directly for the Cartesian force constant matrix avoiding the introduction of internal coordinates [72].

Utilizing one of the improved scaling methods one can reduce average deviations from experimental frequencies from originally close to 15 cm^{-1} to currently just 3 cm^{-1} wave numbers in selected cases [73]. For 19, most frequently used methods and basis sets, average scaling factors are available based on a reference set of 122 small molecules with 1062 different frequencies [67]. These scaling factors are directly applied to all calculated frequencies. Although the scaling procedures in use cannot reproduce experimental frequencies exactly, they are sufficiently accurate to complement the frequencies of an experimental vibrational spectrum where the scaling is done in a small fraction of the time that would be needed to obtain anharmonic corrections with the perturbation theory approach in use today [56].

2.3. Localizing Vibrational Normal Modes

Normal vibrational modes are delocalized modes where the degree of delocalization increases for lower frequency modes. Delocalization can result from different causes. Vibrational modes which are equivalent because of symmetry (e.g. the CH stretching modes of a CH_3 group) mix with each other and lead to delocalized modes. Coupling phenomena such as Fermi resonance or Darling-Dennison resonance coupling [74,75] leads to mixing and a change in vibrational frequencies. Apart from these special cases, the degree of delocalization can be assessed by the following considerations based on Eq. (2.1) expressed in 3*N* Cartesian coordinates:

$$\mathbf{f}\mathbf{l}_{\mu} = \omega_{\mu}^{2}\mathbf{M}\mathbf{l}_{\mu}, \quad \mu = 1,\ldots,N_{vib} \tag{2.9}$$

where **f** is the force constant matrix, $\mathbf{l}_{\mu}$ the μth vibrational eigenvector, and **M** the mass matrix of the molecule in question. It may be assumed that $\mathbf{l}_{\mu}$ is identical to the local mode $\mathbf{v}_m$ associated with the internal coordinate q_m. This assumption will not be fulfilled if one of two or both coupling mechanisms suggested by Eq. (2.9) occur: i) An *electronic coupling* involving the potential energy part of the vibrational problem according to

$$\mathbf{v}_n^{\dagger}\mathbf{f}\mathbf{v}_m \tag{2.10}$$

or a *mass coupling* involving the kinetic energy part

$$\mathbf{v}_n^{\dagger}\mathbf{M}\mathbf{v}_m \tag{2.11}$$

The delocalized nature of vibrational normal modes is a result of electronic and mass coupling as reflected by the fact that neither the force constant matrix nor the Wilson **G** matrix are diagonal. The off-diagonal force constants reflect the electronic coupling and the off-diagonal elements of **G** the mass coupling. Naively, one could say that only if all off-diagonal elements are zero, local modes are enforced for the molecule in question. This however would correspond to the unrealistic situation that the molecule would be an union of diatomic (bond stretching vibrations), triatomic (bending vibrations), tetratomic (torsional vibrations), and higher entities whose interplay would not be clear. Any partitioning into local modes would require that for a linear N-atom molecule N-1 local bond stretching vibrations are complemented by N-2 angle bending, and N-3 torsion vibrations. Sizable bending (torsion) force constants would imply an interaction between the bonds, which would be excluded by the picture of local, non-interacting bonds needed for the description of local bond stretching modes. Such a situation may be partly given in a van der Waals complex containing two monomers (e.g. two H_2 molecules), however cannot be adopted for the electronic structure of a molecule that is characterized by the interplay of bonding and non-bonding interactions. These considerations reveal that it is not possible to partition delocalized normal modes into local modes. However, it should be possible to project local modes out from normal modes or to transform the latter into the former where of course the question arises whether the resulting modes will be physically reasonable. It will be essential to clarify whether the modes in question lead to a local mode frequency, force constant, mass, and intensity that describe the local electronic structure. Furthermore, it is important that normal modes can be described in terms of local modes, which implies the definition of a weighting factor or amplitude. Finally, it must be possible that local modes can be derived from measured vibrational modes to guarantee a general applicability of the local mode concept in question. Apart from listing these requirements it may be useful to further discuss the nature of a local mode in somewhat more detail.

If a local AB bond stretching vibration is initiated, local mode behavior would imply that all atoms bonded to either atom A or atom B should follow this motion without resistance. This rigid vibration would truly be localized since no other vibration will be triggered. Of course, the rigid local bond stretching vibration would imply a much too strong energy increase since the molecule would not be able to adjust to the displacements of atoms A and B and the periodic change in the bond length. The stretching force constant of the rigid, local motion would be too large and when used to describe the strength of bond AB would predict a much too strong bond. A more realistic situation would result if the rest of the molecule could always adjust to the changes in the bond length AB so that the molecular energy would always be minimal for any displacement $\Delta r(AB)$. The relaxation of the molecular geometry for a given vibrational motion does not imply that the latter is delocalized within the rest of the molecule. The other atoms still follow the AB stretching motion, however now in a non-rigid fashion. This is the principle of the adiabatic internal coordinate modes (AICoMs), [50-54] which will be discussed in Section 2.4. However before doing so, other approaches aimed at the determination of local vibrational will be summarized.

Averaging of Frequencies: Intrinsic Frequencies

The OH stretching modes of water split up into a symmetric and an asymmetric stretching mode possessing vibrational frequencies of 3657 and 3756 cm^{-1} (Fig. **1**), [76] neither of which presents a measure of the strength of the OH bond in water. One could assume that the arithmetic mean of the two frequencies,

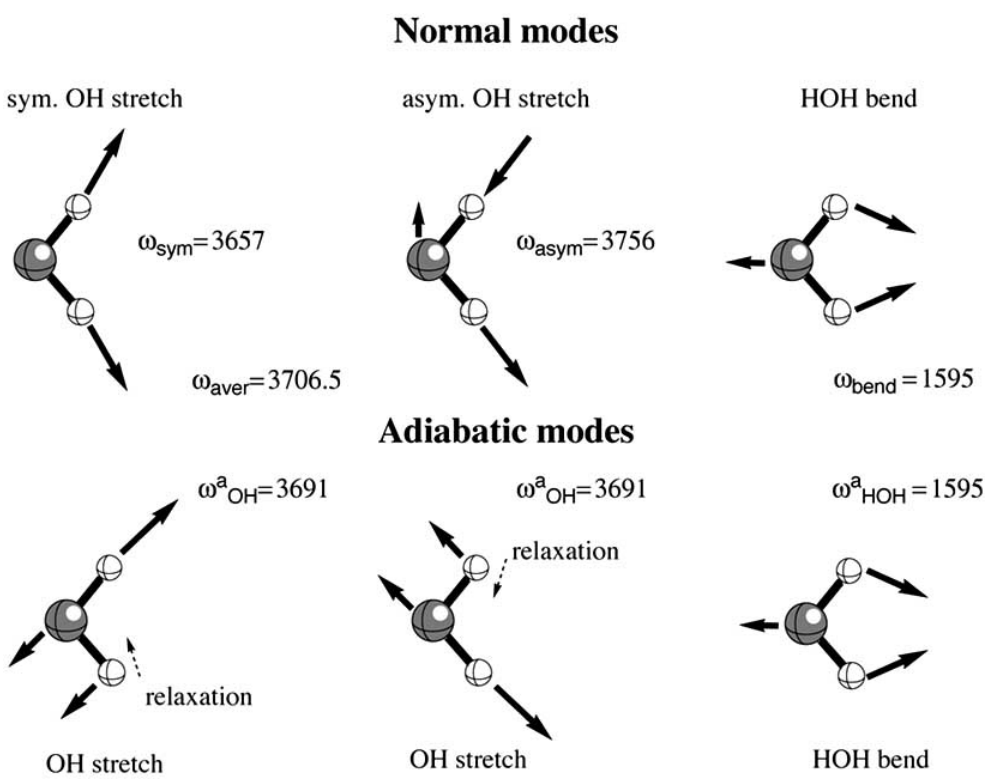

Fig. (1). Schematic representation of the three normal modes of the water molecule (from left to right): symmetric OH stretching, asymmetric OH stretching, and HOH bending mode (top); adiabatic OH stretching and HOH bending modes (bottom). Experimental normal [76] and adiabatic mode frequencies are given in cm^{-1}. Displacement arrows are given not to length scale to illustrate atom movements. Dashed arrows indicate movement of H atoms due to adiabatic relaxation.

3706.5 cm^{-1}, is such a measure. A theoretical approach based on this idea was suggested by Boatz and Gordon [77], who derived the *intrinsic frequencies* ω_n^{in} as representatives of local mode frequencies associated with an internal coordinate q_n.

$$\left(\omega_n^{in}\right)^2 = \sum_{\mu=1}^{N_{vib}} \sum_{m=1}^{N_{Parm}} P_{nm}^{\mu} \omega_{\mu}^2 \tag{2.12}$$

where P_{nm}^{μ} is an element of the PED density matrix measuring the contributions of the internal vibrational modes $\mathbf{c}_m$ associated with the internal coordinate q_m [77] and N_{Parm} defines the number of internal parameters used in the set of internal coordinates. The matrix **C** that collects all vectors $\mathbf{c}_m$ relates normal mode eigenvectors expressed in Cartesian coordinates, $\mathbf{l}_\mu$, to those expressed in internal coordinates, $\mathbf{d}_\mu$, according to

$$\mathbf{l}_\mu = \mathbf{C}\mathbf{d}_\mu \tag{2.13}$$

Considering that **D** relates internal coordinates **q** to normal coordinates **Q** according to

$$\mathbf{q} = \mathbf{D}\mathbf{Q}, \tag{2.14}$$

a local mode driven by internal coordinate q_m would require that the corresponding mode vector $\mathbf{d}_\mu$ fulfills the requirement $d_{\mu,m} = \delta_{m,\mu}$ for all its elements $d_{\mu,m}$ thus yielding $\mathbf{l}_\mu = \mathbf{c}_m$. Local modes expressed in form of **c**-vector modes will not couple if all off-diagonal force constant and **G**-matrix elements are zero, which leads as pointed out above to an unrealistic electronic structure. Hence, they couple as is reflected by $F_{n,m}$ and $P_{n,m} \neq 0$. Averaging of vibrational frequencies leads to different values for different sets of internal coordinates (unless redundant coordinate sets are used), a large scattering of frequencies for similar bonds. Negative frequencies may result, which prohibit an electronic structure analysis because they cannot be associated with a vibrational mode and a force constant.

Projecting Out Local Modes

Local modes are the appropriate tool to analyze delocalized vibrational modes in biomolecules. Therefore various attempts have been made to calculate local vibrational modes. Jacob and Reiher [78] recently suggested a procedure that leads to modes which are maximally localized with respect to a suitably defined criterion. They chose two localization criteria in analogy to mathematical procedures used for the localization of molecular orbitals. The authors showed how the application of localized modes to the vibrational spectrum of the alpha helix of $(Ala)_{20}$ polypeptide makes it possible to visualize which atoms dominantly contribute to each normal mode leading to a characteristic pattern for each residue. The coupling between the local modes defines the interaction between the residues. Choi and Cho [79] describe the extent of delocalization and the vibrational properties of amide normal modes in dipeptides by amide local mode frequencies and intermode coupling constants utilizing suitable local vibrational modes. The latter are derived by a generalized form of the Hessian matrix reconstruction method [80]. In this procedure, the mass-weighted Hessian defined in atomic Cartesian coordinates is divided into submatrices associated with the peptide fragments. Diagonalization of the fragment submatrices leads to the frequencies of vibrations localized at the two fragments. The diagonal elements of the submatrices correspond to the force constants of the fragments and the off-diagonal elements describe their coupling. This method can be applied to other systems with a repeating fragment unit such as nucleic acids. In each case, the

degree of localization of the reference modes can be determined according to worked out procedures [81].

Local Vibrational Modes in Crystals

In solid state physics, crystal defects or impurities lead to a lowering of the lattice symmetry and the appearance of additional vibrational modes [82]. These modes possess frequencies significantly separated from the lattice frequencies provided the mass of the impurity atom (H, C, etc.) is smaller than that of the lattice atoms. Therefore, one speaks of local vibrational modes that can be used to localize and analyze the lattice impurity [82-84]. The use of the term local vibrational mode differs in this case clearly from that used in molecular vibrational spectroscopy, since the former modes couple with the modes of the surrounding lattice and are only in so far localized as they do not involve lattice positions beyond the immediate surrounding.

Site-specific Modes from Nuclear Resonance Vibrational Spectroscopy

Related to the local vibrational mode spectroscopy of solid state physics is nuclear resonance vibrational spectroscopy (NRVS) [85-88] in so far as it leads to site-specific vibrational modes. NRVS uses synchrotron radiation to excite Mössbauer active isotopes such as ^{57}Fe and measures beside the zero-phonon resonance also transitions corresponding to the complete set of vibrational modes involving the excited nucleus. Hence, NRVS can be considered as Mössbauer spectroscopy with vibrational sidebands. Localized vibrational modes are obtained, however no real local modes because the modes measured exhibit a significant degree of delocalization [88].

Isolated Stretching Modes

Local modes in the sense of the AICoMs to be discussed in Section 2.4 are the isolated XH stretching modes originally investigated by McKean [89-95]. The CH stretching mode undergoes a Fermi resonance with the first overtone of the CH_3 and CH_2 bending modes, which leads to a CH stretching frequency that does no longer reflect the true nature of the CH bond [44]. A way of suppressing Fermi resonances is to replace all H atoms but the targeted H atom by deuterium. This has also the advantage that in CH_3 or CH_2 groups mixing of CH stretching modes is suppressed so that the stretching mode of the remaining CH bond is largely localized. McKean investigated D-isotopomers of many organic compounds and presented the corresponding CH stretching frequencies [89]. They nicely correlated with known $r_0(CH)$ bond lengths and could be used to predict unknown values with a precision of 0.001 Å [89]. Larsson and Cremer [44] calculated isolated CH stretching frequencies and compared them with the corresponding AICoM CH frequencies. Their work revealed that AICoMs are the theoretical equivalences of McKean's isolated stretching modes: The two types of local CH stretching modes overlap by more than 98%, which is reflected by a linear relationship between them with R^2 = 0.997. The only exceptions were found for CH stretching in alkines where the isolated CH modes were still contaminated due to some coupling with the CC stretching motion [44].

The isolated stretching frequencies are based on a suppression of mass coupling, Fermi resonances, and other mode-mode coupling effects. Due to a doubling of the hydrogen mass, frequencies for C-H/C-D stretching vibrations are significantly shifted to lower values thus eliminating a mixing with the remaining CH stretching motion. Isolated stretching frequencies, despite of reducing mass coupling, still suffer from electronic coupling since the CH stretching force constants are not affected by D substitution. Also, an extension of the original concept of the isolated stretching frequencies to other than just XH bonds [96, 97] is difficult since a doubling of the nuclear mass is not possible for any other element frequently used in organic chemistry.

Local Vibrational Modes from Overtone Spectroscopy

Information on local XH stretching modes can also be obtained from the overtone spectra of these vibrational modes [98]. Henry has shown that the higher overtones of a XH stretching mode can be described with an anharmonic potential of a quasidiatomic molecule [98]. Higher overtones ($\Delta v \geq 3$) possess considerable local mode character [99-101]. For overtones with Δv = 5,6 one observes mostly one band for each unique XH bond, even if there are several symmetry equivalent XH bonds in the molecule. In fundamental and lower overtone modes, there is always a splitting of the frequency into, e.g., a symmetric and an antisymmetric mode frequency of two symmetry equivalent XH stretching modes, whereas this splitting virtually disappears for overtones with $\Delta v \geq 5$. In general, the different linear combinations of symmetry equivalent XH stretchings become effectively degenerate for the higher overtones.

The local mode behavior of the fifth overtone (v=6) of CH stretching modes can be verified by comparison with the corresponding AICoM frequency [49]. There is a linear relationship between the two quantities (correlation coefficient R^2 = 0.990), which again confirms that AICoMs are suitable local vibrational modes. The use of overtone spectroscopy as a means of obtaining information on local vibrational modes and their properties is limited to terminal bonds, of which so far only XH (X = C, N, O, S, etc. [102,103]) bonds were investigated. An extension of the local mode description by overtone spectroscopy is rather limited.

Local Mode Information from Compliance Force Constants

Another way of obtaining local mode information seems to be provided by the compliance force constants [104-110]. The latter are obtained by expressing the potential energy of a molecule in terms of generalized displacement forces rather than internal displacement coordinates [104, 105]:

$$V(\mathbf{g}) = \frac{1}{2}\mathbf{qFq} \tag{2.15}$$

$$V(\mathbf{g}) = \frac{1}{2}\mathbf{g}_q\mathbf{Cg}_q \tag{2.16}$$

where the elements of the compliance matrix **C** are given as the partial second derivatives of the potential energy V with regard to forces $f_i = -g_i$ and $f_j = -g_j$:

$$C_{ij} = \frac{\partial^2 V}{\partial f_i \partial f_j} \tag{2.17}$$

The gradient vector $\mathbf{g}_q$ of Eq. (2.16) can be obtained by differentiation of Eq. (2.15):

$$\mathbf{g}_q = \mathbf{Fq} \tag{2.18}$$

thus yielding

$$V(\mathbf{g}) = \frac{1}{2}\mathbf{q}^\dagger\mathbf{F}^\dagger\mathbf{CFq} \tag{2.19}$$

Hence, the compliance matrix **C** is identical with the inverse of the force constant matrix:

$$\mathbf{C} = \mathbf{F}^{-1} \tag{2.20}$$

From Eq. (2.18) one sees that

$$\mathbf{q} = \mathbf{F}^{-1}\mathbf{g} \tag{2.21}$$

The diagonal compliance force constant C_{ii} gives the displacement of internal coordinate q_i under the impact of a unit force whereas all other forces are allowed to relax [105]. This leads to the fact that off-diagonal elements of **C** are largely reduced suggesting a suppression of electronic coupling. There is no indication that also mass coupling is reduced. In addition, the compliance force constants are force constants without a vibrational mode. Nevertheless, there is need in view the increasing use of compliance force constants to investigate to which extend local mode information is provided by the compliance force constants.

2.4. The Adiabatic Mode Concept

In Section 2.3, it has been described how the molecule should move under the impact of a local vibrational motion. Considering the similarity of internal coordinates and internal coordinate force constants between molecules of the same type, one can expect that electronic coupling is small. However, there is no guarantee that mass coupling is also small. Accordingly, it is important to eliminate mass coupling to obtain an internal vibrational mode $\mathbf{v_n}$ associated with the internal coordinate q_m that describes a molecular fragment ϕ_m (bond length r_m for a diatomic entity, bending angle for a triatomic entity, etc.) that leads to atom movements exactly as described in Section 2.3. Clearly, a suppression of mass coupling could be accomplished if all masses but those of the fragment ϕ_m would be zero. This is the idea of the AICoMs as first realized by Konkoli and Cremer [50]. For the purpose of deriving the AICoMs the Euler-Lagrange equations of a molecule are written in the modified form of Eq. (2.22).

$$\dot{p}_i = \frac{\partial V}{\partial x_i}, \quad i = 1,\ldots,3K_m \tag{2.22a}$$

$$0 = \frac{\partial V}{\partial x_j}, \quad j = 3K_m + 1,\ldots,3N \tag{2.22b}$$

where it is assumed that fragment ϕ_m has K_m atoms and is described by $3K_m$ Cartesian coordinates (a formulation in internal coordinates has been given in the original literature [50-54]. The masses of the other nuclei (K_m+1,…,N) are zero, which leads to $\dot{p}_j = 0$ ($j = 3K_m + 1,\ldots,3N$) for the momenta related to the Cartesian coordinates of the nuclei outside fragment ϕ_m, where

$$p_i = \frac{\partial L}{\partial \dot{x}_i} = m_i \dot{x}_i, \quad i = 1,\ldots,3N \tag{2.23}$$

and,

$$p_j = 0, \quad j = 3K_m + 1,\ldots,3N \tag{2.24}$$

Eqs. (2.22) can be solved by rewriting them in the form of (2.25)

$$\lambda_i = \frac{\partial V}{\partial x_i}, \quad i = 1,\ldots,3K_m \tag{2.25a}$$

$$0 = \frac{\partial V}{\partial x_j}, \quad j = 3K_m + 1,\ldots,3N \tag{2.25b}$$

with

$$\dot{p}_i = \lambda_i, \quad i = 1,\ldots,3K_m \tag{2.26}$$

Using (2.25),

$$x_k = x_k\left(\lambda_1,\ldots,\lambda_{3K_m}\right), \quad k = 1,\ldots,3N \tag{2.27}$$

and combining (2.23), (2.26) and (2.27) the time dependence of λ_i and thereby x_k can be found [50]. In the harmonic approximation, the solution of dynamical Eqs. (2.24) leads to the vibrational problem and an eigenvalue equation, which determines the set of local mode vectors $\mathbf{v}_n^u \mathbf{a}_n^u$ (u = 1,…,$3K_m$–L_m) that describe the AICoM vibrations of the fragment ϕ_m of the molecule.

If one uses Eq. (2.22b) instead of Eq. (2.27), one can obtain,

$$x_j = x_j\left(x_1,\ldots,3K_m\right), \quad j = 3K_m + 1,\ldots,3N \tag{2.28}$$

which reveals that nuclei not belonging to fragment ϕ_m follow exactly the motions of the fragment nuclei due to their zero mass, i.e. the fragment nuclei determine the motion of the whole molecule for the AICoMs determined. This fulfills exactly the requirement for a local vibrational mode formulated in Section 2.3.

The second requirement for the local vibrational modes implies that for any displacement of the nuclei belonging to ϕ_m, the other parts of the molecule are relaxed so that the molecular energy always adopts a minimum. This is expressed in Eq.s (2.29).

$$V(\mathrm{x}) = min \tag{2.29a}$$

$$x_i = const, \quad i = 1,\ldots,3K_m \tag{2.29b}$$

where the coordinates x_i give the displacements of the fragment nuclei from their equilibrium value x_i=0. These displacements are kept frozen whereas those of the other nuclei are relaxed until the molecular energy adopts a minimum. Using the method of Lagrange multipliers with $3K_m$ multipliers λ_i leads to the Eqs. (2.29), which are equivalent to Eqs. (2.25) [50]. Actually, Eqs. (2.29) describe the motion of a molecule where the nuclei leading the motion move infinitesimally slowly, which has led to speaking of *adiabatic motions*. Hence, the AICoMs fulfill via Eqs. (2.28) and (2.29) both requirements of a local vibrational mode.

Properties of Adiabatic Internal Coordinate Modes

Each AICoM is driven by a specific internal coordinate. In this work, we will focus on the AICoMs associated with bond lengths, i.e. the bond stretching modes. Hence, a molecule is considered as the union of quasi-diatomic units. The adiabatic internal mode $\mathbf{a}_m^Q$ associated with internal coordinate q_m and expressed in terms of normal coordinates is given by Eq. (2.30):

$$Q_\mu^{(m)} = (\mathbf{a}_m^Q)_\mu q_m^* \tag{2.30}$$

where q_m^* is the internal coordinate driving the AICoM by adopting a fixed displacement value as indicated by the *. The elements of vector $\mathbf{a}_m^Q$ are given by Eq. (2.31):

$$\left(\mathrm{a}_m^Q\right)_\mu = \frac{\frac{D_{m\mu}}{k_\mu}}{\sum_{\nu=1}^{N_{Vib}} \frac{D_{m\nu}^2}{k_\nu}}, \tag{2.31}$$

The AICoM $\mathbf{a}_m^Q$ can be transformed into an AICoM expressed in Cartesian coordinates, $\mathbf{a}_m$, with the help of the **L**-matrix

containing the normal mode eigenvectors $\mathbf{l}_\mu$ expressed in Cartesian coordinates.

$$\mathbf{a}_m = \mathbf{L}\,\mathbf{a}_m^Q \tag{2.32}$$

so that AICoMs are completely specified no matter whether internal coordinates, normal coordinates or Cartesian coordinates are used.

Each AICoM possesses a force constant k_m^a

$$k_m^a = \mathbf{a}_m^\dagger \mathbf{f} \mathbf{a}_m \tag{2.33}$$

and a mass m_m^a

$$m_m^a = \frac{(\mathbf{b}_m^\dagger \mathbf{a}_m)^2}{\mathbf{b}_m^\dagger \mathbf{M}^{-1} \mathbf{b}_m} = G_{mm} \tag{2.34}$$

where G_{mm} is a diagonal element of the **G** matrix, vector $\mathbf{b}_m$ corresponds to the mth column of the **B** matrix, and

$$\mathbf{b}_m^\dagger \mathbf{a}_m = 1 \tag{2.35}$$

since the AICoMs are properly normalized. Hence, the AICoM mass is based on a generalization of the reduced mass to internal coordinates connecting more than two atoms. With the AICoM force constant and the AICoM mass, it is straightforward to obtain the AICoM frequency

$$\omega_m^a = (\mathbf{a}_m^+ \mathbf{f} \mathbf{a}_m G_{mm})^{1/2} = (\frac{k_n^a}{m_m^a})^{1/2} \tag{2.36}$$

The force constant, frequency, and mass associated with a given AICoM for internal coordinate q_m fully characterize it. This information can be used to investigate normal modes by considering them as being composed of AICoMs. If one knows the decomposition of a normal mode in terms of AICoMs, then one can clarify whether the normal modes are more or less delocalized and what electronic or geometric information they contain.

The AICoMs are the dynamic counterparts of the internal coordinates, i.e. the latter are used to describe the equilibrium geometry of a molecule (static property) whereas the former describe the dynamic behavior of a molecule including the vibrational motions and the translational motion of a reaction complex during a reaction (dynamic behavior of a molecule). The dissection of the normal modes into AICoMs cannot be done in the sense of a simple partitioning. Instead, amplitudes $A_{m\mu}$ are determined that reflect the contribution of an AICoM to a given normal mode according to three essential criteria: [52,53] 1) Symmetry criterion: symmetry equivalent AICoMs have the same amplitude in a normal mode provided the normal mode retains this symmetry. 2) Stability criterion: AICoM amplitudes are not influenced by the choice of the internal coordinate set. The amplitudes should not change for a normal mode if they are calculated with different redundant internal coordinate sets and the differences in the parameter sets only concerns coordinates irrelevant to the normal mode. 3) Dynamic criterion: There is a relationship between the amplitude $A_{m\mu}$ of an AICoM contained in a normal mode and the difference $\Delta\omega_{m\mu} = \omega_m - \omega_\mu$ in the way that a small difference implies large amplitudes while large differences lead to very small amplitudes. In other words, the scattering of points $A_{m\mu}$ in dependence of $\Delta\omega_{m\mu} = \omega_m - \omega_\mu$ should be enveloped by a Lorentzian curve. - Based on these three criteria the AICoM amplitudes $A_{m\mu}$ are given by Eq. (2.37):

$$A_{m\mu} = \frac{\left\langle \mathbf{l}_\mu \,|\, \mathbf{f} \,|\, \mathbf{a}_m \right\rangle^2}{\left\langle \mathbf{l}_\mu \,|\, \mathbf{f} \,|\, \mathbf{l}_\mu \right\rangle \left\langle \mathbf{a}_m \,|\, \mathbf{f} \,|\, \mathbf{a}_m \right\rangle} \tag{2.37}$$

Eq. (2.37) provides the basis of a *Characterization of Normal Modes (CNM)* in terms of AICoMs and as such it is the counterpart of the PED analysis [111-114]. Contrary to the CNM approach, the PED analysis suffers from several deficiencies that can lead to non-physical results as has been demonstrated elsewhere [49,52,53].

Advantages of AICoMs

AICoMs have the following advantages that distinguish them from other attempts of defining local vibrational modes:

1) They are derived from a clear dynamic principle, namely the leading parameter principle, which points out that a single internal coordinate q_m (in general, a single internal parameter) defines the displacements of the nuclei from their equilibrium positions and, by this, leads the internal mode $\mathbf{a}_m$. This *leading parameter principle* [50,51] implies a new set of Euler-Lagrange equations because the generalized momenta for all other internal coordinates q_n ($n \neq m$) become zero [50], which can be pictured in the way that all atomic masses outside the molecular fragment are considered as massless points. This is equivalent to requiring that the potential energy V is minimized for a geometry perturbation under the constraint that the perturbation is defined by $\mathbf{q}_m^*$ [50].

2) All vibrational mode properties (adiabatic force constant, adiabatic mass, and adiabatic frequency) are clearly defined.

3) AICoM amplitudes $A_{m\mu}$ lead to the CNM analysis of normal modes in a more sound and physically meaningful way than provided, for example, by the PED analysis. The CNM analysis provides an easy way of analyzing vibrational spectra and quantitatively specifying the degree of delocalization of each vibrational mode.

4) AICoMs and the CNM analysis simplify the correlation of the vibrational spectra of different molecules.

5) AICoM intensities can be used to investigate the charge distribution in a molecule [54].

6) AICoMs are easily calculated utilizing measured vibrational frequencies as described in Section 2.1. In this way experimental information can be used in the sense of a Cal-X method thus leading to Vib-Cal-X.

7) Harmonic AICoMs can be scaled to resemble experimental AICoMs. In this way, they provide the basis of a powerful general scaling procedure.

8) AICoM bond stretching force constants can be used to define bond order and bond strength for any bond type [48,49].

9) AICoMs can also be defined for and applied to a reacting molecule. In this case, the AICoMs are based on generalized vibrational modes. They can be used to analyze the changes of the vibrational modes along the reaction path, the curvature and the Coriolis coupling constants, energy transfer and energy dissipation as well as other properties of the reaction complex along the reaction path [115-124].

10) Special AICoMs can be defined to analyze the translational motion of the reaction complex along the reaction path, which leads

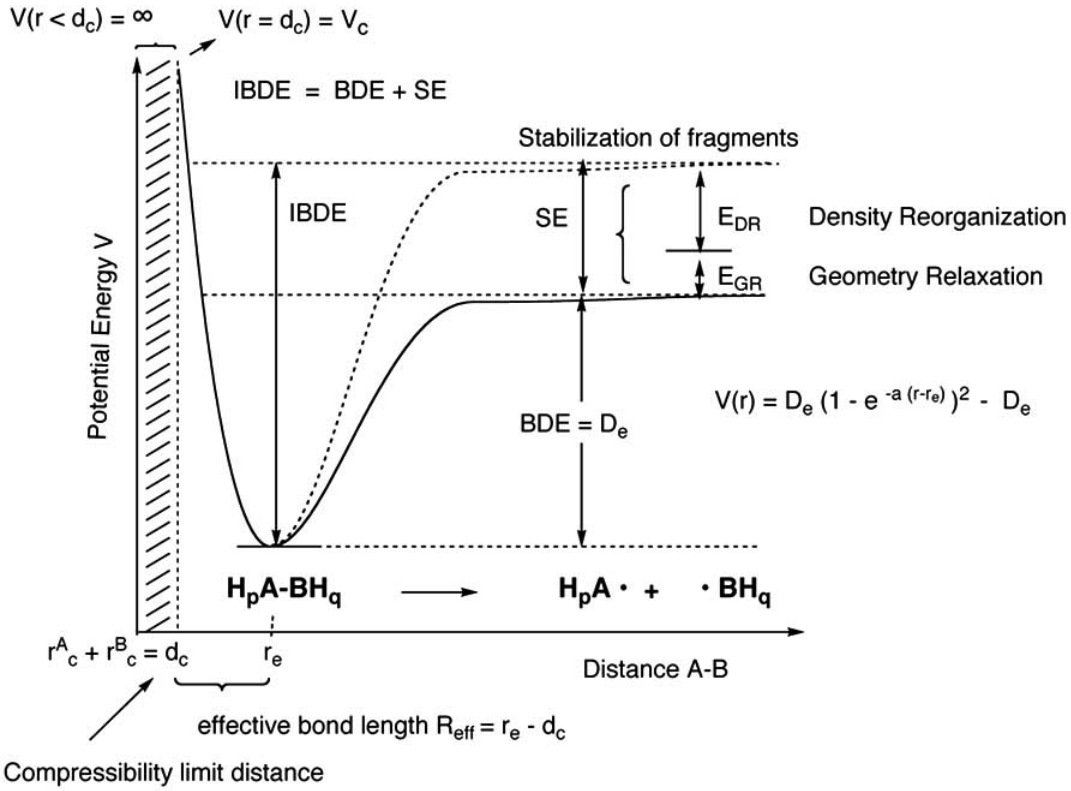

Fig. (2). Schematic representation of a Morse potential for the dissociation of the bond AB in H_pA-BH_q. Bond dissociation energy BDE, intrinsic bond dissociation energy IBDE, fragment stabilisation energy $E_S=E_{DR}+E_{GR}$, density reorganization energy E_{DR}, geometry relaxation energy E_{GR}, and compressibility limit distance d_c are indicated.

to an analysis of the reaction path direction and its curvature [115-124].

There is a large application spectrum for AICoMs, which is currently exploited. This includes the automated analysis and comparison of vibrational spectra [125], their use in connection with the Vib-Cal-X approach to obtain geometry, bonding, and electronic structure information, the set up of force fields based on AICoM force constants, and the systematic investigation of the mechanism of chemical reactions. Some of these application possibilities will be discussed in Section 3. We will show that AICoM force constants are suitable descriptors for the strength of a chemical bond.

3. A BASIC VIEW ON THE CHEMICAL BOND AND ITS DESCRIPTION BY MEASURABLE QUANTITIES

Both structure, stability, and reactivity of a molecule can be predicted if the nature of its chemical bonds is understood [126-132]. One of the central questions in chemistry is how to find easily accessible bond properties that reflect the strength of the chemical bond. Frequently mentioned in this connection are bond length $r(AB)$, bond dissociation energy (BDE) and bond energy (BE) of bond AB, bond density $\rho(AB)$, one-bond spin-spin coupling constant $J(AB)$, bond stretching frequency $\omega(AB)$, and bond stretching force constant $k(AB)$. One has also defined the bond order n (number of bonding - number of antibonding electrons) as a simple measure of the bond strength. The bonding character of the electrons is determined via the molecular orbitals they occupy. The orbital-based definition of the bond order will work only if the orbital in question is localized in the bond and can be identified as being bonding or antibonding via its nodal surfaces. In polyatomic molecules, especially when hetero atoms are involved, these requirements are seldom fulfilled. However, even if the requirements would be fulfilled, the bond order defined in this way could only be used to describe different bonding situations for one type of bond, e.g. just for CC bonds. Use of a bond order to compare the strength of different bonds is problematic.

In general, the strength of the chemical bond is the result of a covalent and a polar (ionic) contribution [126,127]. In perturbational MO theory [127,128], the covalent part can be assessed by the overlap of the fragment orbitals forming the bonding MOs and the stabilization of the latter, which is also related to the energies of the fragment orbitals forming the MOs. If both bonding and antibonding orbitals are occupied, all stabilizing and destabilizing contributions have to be considered where the antibonding MO is always more destabilized than the bonding MOs stabilized. The ionic character of the bond always leads to an increase of the bond strength [126]. It has to be assessed via the electronegativity difference between the atoms involved in bonding and the resulting charge transfer from the more electropositive to the more electronegative atom.

3.1. Assessing Bond Strength from Bond Energy (BE) or Bond Dissociation Energy (BDE)

BE and BDE are the two quantities that are often used to describe the strength of a chemical bond [45]. The BE accounts for both covalent and ionic contributions to the bond strength. However, the BE is a model quantity that cannot be measured. Normally, one uses the atomization energy (AE) to derive BEs. For example, the BE(XH) of a highly symmetrical molecule XH_n is just the nth part of the corresponding AE. However, if there are

different bonds in a molecule it is no longer clear how to split up the BE between the individual bonds. One has to revert to assumptions that are in general difficult to make in a reasonable, insight providing way. Therefore, there is currently no reliable BE model by which the strength of the bond or a bond order *n* can be determined in an unambiguous, straightforward way.

It is still a wide-spread custom to utilize measured BDE values to describe the bond strength. This is however misleading since the BDE depends on two quantities as is illustrated in Fig. (**2**) where for a molecule H_pABH_q the Morse potential

$$V(r) = D_e(1 - e^{-a(r-r_e)})^2 - D_e \quad (3.1)$$

is schematically drawn. D_e, r_e, a denote the BDE at equilibrium, the equilibrium bond length, and the Morse constant, respectively, which reflects the anharmonicity ("width") of the potential function V(r) for dissociation of the AB bond. Besides the bond strength of bond AB being broken, also the stabilization energies (SEs) of the fragments generated determine the magnitude of the BDE (Fig. **2**). If the SE values are large because of geometry relaxation effects (pyramidal to planar, bent to linear, etc.) and density reorganization (conjugation, hyperconjugation, or anomeric delocalization), the BDE becomes small (see Fig. **2**), perhaps disguising the fact that the actual bond strength is large. Hence, the BDEs do not provide a reliable measure for bond strength.

In Fig. (**2**), it is indicated that the sum of BDE and SEs, henceforth called the intrinsic bond dissociation energy, IBDE = BDE + SE, would provide a reliable measure of bond strength. Of course, IBDEs are model quantities, which cannot be measured [45]. Nevertheless, it is advantageous to estimate the magnitude of the IBDE. It corresponds to an electronic situation of the fragments that exactly mirrors the situation in the molecule, i.e. geometry, charge distribution, hybridzation are kept frozen in the situation of the molecule and in this way all SE effects are excluded. This hypothetical situation is difficult to model and even more difficult to calculate. An estimate however can be given in the case of methane. In the atomization process, C(^{3}P) and four H(^1S) atoms are formed that possess different electron density distributions than C and the H atoms in the methane molecule. The electronic situation for carbon being bound in methane can be modeled by promoting a 2s electron into the empty 2p orbital thus yielding the C(^{5}S) or C(^{3}D) state and then mixing s and p orbitals to form four, tetrahedrally oriented sp^3 orbitals. The energy needed for these two processes is about 100 + 60 kcal/mol, [45] which leads to a 40 kcal/mol contribution to the BE(CH) value of methane being AE/4 = 104 kcal/mol. Hence the intrinsic BE (IBE) of methane is at least 104 + 40 = 144 kcal/mol because the actual density distribution in methane cannot be remodeled utilizing a hybridization model and the energy required to restore the exact density distribution of methane (anisotropic density around the H nuclei, density paths extending into the directions of the 4 H atoms) is not known. A distortion of the density in this way leads to a non-negligible increase in energy even at the H atoms so that IBE(CH) values between 150 - 170 kcal/mol are likely.

The IBE(CH) value of methane can be used to obtain the IBDE(CH) value for the dissociation of methane into methyl radical and H atom since in both cases the same reference densities and geometries are used (which is no longer the case for the methyl, methylene, or methine dissociation that start from different references with relaxed geometry and electron density). Contrary to the AE of methane, which is equal to the sum of the four different BDEs, the sum of the four IBDE values will not be equal to intrinsic atomization energy (IAE) because for each of the four intrinsic processes a new reference state of lower energy will be set (frozen CH_3 vs. relaxed CH_3, frozen CH_2 vs. relaxed CH_2, etc.) so that the sum of the IBDE should become smaller than the IAE value (but still larger than AE).

For diatomic molecules AB, the BE is identical to the BDE and one tends to consider the BDE as a direct measure of the bond strength [133]. We note that the BDE, even in this case, is not equal to the IBDE (keeping the electron density distribution of A and B frozen at that of the molecule AB). Hence, the comparison of the BDE(AB) values of different AB molecules does provide only qualitative rather than quantitative answers to the relative strength of different bonds AB. Clearly, relaxation of the electron density of a Li atom upon dissociation of Li_2 is clearly smaller than that of N upon dissociation of N_2. Accordingly, the SE value is larger for N_2 and the use of its BDE as bond strength indicator leads to an underestimation of the bond strength as compared to that of Li_2. This has to be considered when using listed BDE values to describe bonding in diatomic molecules [133]. We conclude that neither BE nor BDE values provide a reliable measure for the bond strength because they always depend on both bond strength and the fragment stabilization energies.

3.2. Assessing Bond Strength from the Bond Length

In chemistry, it is largely accepted that a shorter (longer) bond length is indicative of a stronger (weaker) bond, especially if the same bond type AB is considered [126,127]. One might argue that it is difficult to define the actual bond length. Bonds can be bent as found in small ring molecules [131,132,134,135]. In such a case the internuclear connection line between two bonded atoms does no longer coincide with the bond path and it is the question how to experimentally determine the bending of the bond. It has been argued that the maximum path of electron density connecting the atoms is an image of the bond [131,132] and therefore leads to a reasonable definition of the bond length. Bending of bonds, if described via electron density paths, is actually also relevant for acyclic molecules since there is indication for small molecules that the path of maximum electron density does generally not follow the internuclear connection line although deviations are small [131,134,135]. These considerations reveal that a strict definition of bond length seems to be only possible within a given model or concept (electron density model, orbital model, geometric model, etc.), which of course is a result of the fact that the chemical bond itself is just a model quantity rather than an observable quantity, which leads in consequence to the fact that none of the so-called "bond properties" are observable. There is no experiment that could measure a bond length. Measurable are (vibrationally averaged) atomic positions from which one can derive bond lengths using some model of the chemical bond. Common bond models used in chemistry are applicable only in a limited sense. They fail when bonded and non-bonded situations have to be distinguished in border cases.

For the moment, we set aside these basic considerations and examine whether at least in a semiquantitative sense bond lengthening (shortening) is an indicator of bond strength. The bond distance is the result of two different contributions. First of all, the size of the atoms connected by a bond determines the magnitude of the atom, atom distance. Often this dependence is estimated on the basis of known atomic radii, covalent radii, or ionic radii depending on the type of bonding. Clearly, these radii depend on the number of core shells of an atom A, i.e. with increasing period within a

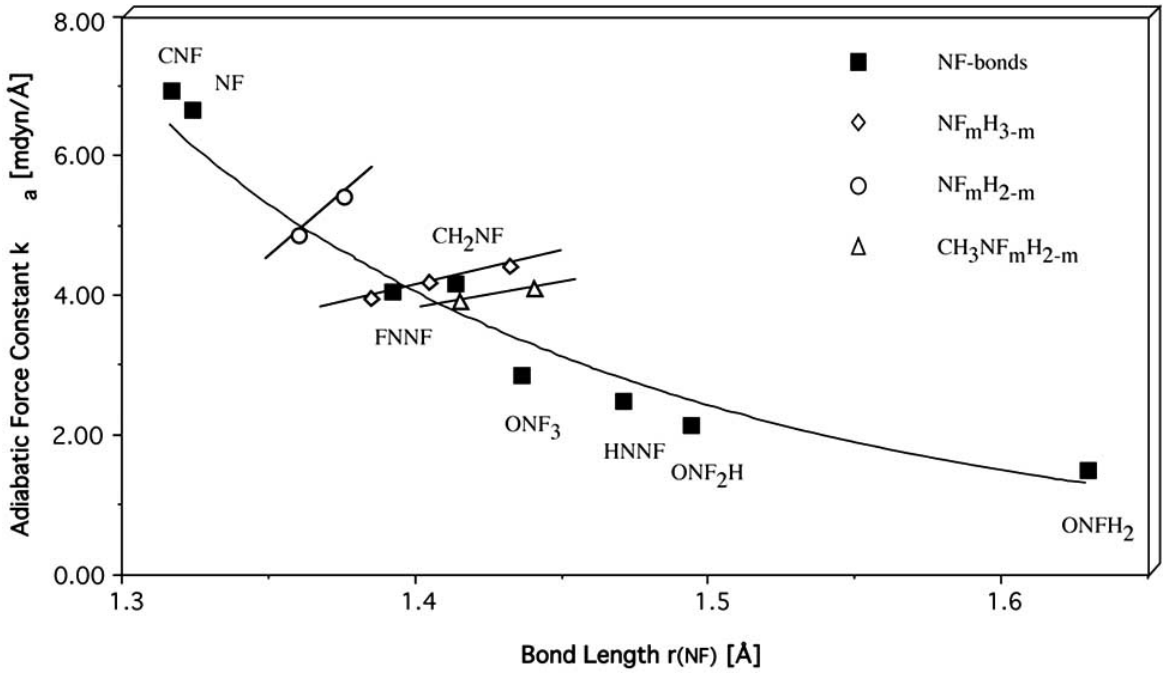

Fig. (3). Adiabatic stretching force constants of NF bonds in dependence of equilibrium bond lengths r(NF) calculated at B3LYP/6-31G(d,p) [139]. The general exponential decay of $k_a(NF)$ for increasing r(NF) is not fulfilled by three fluoroamine classes: In these cases, the NF stretching force constant and thereby the bond strength increases with increasing bond length.

given group the atom-specific radii increase thus leading to larger bond lengths. Since atoms are polarizable and compressible, it is useful to define a situation of highest atom compressibility (compressibility limit) given by the steep increase of the potential V of Eq. (3.1), which accordingly can be rewritten in the form of Eq. (3.2) (see also Fig. **2**):

$$V(r > r_c) = D_e(1 - e^{-a_e(r-r_e)})^2 - D_e \quad (3.2a)$$

$$V(r_c) = V_c = D_e(1 - e^{-a_e(r_c-r_e)})^2 - D_e \quad (3.2b)$$

For r-values smaller than the compressibility limit value, the potential takes the value $V(r < r_c)=\infty$. The atom-specific compressibility limit radius r_c of an atom is more useful than any other atom radius to specify the influence of atomic size on the bond length. The value of r_c is about half the magnitude of the covalent radius and is either calculated or empirically determined [136-139]. The sum of the compressibility limit radii of atoms A and B determines the distance d_c identical to a minimum contact distance (see Fig. **2**), which turns out to be largely independent of the nature of A and B. Badger [136,137] showed that in a first approximation the distance d_c for all bonds AB with A being located in period i of the periodic table and B in period j exclusively depends on i and j, i.e. $d_c(AB)=d_c(i,j)$ for all atoms A with the same i and all atoms B with the same j.

If the minimum contact distance $d_c(i,j)$ of a given bond AB is known, the difference $R_{eff} = r_e - d_c(i,j)$ provides an effective bond length R_{eff} that is directly related to the bond strength of AB. The smaller R_{eff} the stronger is the bond. Since effective bond lengths have been determined for many different bonds, the geometry of a molecule may provide a simple basis to discuss the strengths of its bonds provided one sets aside all principle qualms on the definition of the bond. In practise however, effective bond lengths determined via universal compressibility distances turn out to be too inaccurate to be reliable bond strength descriptors. The compressibility limit radius critically depends on the charge situation of a bonded atom. A cation A^+ has clearly a smaller, and an anion A^- clearly a larger compressibility radius than A itself. In molecules, electronegative (electropositive) substituents generate partial positive (negative) charges on A. For example, DFT calculations reveal that in fluoroamine radicals and fluoroamines of the formula NF_nH_{2-n} (NHF, NF_2), NF_nH_{3-n} (NH_2F, NHF_2, NF_3), and $CH_3NF_nH_{2-n}$ (CH_3NHF, CH_3NF_2) the shorter NF bonds are weaker than the longer ones (see Fig. **3**). This effect is significant and confirmed by structural and spectroscopic measurements in the case of the amines NF_nH_{3-n} [140-143]. The compound with the largest number of fluorine atoms is always the one with the shortest NF bond length. In this case, the F atoms strongly withdraw electron density from the N atom they are attached to. Consequently, the N atom approaches the situation of an N^+ ion, which possesses a smaller compressibility (and covalent) radius than N itself. With increasing F substitution, the NF bonds become shorter because they correspond more to $N^+{-}F^-$ rather than $N{-}F$ bonds. The bond shortening causes an increase in electron pair repulsion between the lone pairs at F and N. Despite the bond shortening, destabilizing four electron interactions reduce the bond strength. The NF stretching force constants decrease with decreasing bond length and reflect the weakening of the NF bonds (Fig. **3**). This observation seems to be in conflict with common chemical thinking that expects bond strengthening upon bond shortening. However when adjusting the compressibility limit radius of the N atom to the value of an N^+ ion, the effective bond length R_{eff} becomes larger with increasing F substitution confirming the general observation that (effectively) longer bonds are weaker bonds.

A similar effect is observed for the OF bonds in OF_2 and HOF, FOF [144-146] however not in the series ONF_nH_{3-n} (ONH_2F, $ONHF_2$, ONF_3; included in Fig. **3**) nor for the CH bonds in the series CF_nH_{4-n} (CH_3F, CH_2F_2, CHF_3, CF_4) since there are no vicinal

lone pair-lone pair repulsions in these molecules. In the case of the anions $CF_nH_{3-n}^-$(CH_2F^-, CHF_2^-, CF_3^-), there are vicinal lone pairs which repel each other. However, the lone pair at C is diffuse and, accordingly, repulsion is rather small so that there is only a small weakening of the CF bond. The CF bond length is decreased from 1.520 Å(CFH_2^-) to 1.486 Å(CF_2H^-) and 1.445 Å(CF_3^-). Contrary to molecules $CH_3NF_nH_{2-n}$ the NF stretching force constant becomes larger with decreasing bond length (indication of bond strengthening, see below) since lone pair-lone pair interactions do not dominate in this case.

Computed lengths of bonds involving heavy transition metal atoms as for example mercury or gold decrease when relativistic effects are included into the quantum chemical calculation [147-149]. This is often connected to a relativistic 6s-orbital contraction although the actual bond length contraction is due to changes in the one-electron contributions caused by the relativistic mass-velocity effect. The quantum chemical calculations reveal that in most cases the shorter bonds are weaker than the longer bonds. In the case of HgX (X = halogen, chalcogen), this is due to reduced charge transfer from the mercury 6s-orbital to X (consequence of the relativistic 6s-orbital contraction) thus causing a lower bond polarity (bond weakening) and an increase in lone pair repulsion (consequence of bond shortening) [147-149] Again, an adjustment of the compressibility limit radius of the transition metal atom leading to a longer effective bond length clarifies the qualitative relationship between bond length and bond strength.

There is no unique way of determining compressibility distances d_c for individual bonds in dependence on their electronic environment. Those parameters d_c given in the literature have been derived empirically for certain bond types (period 1 - period 2 bonds, period 2 - period 2 bonds, etc.) [49,136,137]. The resulting effective bond lengths are far too inaccurate to provide reliable bond strength indicators. We conclude that the bond length is not a useful starting point for deriving bond order or other bond strength parameters, which, apart from the fact that there are principal difficulties to define a bond length, predominantly results from the dependence of r_e on both the size of the bonded atoms (compressibility limit radii) and the bond strength, which are are difficult to separate.

3.3. Assessing Bond Strength from the Bond Density

Bader's work on the virial partitioning of the molecular electron density distribution $\rho(\mathbf{r})$ [131] suggests that a much better descriptor of bond strength should be directly derived from the bond density. However, the bond density is a quantity that lacks a rigorously defined bond region. The virial partitioning approach leads to a definition of atoms in molecules separated by zero-flux surfaces of the electron density [131]. The point of largest electron density in a zero-flux surface is the bond critical point r_{bc}, which is at the same time a point of minimum density along a path of maximum electron density (MED path) perpendicular to the zero-flux surface connecting atoms A and B [131]. There have been attempts to derive from the density ρ_{bc} at r_{bc} relationships for the bond order of a bond AB [132,150]. For closely related bonds (for example, different CC bonds) with chemically well-accepted references (the CC bonds in ethane and ethene defining n = 1 and n = 2) these relationships lead to the prediction of useful bond orders as measures for bond strength. However, a generally defined bond order on the basis of ρ_{bc} is difficult to justify when considering the following. A single bond-density value, even if determined at a characteristic and unique location of the bond region, is an insufficient measure for the bond strength as was shown in several investigations [45,48]. The bond strength depends on the total electron density in the bond region, which of course can only vaguely be described as the region between the bonded atoms. In addition, it includes also to some extend the lone-pair regions (lone pair repulsion) and core regions of the atoms (core-valence electron polarization) as well as regions of substituents attached to the bonded atoms that indirectly contribute to the bond strength via steric and electronic effects between the substituents.

A better assessment of the bond density was made by Cremer and Gauss [151] who determined the density in the zero-flux surface between the bonded atoms by appropriate integration. The zero-flux surface density is a measure for the number of electrons involved in the formation of the bond AB. Theory shows that by dividing the zero-flux surface density by the square of the internuclear distance an energy quantity is obtained that reflects the bond strength in the case of simple hydrocarbons [151]. For CC and CH bonds in hydrocarbons, the covalent part of bonding dominates because the bond polarity is rather low. The zero-flux surface density is a measure for the covalent part of the bond strength whereas ionic (polar) contributions are not considered. Bond polarity is reflected by the position of r_{bc} (shifted from the bond midpoint towards the more electropositive atom) or the charge transfer from A to B using calculated virial charges. There is no reliable and generally applicable way of including contributions from bond polarity into the description of the bond strength so that a generalization of the Cremer-Gauss approach has so far not been pursued.

Apart from the question how both covalent and polar part of the bond strength can be determined, there is also the problem how to assess other bond strength-relevant features of the bond density. For example, density may be contracted toward one nucleus thus shielding it effectively, reducing nuclear repulsion, and increasing the bond strength. Such an effect is not necessarily reflected by the zero-flux surface density, which underlines the need of considering all density in the bond region. A solution to this problem has not been found yet.

In the work of Cremer and Gauss, [151] an energy quantity was directly obtained from the calculated density utilizing quantum mechanical properties of the zero-flux surface. Alternatively, the energy density $H(\mathbf{r})$ can be determined along the MED path or for the zero-flux surface and integrated [151-153]. Cremer and Kraka used $H(\mathbf{r})$ to distinguish covalent from non-covalent bonding [152,153]. It should be possible to extend their work to obtain useful bond strength descriptors. So far, no attempts have been made in this direction. In summary, the bond density parameters discussed do not provide a reliable account on the bond strength and the progress reported was restricted to a limited number of bonds mostly found in organic molecules.

3.4. Assessing Bond Strength from the NMR Spin-Spin Coupling Constant

NMR spin-spin coupling constants are sensitive probes for the electronic structure, geometry, and conformation of molecules. Therefore, it has repeatedly been tried to relate the one-bond $^{13}C,^{13}C$, spin-spin coupling constant with the strength of the CC bond, e.g. in ethane, ethene, and acetylene [154]. We note that these attempts cannot be successful because the indirect spin-spin

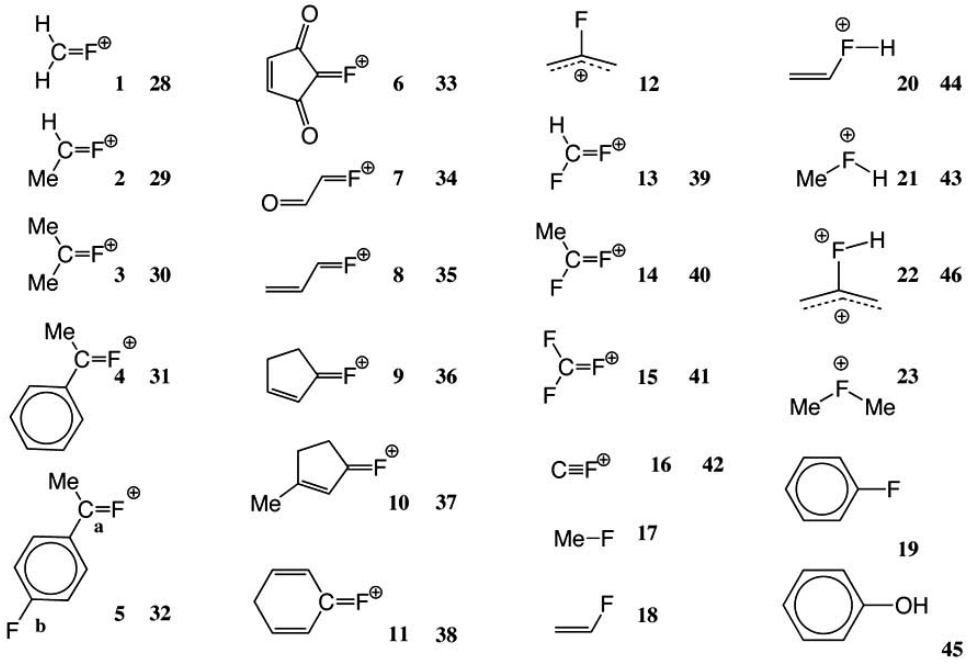

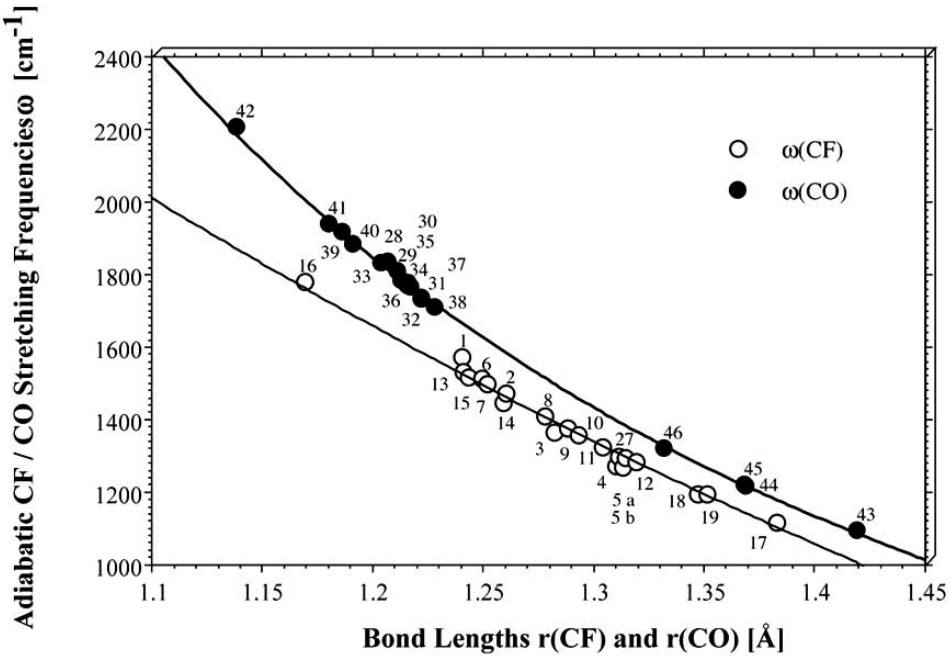

Fig. (4). Adiabatic bond stretching frequencies $\omega_a(CO)$ and $\omega_a(CF)$ given as a function of the corresponding bond lengths (bottom) for 27 structures (top) (**1-16**: F-substituted carbocations; **17-19**: reference compounds with normal C-F bond; **20-23**: fluoronium ions; **24-27**: transition states with loose or normal CF bonds; **28-42**: C=O analogs of **1-16**; **43-46**: reference compounds with C-O(H) bond some of which being isoelectronic with **20-22**. Correlation coefficient R^2 for $\omega_a(CO)$: 0.999, and for $\omega_a(CF)$: 0.993 [48].

coupling constant depends on the first order rather than the zeroth order density (the latter is responsible for bonding), probes spin polarization and density currents, and strongly depends on the environment of the bond [155]. Spin-spin coupling is not just the result of the transport of spin information along the bond path, but also includes transport along bond paths involving substituents and through-space interactions. There has been only one attempt to determine the π-character of CC bonding in typical hydrocarbons with the help of the spin dipole and paramagnetic spin orbit terms of the one-bond spin-spin coupling constant, which however did not lead to any quantitative insights with regard to the bond strength [156].

3.5. Assessing Bond Strength from the Vibrational Bond Stretching Frequency

Vibrational spectroscopy is a frequently used tool to identify and characterize a molecule with the help of its vibrational modes. Depending on its geometry, conformation, and electronic structure,

each molecule has typical vibrational spectra, which are measured with the help of infrared or Raman spectroscopy [27-31]. For example, an infrared band at 1700 cm^{-1} is typical of a carbonyl stretching frequency or one at 1250 cm^{-1} of a Si-C bond stretching frequency. However, this kind of information does not qualify as bond strength descriptor since the vibrational modes are delocalized and contain besides the contribution from a given stretching mode also other stretching, bending, etc. contributions. The AICoMs [50-54] solve this dilemma by providing bond specific vibrational information in form of AICoM frequencies. However, the use of AICoM frequencies is hampered by the fact that they depend again on two quantities, one of them being the bond strength and the other being the adiabatic mass of the bond. This may not matter in the case of the isolated stretching frequencies, which were originally exclusively investigated for CH bonds. However, as soon as one wants to compare different bonds, vibrational frequencies are more an obstacle than the answer to the problem. This was demonstrated by Kraka and Cremer in the case of the CF and the CO bonds [48]. These two types of bonds were first investigated utilizing measured vibrational frequencies in the sense of a Vib-Cal-X approach [47] (for other Vib-Cal-X studies, see Ref. [49]). Correlating CF and CO AICoM bond stretching frequencies with the corresponding bond lengths [47] or bond densities $\rho(r_{bc})$ [48] two different relationships, one for the CF and one for the CO bonds, resulted. Later it was found that this was just a result of the different masses of O and F atoms [48]. In view of the fact that the compressibility limit radii of the two atoms are almost identical, one relationship resulted for both CF and CO bonds irrespective of the fact whether isoelectronic *C=O* and *C=F*$^+$ bonds were compared or the non-isoelectro-nic C-O(H) and C-F bonds. Although vibrational frequencies, contrary to vibrational force constants can be measured it is of advantage to use the latter rather than the former for the purpose of assessing the strength of a chemical bond. This is in line with the original work of Badger and many other investigations who focused on the stretching force constant of a bond rather than on its stretching frequency.

3.6. Assessing Bond Strength from the Vibrational Bond Stretching Force Constant

IBDEs are difficult to determine because the geometry and the density distribution of the undissociated molecule must be kept frozen during the dissociation process so that the fragments still have the electronic structure of the undissociated molecule. An alternative to the dissociation process is an infinitesimally small shift of the dissociation coordinate causing such a small change in the electron density distribution that it can be considered to be preserved. This shift leads to an increase in the potential energy *V*, which can be determined by expanding *V* into a Taylor series. At the equilibrium, there is no first order correction to *V* so that the correction is dominated by second order term. Hence, the magnitude of the correction is reflected by the curvature of *V* in the direction of the dissociation coordinate as described by the corresponding stretching force constant. The stretching force constant is in this way directly related to the IBDE and, therefore, it can replace the latter as a suitable measure for the bond strength.

One might argue that there should not be any difference as to whether the bond stretching vibration is expressed in terms of AICoMs or **c**-vector modes, i.e. whether force constants k_a or k_c are

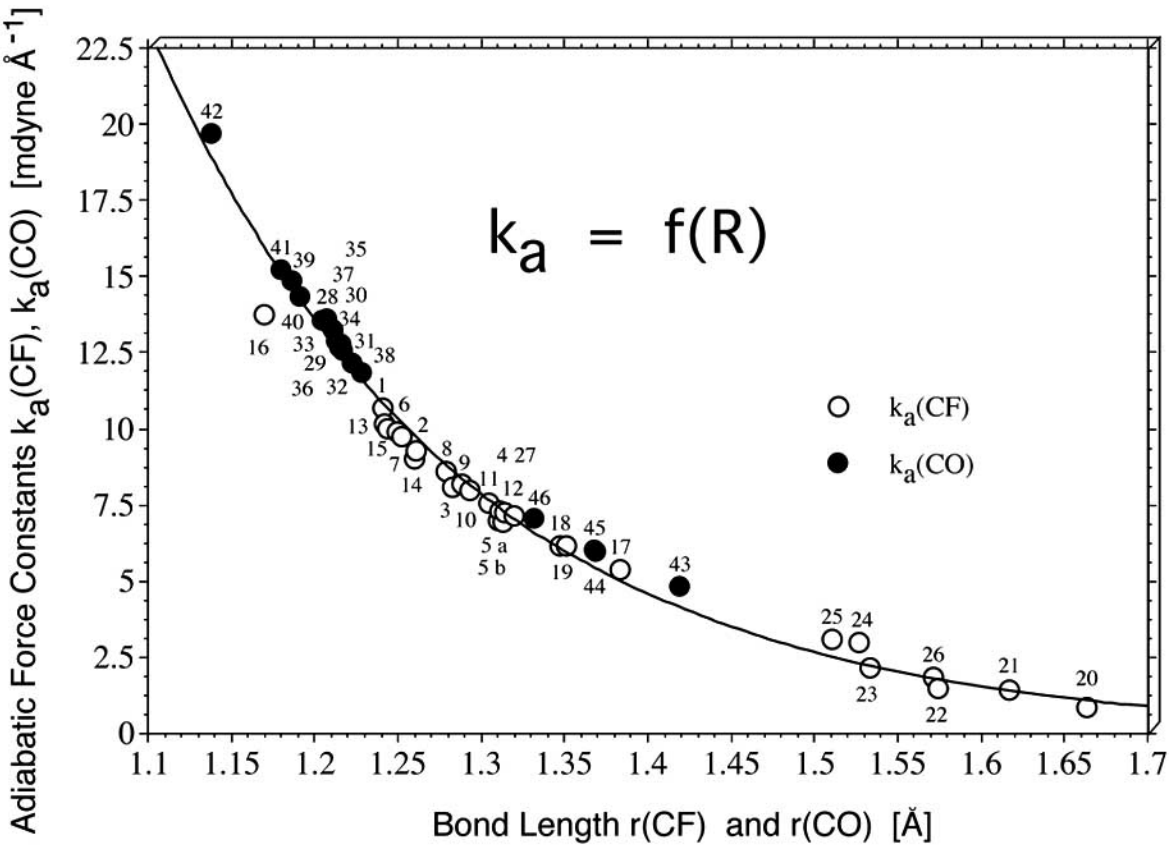

Fig. (5). Adiabatic CF and CO stretching force constants of structures **1** - **46** (Fig. **4**) expressed in form of an exponential relationship of the corresponding bond lengths. Correlation coefficient R^2 for $k_a(CO)$: 0.998, and for $k_a(CF)$: 0.982. If both sets of data are correlated with the bond length, R^2 is 0.985. B3LYP/6-31(d,p) calculations [48].

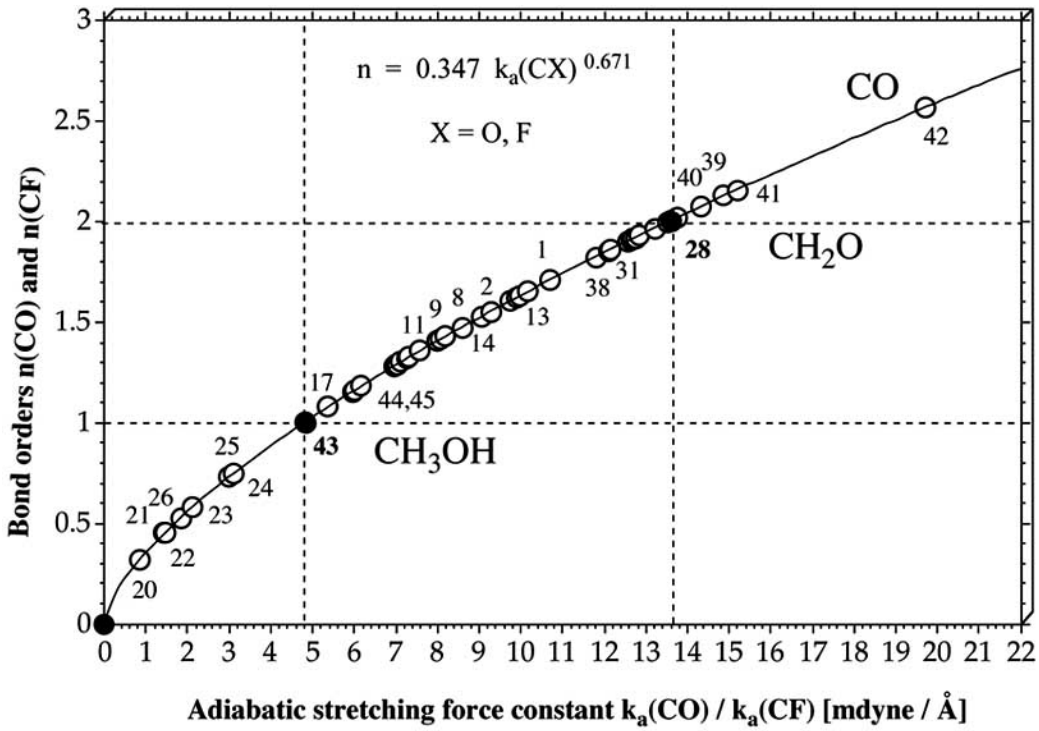

Fig. (6). CF and CO bond orders *n* based on the adiabatic CF and CO stretching force constants of structures **1 - 46** shown in Fig. **4**. Reference points are given by the black, solid circles at $n = 0$, $n = 1$ (CH_3OH), and $n = 2$ ($CH_2=O$). All other bond orders *n* were calculated using the available adiabatic stretching force constants and the power relationship given in the upper part of the diagram.

used to determine the strength of the bond. The latter do not include a relaxation of the geometrical parameters of the molecule upon bond stretching. Therefore, k_c force constants are always larger than k_a force constants [48]. The adiabatic stretching mode, contrary to the **c**-stretching mode, initiates bond dissociation and accordingly provides a natural measure for the strength of the bond. As has been shown, k_c force constants in general can lead to unphysical values ($k_c<0$ k_c not complying with symmetry, etc. [45,50,51]) and therefore their use is not recommended. The following discussion will be exclusively based on adiabatic stretching force constants k_a as the most reliable bond strength descriptors.

When the calculated $k_a(CF)$ and $k_a(CO)$ values for the structures shown in Fig. (**2**) are related to the corresponding bond lengths the two relationships observed for the adiabatic stretching frequencies (Fig. **4**) merge into just one exponential relationship despite the different nature of CO and CF bonds. The scattering of data points is moderate, which suggests that the variation in the compressibility limits of C, O, and F atom in dependence of their substituents is small. This is observed for the $C{=}F^+$ ion, the normal C-O single bonds (**43 - 46**), and some of the transition states, i.e. in those situations where the positive charge on C is different from that found for the fluoro carbocations and the keto structures. Apart from this, the results found for CO and CF bonds clearly support the view that adiabatic stretching force constants provide a measure for bond strength and that it is therefore reasonable to use them to define a common bond order *n* (Fig. **5**). The definition of a bond order implies the use of suitable reference values, which were chosen to be n=1 and n=2 for the CO bonds in methanol (**43**) and formaldehyde (**28**) in agreement with general chemical understanding. In addition, it was required that for a vanishing stretching force constant the bond order is equal to zero. In this way the power relationship shown in Fig. (**6**) was obtained (some selected values are shown in Fig. **7**). The calculated bond orders reveal that the bond in carbon monoxide has less than triple bond character in agreement with the measured and calculated BDE values of methanol, formaldehyde, and carbon monoxide [48]. Furthermore, the CF^+ ion is found to have just a double bond because F is too weak a π donor to share more than one electron lone pair with the positively charged carbon atom. Otherwise F-substituted carbocations possess significant double bond character (Fig. **7**) with bond orders between 1.3 and 1.7. The magnitude of the bond order sensitively depends on the presence of electron-donating substituents (methyl, phenyl groups) that by charge donation to C^+ reduce π-donation of F and by this the double bond character. The opposite effect is found for electron-withdrawing groups (acyl) that increase the CF^+ double bond character. Hence, the CF^+ double bond character can be used as a sensitive antenna for the electronic environment of a carbo cation.

Fluoronium, cations have rather weak CF σ-bonds (n = 0.3 - 0.6; BDE values between 14 and 47 kcal/mol; Fig. (**7**) and Ref. [48]). Although they are isoelectronic with CO single bonds, the electron-deficient F atom is no longer sufficiently shielded and therefore strong nuclear, nuclear repulsion leads to lengthening and weakening of the CF bond. The CF bonding situation in the transition states investigated (FH elimination reactions, Fig. **4**, top) can be assessed by comparison with the different types of CF bonding ($C{-}F$, $C{=}F^+$, $C{-}F^+$, Fig. **7**) investigated. In Section 4, we will discuss the use of vibrational information in the situation of a chemical reaction.

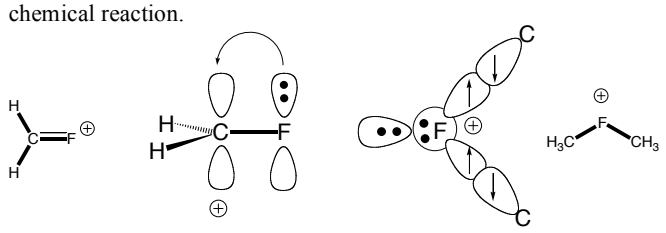

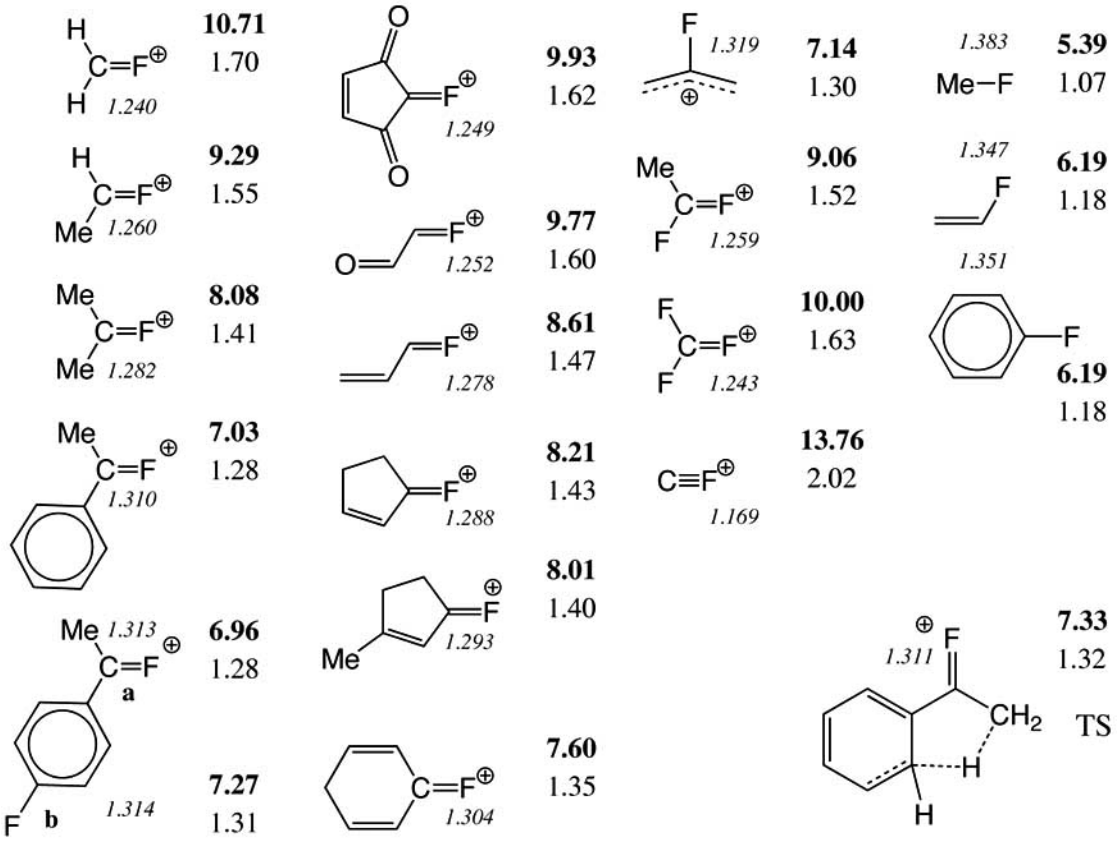

Fig. (7). Some selected adiabatic CF stretching force constants in mdyne/Å (bold face), bond lengths in Å (italics), and bond orders (normal print) of F-substituted carbocations [48].

4. FROM VIBRATING MOLECULES TO CHEMICAL REACTIONS

Thermally triggered chemical reactions are mostly started by an energy transfer during a collision. This energy transfer leads to vibrational excitation, for example, of a bond stretching vibration in an unimolecular dissociation. One can say that the chemical reaction is the consequence of the favorable interaction of two events, a molecular collision at an angle that enables energy transfer and a vibrational excitation that leads to bond loosening and cleavage. Chemical reactions start with a vibrational motion that is forced to adopt larger and larger vibrational amplitudes until bond cleavage occurs. The situation is similar for a photolytically triggered reaction, however with the difference that an excitation to a higher electronic state takes place. This state is dissociative when a vibrational mode converts into a translational motion thus leading to bond cleavage. Molecular vibrations always play an important role in chemical reactions and the purpose of this section is to describe this role. However, before doing so some useful terms in connection with the mechanism of chemical reactions have to be clarified.

4.1. Chemical Processes, Reaction Complex, and Energy Landscape of a Reaction

The understanding of chemical reactivity and the mechanism of chemical reactions is the primary objective of chemical research. This understanding is essential because it enables chemists to control chemical reactions and to synthesize materials with desired properties. In a chemical reaction, one or more reactants are interconverted into new products. Normally, this implies one or more chemical processes each of which leads to a change in chemical bonding. More specifically, we define bond breaking or bond forming as chemical processes to distinguish them from other processes such as van der Waals processes, conformational processes, (de)solvation processes, self-assembly (self-organized) processes, electron-transfer processes, excitation processes, or ionization processes. All these processes can occur in the course of a chemical reaction and therefore are investigated by chemists although they are often more physical than chemical in nature. For example biochemists investigate folding processes of proteins, which include predominantly conformational but also solvation processes. Medicinal chemists and drug developers study docking processes, which involve van der Waals, conformational, and solvation processes. Compared to these processes, chemical processes are at the core of chemistry and the study of reaction mechanism focuses primarily on these processes.

What is a Chemical Bond?

Since chemical interconversions imply changes in the bonding pattern there is a need to distinguish between bonding and nonbonding situations. This can only be done if one defines a chemical bond [126-133]. Most chemists would not claim that a dispersion-stabilized van der Waals complex is kept together by chemical bonds although the term *van der Waals bond* is sometimes used. Considering a weakly bonded donor-acceptor complex it becomes more problematic to distinguish between a bonding or non-bonding situation. The actual reason for all problems in connection with specifying the nature of a chemical bond results from the fact that the chemical bond is a model quantity rather than an observable quantity developed within a given concept to

understand molecular structure and stability (see Section 3). There is no experiment that could measure properties of the chemical bond and by this help to clearly distinguish between a bonding and a non-bonding situation. It is only possible within a given model to define the chemical bond and bond forming / bond breaking, i.e. the chemical processes and the chemical reaction caused by the chemical processes. This may be illustrated by an example: Ethane-1,2-diol is stabilized in a gauche conformation due to H bonding between the OH groups. A rotation at the CC bond leads to a cleavage of the H-bond and a change in energy by just 2.0 kcal/mol, [46] which is definitely not typical of the energy changes accompanying normal bond ruptures. Without a specific model of the chemical bond also applicable to H bonding, it is not possible to distinguish in this case between a chemical reaction and a conformational process although most chemists would emphasize the latter in this case. Hence, we have to clarify this question in the following.

Reaction Complex and Reaction Path

One characterizes chemical reactions according to their molecularity (unimolecular, bimolecular or a few trimolecular processes). In the quantum chemical study of reaction mechanism one simplifies by focusing on a *reaction complex* that is the union of all reactants. By determining the properties of the reaction complex one unravels the reaction mechanism. It is a non-trivial problem to describe the vibrating and rotating reaction complex during the reaction. For this purpose two conceptual simplifications are introduced. First, the Born-Oppenheimer approximation separating nuclear and electronic motion is applied. Second, the changes of the reaction complex are modeled on the potential energy (hyper)surface (PES) V(**q**), which is spanned by the 3N-L internal coordinates q_m of the reaction complex, i.e. the reaction is described in a model space rather than in real space. Although any function depending on more than 2 variables is difficult to visualize, one determines internal coordinates that describe major deformations of the reaction complex and makes two-dimensional cuts through the PES to represent energy changes in dependence on these two coordinates in form of contour line diagrams or perspective drawings. In addition, one uses the geographical terms of a mountain region to describe the multi-dimensional energy landscape of the PES. In a chemical reaction, the reaction complex follows a minimum energy path (*reaction path*) from a minimum occupied by the reactants up an energy valley called the *reaction valley*, to an energy pass between energy mountains (the transition state of the reaction determining the energy barrier and corresponding to a first order saddle point of V(**q**)). From the energy pass, the reaction complex follows down another energy valley to an energy minimum occupied by the product(s).

4.2. Reaction Step, Reaction Phase, and Reaction Mechanism

A reaction from reactants to products via a single transition state is called a one-step or elementary reaction. A two step reaction passes through an intermediate minimum occupied by a chemical reaction intermediate. The kinetic stability of the intermediate decides whether the compound in question can be experimentally intercepted. There are intermediates of low stability on the PES which vanish on the Gibbs energy surface G(**q**). From an experimental point of view, these pseudo-intermediates can be ignored. However, they are of high importance for the mechanistic analysis because they indicate the possibility of obtaining stable intermediates if the electronic situation and/or the environment is changed in a way that can be assessed from an analysis of the pseudo-intermediate. Clearly, the first and most important step of any mechanistic analysis has to focus on electronic structure features of the reaction complex as they relate to the features of the PES. Features of the Gibbs energy surface along the reaction path can be analyzed to determine entropy, temperature and other effects. However, they will not be subject of this review that focuses exclusively on electronic structural features of the reaction complex.

When Does One Speak of a Reaction Mechanism?

Experimentalists use the term reaction mechanism when discussing the elementary reactions leading from reactants to products. This is distinguished from a *reaction sequence*, which is a proposed reaction mechanism based on incomplete experimental data. It is unusual in experimental chemistry to use the term reaction mechanism in the case of a one-step reaction with or without transition state. In a quantum chemical investigation of a reaction, one describes the properties of the reaction complex at any transient point along the reaction path to obtain a detailed analysis of the chemical processes. For decades, it was a common practice among quantum chemists to study the reaction complex just at the stationary points (reactant or product minima and transition states), which leads to an incomplete and sometimes even misleading picture of the reaction mechanism as will be shown in Section 4.5. A continuous description of the reaction complex along the reaction path has the advantage that all changes in its properties can be registered and their influence on the course of the reaction assessed. In such a description, it makes sense to speak of the reaction mechanism of a one-step reaction even if this is proceeding without barrier and transition state. For example, the dissociation of H_2 is an elementary reaction without transition state but with a distinct reaction mechanism consisting of two *reaction phases* (Fig. **8**). The first is characterized by a "reaction complex" with continuously elongated H-H bond. Any bonding interaction ceases when the electron pair responsible for bonding undergoes spin decoupling to an open-shell singlet. Then, Coulomb repulsion facilitates lengthening of the H,H interaction distance. A second reaction phase starts, which is characterized by H atoms quickly drifting apart. It ends when the energy asymptote representing two completely free H atoms is reached. In the first reaction phase, the potential energy V(r) possesses a positive curvature (d^2V/dr^2), i.e. for each step Δr of the dissociation reaction the energy increases stronger as predicted by the gradient dV/dr. The reaction complex resists the bond breaking motion. This changes as soon as the electron pair of H_2 is spin-decoupled. The function V(r) becomes concave with a negative second derivative, i.e. the reaction complex does no longer resist an elongation of the HH distance. the reaction force is negative, and the predicted energy changes for an increase Δr are larger than actually given by the energy curve and the reaction force.

The two-phase mechanism of the H_2 dissociation, although rather simple, leads to several questions: 1) Does the inflection point (IFP, change from positive to negative derivative $d^2V(r)/dr^2$; Fig. **8**) of the V(r) potential relate to the distance r, at which spin decoupling occurs? 2) Is spin decoupling a sudden or a gradual process and what triggers it? 3) How is the position of the IFP related to the values of BDE and IBDE of H_2? 4) Which part of the BDE is needed for spin decoupling and which part for complete H,H separation? 5) Does the stretching vibration support or hinder spin decoupling? - Answering these questions leads to the establishment of a dissociation mechanism, which passes through at least two different reaction phases. The physical importance of the

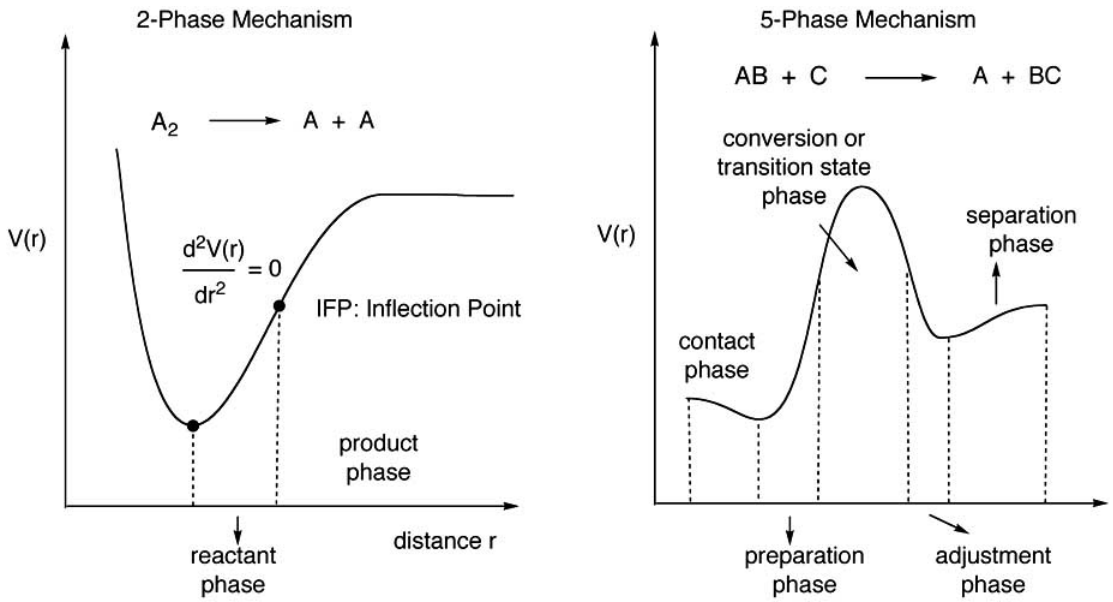

Fig. (8). Two-phase mechanism of an A-A single bond dissociation (left side). Five-phase mechanism of the reaction *AB+C→A+BC* (right side). The reaction phases are separated by vertical dashed lines. Note that the phase borders are not specified on the right side.

IFP as the point that separates two reaction would be clarified if the IFP is also the point of spin decoupling. However, it is more likely that spin decoupling is not a sudden but a slowly developing process that depends on bond strength and the (spin) polarizability of the bond density. Several authors have agreed to the special role of the IFP and connected it with other properties of the reaction complex [157-159].

The H_2 example underlines that transient points along the reaction path, not identical with the stationary points, can be mechanistically relevant. This is taken care of by the phase model of the reaction mechanism [115,117,119-124], which dissects the elementary reactions into different phases. In general, one can expect that a bimolecular elementary reaction with transition state proceeds in five phases: i) a contact or van der Waals phase between the reactants where first van der Waals interactions (possibly leading to a van der Waals complex) result in a preferred configuration of the reaction complex that will influence the stereochemistry of the reaction; ii) a preparation phase, in which the reaction complex distorts to prepare for the actual chemical processes; iii) a conversion or transition state phase, in which the chemical processes take place; iv) an adjustment phase, in which the reaction complex adjusts to the electronic structure, geometry, and conformation of the products; v) a separation phase, in which weak van der Waals interactions are dissolved. - Clearly, contact and separation phase, preparation and adjustment phase reverse their roles for the reverse reaction. There is no general rule that requires that the energy transition state is always located in the conversion phase. If this would be the case, the energy barrier was primarily a result of the bond breaking or forming processes. If however the barrier is due to the preparation process of the reaction complex, the energy transition state can also be positioned in the preparation (adjustment) phase. These considerations already reveal that the transition state location and its energy may disclose little about the detailed reaction mechanism.

Macroscopic and Atomistic Descriptions of Chemical Reactions

Clearly one has to distinguish between a macroscopic and atomistic (microscopic) description of the chemical reaction both adding to the understanding of the reaction mechanism as it is needed to control the reaction. The macroscopic description includes the energetics as given by the free reaction energy $\Delta_R G$ and free activation energy $\Delta G^{\ddagger}$, the reaction temperature and pressure, solvent, reaction rate, yield, etc. The microscopic description includes the geometric distortion of the reaction complex, its energy change, changes in the electron density distribution, in electric and magnetic properties, all given along a representative reaction path. Important are also the vibrations of the reaction complex as they change in the course of the reaction. Since the reaction is a dynamic process described as a translational motion along the reaction path, it may be connected to other dynamic processes such as the vibrational and rotational movements of the reaction complex. For reasons of simplicity, we do not consider here the rotation of the reaction complex (although it may be relevant as for example in unimolecular reactions [160,161]) and instead focus on the vibrations of the reaction complex.

4.3. Vibrations of the Reaction Complex

Chemical reactions are normally triggered by some uptake of energy in a collision or excitation process. However, the actual chemical process starts by a vibrational motion that is converted into a translational motion along the reaction path. This is often accompanied by strong coupling to other vibrational modes of the reaction complex and therefore the mechanism of a chemical reaction can only be clarified by analyzing the vibrations of the reaction complex and their interplay. Upon conversion of one vibrational mode into a translational movement, the remaining 3N-7 vibrations orthogonal to the reaction path reflect in a characteristic way the changes in the reaction complex. Bond stretching vibrations of bonds being broken vanish and those of bonds being formed appear, by this giving an account on structural and stability changes of the reaction complex. Also, certain vibrations of the reaction complex can couple with its translational motion thus making an energy transfer between these two dynamic processes possible [162,163]. Alternatively, different vibrational modes of the reaction complex can couple, which facilitates the energy transfer

between the vibrational modes and by this the energy dissipation in the reaction complex. Energy dissipation can occur whenever the eigenstates of two vibrational modes approach each other and undergo an avoided crossing [115,118,162].

As was pointed out in Section 2, normal vibrational modes of a molecule are always delocalized and this also holds for the reaction complex. For the purpose of facilitating the analysis of the reaction complex vibrations as they change along the reaction path, they can be decomposed into AICoMs where the AICoMs are led by the internal coordinates used to describe the geometry of the reaction complex [115,117,119-124]. In this way, the forming and breaking of new bonds can be followed in detail without reference to a specific bond model. Any developing bonding interaction can be detected when the adiabatic frequencies or force constants are displayed as a function of the reaction path coordinate. The force constant values, which are finally reached in the products, relate to the strength of the bond generated because the adiabatic force constants provide reliable descriptors of bond strength (see Section 3) [44, 45, 48, 49, 54].

4.4. Choice of the Representative Reaction Path

The reaction path of a chemical reaction is like the chemical bond a model quantity. Therefore, many different reaction paths can be chosen when investigating the mechanism of a chemical reaction. It turns out that the mechanistic study can be significantly simplified if a representative path is used for the analysis. In the case of elementary reactions with transition state, the floor line of the reaction valley is suitable as representative path of the reaction complex. There are basically two different strategies for determining reaction paths: i) moving downhill, i.e. starting at the transition state in the direction of the negative curvature and tracing down the steepest decent path toward both the reactant and the product minimum; i) moving uphill, i.e. starting at the minimum occupied by the reactants (products) and following the valley floor line up to the transition state [164, 165]. The most commonly used method belonging to the first category is Fukui's intrinsic reaction coordinate (IRC) approach [166]. The IRC is the steepest descend path starting at the transition state and being expressed in mass-weighted or mass-scaled Cartesian Coordinates [166]. The union of the two steepest descent paths in entrance and exit valley leads to a unique path connecting reactant minimum with product minimum via the transition state [167]. Usually the IRC path tends to follow the valley floor-line, especially in the convex part of the PES between minimum and IFP about halfway up to the transition state [168]. It has been pointed out that in the concave region between IFP and transition state, the IRC path may deviate from the valley floor line [169]. However, small deviations from the floor line are of little consequence for the mechanistic discussion and therefore the IRC path is the path of choice for reactions with a barrier.

Representative Paths for Reactions without Barrier

An IRC path does no longer exist for chemical reactions without a barrier. In this case, one can use an uphill strategy for determining a representative reaction path. For example, gradient extremals [170] can trace out such a path along the uphill going floor line. The floor line fulfills two criteria: i) The energy increases along all directions perpendicular to the direction of the valley floor line. ii) The curvature of the PES along the floor line must be minimal compared to any other direction [171]. Hence, the gradient of the floor line is the eigenvector of the Hessian matrix associated with the lowest eigenvalue. Ruedenberg called lines following the least uphill curvature gradient extremals [172-174]. Quapp and co-workers showed that IRC path and gradient extremal are identical close to the reactant or product minimum (convex PES parts), however when the IRC path becomes curvilinear in the transition state region IRC path and gradient extremal deviate slightly to coincide again at the transition state [169].

Alternatively, Newton trajectories [174] can be used for deriving a representative path in the case of barrierless reactions. Newton trajectories are defined by the condition that a preselected gradient direction is kept by all points on the path, which can be considered as a generalization of the distinguished reaction coordinate approach [175]. Since any gradient direction can be chosen, Newton trajectories do not lead to a unique path. Instead, a family of Newton trajectory curves connects stationary points with a difference of order 1, for example minimum and transition state [174]. Quapp, Kraka, and co-workers [122] showed that Newton trajectories bundle in the exit channel of the reaction valley before merging onto the energy plateau. This makes it possible to determine a central point in the valley from where a representative downhill path can be started. There is also the possibility that the reaction valley opens up to a broad bowl as in case of a cirque created by a glacier. In this case the Newton trajectories can be used to describe size and boundaries of the cirque, which again makes it possible to find a suitable starting point for a representative down hill path. The latter situation was encountered for the chelotropic addition of methylene to ethene yielding cyclopropane [122,123]. There are other definitions of reaction paths, which are however less suited as representative paths because they are used in connection with the statistical averaging of trajectories for the calculation of reaction rates [176,177].

4.5. Reaction Path Splitting

When following the reaction valley, it can happen that it splits into two or even more valleys and the reaction path bifurcates, trifurcates, etc. [178-180]. Two different situations are encountered depending whether path splitting occurs in the exit valley, i.e. for the downhill path (starting from the transition state), or in the entrance valley, i.e. for the uphill path (starting from the reactant minimum). In the first case, valley splitting precedes path branching. On the path down through the valley all curvatures orthogonal to the gradient are positive corresponding to generalized vibrational frequencies larger than zero. If beyond a certain path point, generally called a valley-ridge inflection (VRI) point [181,182], one curvature becomes negative, the eigenvalue of the Hessian matrix corresponding to this curvature must be zero at the VRI. By this condition, the VRI is not a stationary point and therefore there is no path splitting at this point although the valley splits at this point. In this connection, it may be noted that according to the McIver-Stanton rule [183] the reaction complex can change its symmetry only at a stationary point, otherwise it must follow the reaction path. As pointed out by Ruedenberg [181], the reaction path follows after the VRI no longer the floor line of a valley but the crest line of an energy ridge flanked by two (or more) energy valleys or troughs. The curvature from the ridge down to the flanking valleys is negative corresponding to an imaginary generalized frequency. The path follows the ridge until a stationary point (energy gradient equal to zero) is reached which corresponds to the path branching or bifurcation point. In most cases, VRI points and branching points are adjacent points along the path separated by an unspecified path distance. Each of the new paths starts in the direction of the negative curvature downhill until the two valleys

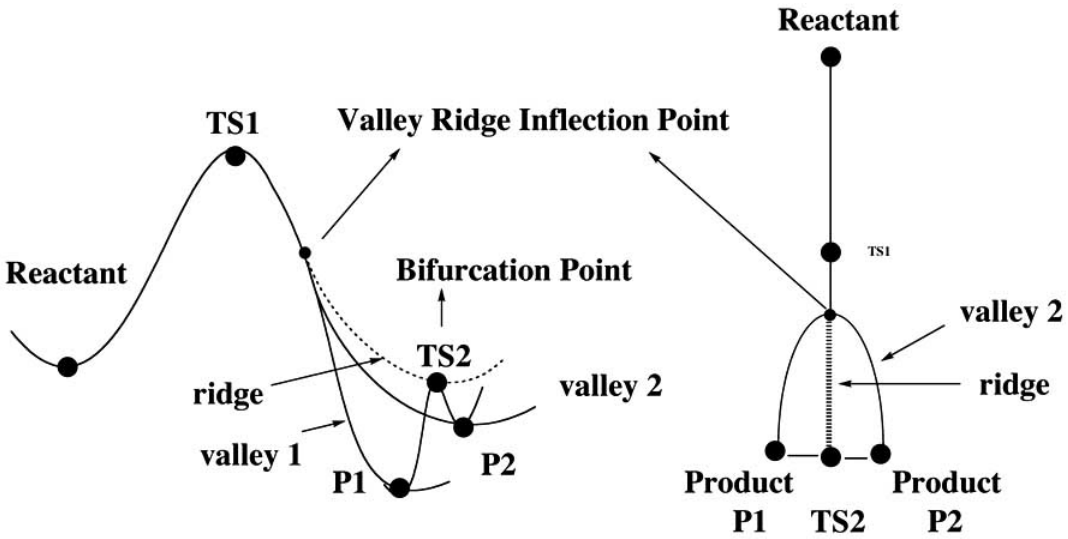

are reached where the reaction path can again follow a floor line to one of the product minima. Two products are generated that may or may not be equivalent by symmetry [178].

VRI points and branching points appear more often than is generally assumed as the work of Caramella and co-workers demonstrates [184-187] (for a recent review, see Houk and co-workers [178]). Examples for reaction valley and reaction path branching processes include many substitution reaction as e.g. the reaction $CH_3+H_2 \rightarrow CH_4+H$ (trifurcation by van der Waals interactions), [117] isomerization of methoxy radical to hydroxymethylene (VRI, bifurcation by rotation) [188-191], bond shifting in cyclooctatetraene (bifurcation by ring puckering) [192], isomerization of cyclooctatetraene to semibullvalene (bifurcation by alternative bond formation) [193], ring-opening of cyclopropylidene to allene (bifurcation by rotation) [194], cope rearrangements of cis-1,2-divinylcyclo-propane (bifurcation by ring inversion), [195] and HF addition to ethene (bifurcation by rotation) [120]. All these examples are characterized by a symmetric branching leading to equivalent products. However, there is also the possibility that the reaction path bifurcation leads to different products and as a consequence the valley splitting is no longer symmetric. Into this category fall for example the Cope rearrangement of 1,2,6-heptatriene leading to the concerted rearrangement product or a biradical intermediate (bifurcation by alternative bond or no-bond formation) [178,196], ene reactions of substituted allenes leading either to the cycloaddition product or a biradical intermediate [197], the cycloaddition of cyclopentadiene with diphenylketene leading to both [4+2] and [2+2] cycloadducts sharing a common transition state (alternative bond formation in transition state) [198].

Many of the path splitting reactions involve symmetry breaking in the reaction complex often as a result of the formation of instable products that can stabilize by equivalent conformational processes (clockwise and counterclockwise rotation, inversion, ring puckering) or van der Waals relaxation processes. In the latter case, bond allineation of the separating group (atom) or movement into corner, edge, or face arrangements can occur where the multiplicity of branching is given by the highest symmetry element of the reaction complex before the VRI point. For example, C_{2v} symmetry can lead to bifurcation, C_{3v} to trifurcation, C_{4v} tetrafurcation, etc. In most of these cases, the reaction path along the valley and the adjoined ridge is clearly representative because valley splitting is a result of non-chemical processes of relatively low energy. However, as pointed out above, there are also reactions involving branching into different chemical processes. These reactions require that, starting from the branching point, two or more new mechanistic studies have to be carried out.

When valley splitting occurs on an uphill path mechanistically a new situation is encountered because the two valleys lead to different transition states associated with different reactions. If the latter are symmetry equivalent only one of them has to be investigated. Usually there is no ridge between the different valleys. If one uses gradient extremals to determine an uphill branching of valley and reaction path, complications may occur due to the existence of turning points at which the nature of the gradient extremal changes from a floor line into a flank line being parallel to an energy ridge. Hence neither VRI nor branching point can be found in this situation. Mathematical recipes have been discussed to get around this problem although no floor line solution has been found so far for these cases [169].

5. CALCULATION OF REACTION COMPLEX PROPERTIES ALONG THE REACTION PATH

For the computational elucidation of the reaction mechanism one has to consider two aspects: i) A reliable calculation of the energetics of a reaction requires high level methods such a couple cluster or multireference configuration interaction, large augmented basis sets, and the inclusion of vibrational and thermal corrections to relate to quantities that are obtained by measurements. Calculational costs set a limit to the size of the reaction complex. For example, nowadays CCSD(T) calculations up to 20 non-hydrogen atoms are feasible on a larger scale provided vibrational corrections are obtained at a lower level of theory. ii) The analysis of the reaction mechanism can also be carried out at a lower level of theory because the sequence of chemical processes is (at least qualitatively) correctly described at all levels of theory. In so far the mechanistic analysis resembles the qualitative molecular orbital analysis, which is mostly correct even when using the simplest quantum chemical methods. Taking both considerations into account, a *dual level approach* is most suitable for the computational description of the reaction mechanism. In the first stage of the analysis, all stationary points are described as accurately as possible. In this way, the energetics of the reaction is

correctly assessed. Then at a lower level of theory the topology of the PES is clarified, for example by connecting reactant and product minima and the associated transition states by reaction paths. This becomes important when there is a large number of reaction possibilities of a reaction complex so that it becomes difficult to determine the relationship between transition states, intermediates, and products. For example, Cremer and co-workers have shown that such means are necessary to unravel the sequence of reactions taking place in the ozonolysis of acetylene and other alkines [199]. The same holds if one wants to explore all possible reactions on a given PES. This was for example done in the case of the C_4H_4 PES for which a total of 106 stationary points (52 minima and 54 transition states) being connected by 32 reactions and reaction sequences (55 elementary reactions in total) were calculated [200,201]. The chemical relationship between these many stationary points could only be assessed by extensive IRC calculations.

The mechanistic investigation that is presented by the *Unified Reaction Valley Approach (URVA)* of Kraka and Cremer [115-124] is based on representative paths such as IRC, gradient extremal, Newton trajectory paths, or down hill paths from an energy plateau through a valley or in a cirque situation. In addition, URVA determines the (harmonic) reaction valley as reflected by the generalized vibrational modes of the reaction complex, their frequencies, and force constants and their changes along the representative reaction path. URVA collects a large number properties of the reaction complex where especially energy, geometry, electron density distribution, and vibrational motions are analyzed. Common basis of all URVA analyses is the Reaction Path Hamiltonian (RPH) of Miller, Handy, and Adams (Section 5.1) [202], the adiabatic mode concept of Cremer and Konkoli ([49-54], see also Section 2.4), and the vibrational mode ordering of Konkoli, Cremer, and Kraka [118].

5.1. Reaction Path Hamiltonian, Adiabatic Mode Concept, and URVA

Once the PES is known for a reaction system, one can apply Newton dynamics to treat the movements of the reaction complex on this surface and calculate reaction rate and other dynamic properties. Apart from the fact that a quantum system should be described with the help of quantum dynamics, there are two major obstacles to proceed in this way. First, there are the high, prohibitive computational costs of determining a PES for a reaction complex with more than 3 atoms. Assuming that about 300 PES points are needed for a reliable description in each direction of the surface, a total of 300^{3N-L} points have to be calculated, which becomes no longer feasible for a large polyatomic system. Secondly, the nuclear dynamics become also costly with increasing size of the reaction complex. Out of this computational dilemma, the idea of a one-dimensional cut through the PES following the reaction path was born [203,204]. The question however remained how to carry out reaction path dynamics that would lead to reasonable rate constants, energy distributions, coupling quantities, kinetic isotope effects, etc. Miller, Handy, and Adams [202] answered this question by developing the RPH. The RPH is a classical Hamiltonian, which facilitates the computational task tremendously when calculating rate constants, but which has to be considered when describing quantum effects.

The configuration space of the RPH is partitioned into the one-dimensional reaction path part and the multi-dimensional valley part orthogonal to the path. The one-dimensional part of the RPH is expanded as a function of the arclength s of the reaction path (Fig. **9**) and the conjugate momentum p_s. Normally, the zero of s is taken as the location of the transition state and positive s values are used for the exit, negative s values for the entrance channel of a chemical reaction. The potential energy of the RPH is given by (i) the term $V_0(s)$, describing the change in energy along the path and (ii) a second term describing the energy change in the $3N-L-1=N_{vib}-1$ (for L = 6: 3N-7)-dimensional harmonic valley, spanned by the $N_{vib}-1$ normal coordinates $Q_\mu(s)$ of as many generalized harmonic modes with frequencies $\omega_\mu(s)$:

$$V[s,\{Q_\mu\}] = V_0(s) + \frac{1}{2}\sum_{\mu}^{N_{vib}-1} \omega_\mu^2(s) Q_\mu^2(s) \tag{5.1}$$

The simplification to a harmonic valley is justified as long as the reaction complex moves close to the minimum energy path, i.e. the floor line of the valley. For the purpose of determining the multidimensional harmonic valley, at each path point s the generalized force constant matrix has to be calculated after projecting out translational and rotational motions and solving the vibrational equation for the remaining degrees of freedom to obtain frequencies ω_μ and normal mode coordinates Q_μ [202]. Despite this extra calculational work, the potential energy part has a simple form, which is no longer the case for the kinetic energy contribution to the RPH. Again, this splits up in a kinetic energy portion for the movement along the reaction path depending on the conjugate momentum p_s and an effective mass of the reaction complex $m_{eff}(s)$ and another part corresponding to the kinetic energy associated with the vibrational motions orthogonal to the path, which depends on $Q_\mu(s)$ and the conjugate momenta $P_\mu(s)$. The complex structure of the kinetic energy part results from the fact that it involves also coupling terms between vibrational motions as well as the coupling between the translational motion along the path and vibrational motions (see Fig. **9**). The magnitude of these couplings is given by mode-mode coupling coefficients (Coriolis coefficients) $B_{\mu,\nu}(s)$ and the curvature coupling coefficients $B_{\mu,s}(s)$: [115,202,205]

$$T[s,p_s,\{Q_\mu\},\{P_\mu\}] = \frac{1}{2}\frac{[p_s - \sum_\mu \sum_\upsilon^{N_{vib}-1} B_{\mu,\upsilon}(s) Q_\mu(s) P_\upsilon(s)]^2}{[1+\sum_\mu^{N_{vib}-1} B_{\mu,s}(s) Q_\mu(s)]^2} + \frac{1}{2}\sum_{\mu}^{N_{vib}-1} P_\mu^2(s) \tag{5.2}$$

where

$$B_{\mu,\upsilon}(s) = \mathbf{l}_\upsilon(s)^\dagger d\mathbf{l}_\mu(s)/ds = B_{\upsilon,\mu}(s) \tag{5.3}$$

$$B_{\mu,s}(s) = \mathbf{t}(s)^\dagger d\mathbf{l}_\upsilon(s)/ds = -\mathbf{l}_\mu(s)^\dagger d\mathbf{t}/ds = -\mathbf{l}_\mu(s)^\dagger \mathbf{k}(s) \tag{5.4}$$

($\mathbf{l}_\mu(s)$: mass-weighted generalized normal mode vector of mode μ at path point s; $\mathbf{t}(s)$: reaction path tangent vector at s giving the path direction; $\mathbf{k}(s)$ is the curvature vector at point s.) The numerator of the first part corresponds to a generalized momentum of the movement of the reaction complex along the path whereas the nominator corresponds to the effective mass of the reaction complex. The curvature coupling coefficients will be large if the reaction path is strongly curved (Fig. **9**, see also Eq. (5.4)) and this will have an impact on the effective mass $m_{eff}(s)$. Curvature is an essential feature of the reaction path, reflects the mechanism of a reaction, is associated with energy transfer and energy dissipation, and reveals at the same time limits of the RPH [115].

Summarizing, the RPH was developed to solve the dimensionality problem of calculating a N_{vib}-dimensional PES for N

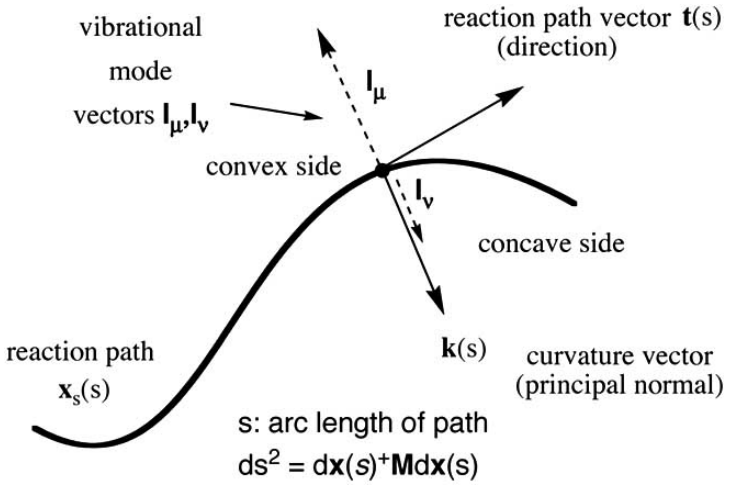

Fig. (9). Direction and curvature of the reaction path as given by the tangent vector **t**(s) and the curvature vector **k**(s). The normal mode vectors $\mathbf{l}_\mu$ are positioned in a plane perpendicular to the path direction. Large curvature couplings require that vectors $\mathbf{l}_\mu$ and **k**(s) are (anti)collinear and have large magnitudes.

≥ 4 and carrying out Newton dynamics (or quantum dynamics) for the reaction complex on this PES to obtain reaction rates and other dynamic reaction properties. The simplifications and assumptions used for the RPH include: 1) It is a classic Hamiltonian based on a reaction path where mostly the IRC path is used, i.e. the mass-weighted or mass-scaled steepest descent path. - 2) It is designed for reactions dominated by a single translational motion of the reaction complex. If this is not the case, a reaction surface Hamiltonian or even more complex Hamiltonians have to be used [115]. - 3) It is assumed that the vibrational motions orthogonal to the path can be described in the harmonic approximation, which is reasonable as the translational motion follows largely the IRC path. - 4) Vibrational adiabaticity is assumed, e.g. the $N_{vib}-1$ vibrations remain in the same adiabatic quantum state throughout the reaction, which for most reactions will be the state v = 0. This assumption is based on the fact that the movement of the reaction complex along the path is slow compared to the transverse vibrational motions. - 5) Rotations of the reaction complex are not considered and therefore a total angular momentum of zero is assumed. - 6) Vibrational eigenstates of modes possessing the same symmetry must not cross along the reaction path (avoided crossing theorem), which is a consequence of the use of an adiabatic Hamiltonian. (For a diabatic reaction path Hamiltonian, see Ref. [206]).

Especially, point 6) has to be fulfilled to determine curvature and Coriolis couplings correctly, which in turn determine mechanism and energy transfer. In this connection, it is useful to point out that the scalar curvature is closely related to the curvature coupling coefficients via Eq. (5.5):

$$K(s) = \| \mathbf{k}(s) \| = [\mathbf{k}^\dagger(s)\mathbf{k}(s)]^{1/2} = [\sum_{\mu}^{N_{vib}-1} B_{\mu,s}^2]^{1/2} \quad (5.5)$$

Curvature and curvature coupling constants are the primary tools used to analyze the mechanism of a chemical reaction and therefore they will be discussed in detail in Sections 5.2 and 5.6.

5.2. Reaction Path Curvature as a Prerequisite of a Chemical Reaction

The reaction path is a curved line in the N_{vib}-dimensional configuration space of the reaction complex. If we consider a reaction $AB+C \rightarrow A+BC$ in which the bond AB is broken and the new bond BC is formed, the configuration space of the reaction complex will be of dimension 3 for the non-linear case where however essential features of the chemical processes can be described in a 2-dimensional space spanned by the internal parameters r(AB) and r(BC) as done in Fig. (**10**). If the reaction path would not be curved, for example, by following the dashed line directly leading from the reactants in the upper left corner of the diagram of Fig. (**10**) to the products located in the lower right corner, the length r(AB) of the bond to be broken would be a linear function of r(BC), the length of the bond to be formed. Furthermore, this would imply that the forces acting in the processes of bond cleavage and bond formation depend linearly on the bond length r, which is a contradiction in itself because these forces are dominated by the Coulomb law and its 1/r-dependence. Hence, a straight, non-curved reaction path can be excluded.

A clear indication of the start of the bond breaking process is a lengthening of bond AB. Four different situations could be hypothetically distinguished (Fig. **10**): 1) Path 7-6-5-4-3-2-1 (path P1): The bond AB keeps its length until C has approached B so much that the value of the bond length BC is adopted. The bond switches from A to C and A moves away from the new molecule BC (increasing r(AB)). For path P1, the chemical processes of bond cleavage and bond formation would be catastrophic ones (an infinitesimally small change in the distance AB would lead from bonding to non-bonding) without gradually developing mutual polarization of the electron density of the reactants that prepares them for the chemical processes. Clearly, the catastrophic description is not correct and therefore a reaction path P1 suddenly changing its direction at the transition state (point 4) is not correct. In the same way, any sudden (catastrophic) change in the reaction path direction is hardly likely, unless the chemical processes are coupled to excitation, ionization or electron transfer processes. - 2) Path 7-6-5-S-E-3-2-1 (path P2): The catastrophic event of P1 is avoided by a smooth curving of the reaction path from S to E. The beginning of P2 curving at point S indicates the beginning of AB bond lengthening and thereby AB bond cleavage. The end of P2 curving at E indicates that the actual bond length BC will no longer change thus suggesting that the bond BC is finalized. Although a unique definition of chemical bonding is difficult, path P2 (as well as P3, P4, etc.) suggests a dynamic definition of chemical bonding based on the curvature of the reaction path: The curvature identifies

changes in the bond and thereby its cleavage or formation. This leaves two questions: a) When does the bond AB cease to exist (at M, E or any intermediate point)? - b) When is the new bond first formed? - Actually these two questions are of little relevance for the dynamic processes of the reaction. Investigation of the reaction complex in the path region S-M-E reveals that the reaction is initialized by a polarization of the density of bond AB leading to a gradual change in the bond properties. Similarly, the newly formed bond adjusts gradually to its equilibrium situation. Therefore, the path curvature increases first slowly from zero, adopts in the middle part close to M a curvature maximum, and then decreases to zero, which is reached close to E. Hence P2 is characterized by one curvature peak. Such a situation is found in degenerate bond processes where the bond cleaved and the bond formed are of the same type as in the reaction $AB+A \rightarrow A+BA$. The curvature peak will be high (low) and its width small (large) if bond AB is strong (weak) and the polarizing power of B is small (large). The situation becomes more complex when one considers that a strong, highly polar bond is difficult to polarize whereas a strong nonpolar multiple bond can easily be polarized. This should also influence magnitude and shape of the path curvature. Hence, the curvature contains detailed information on the chemical processes, but it has to be unraveled.

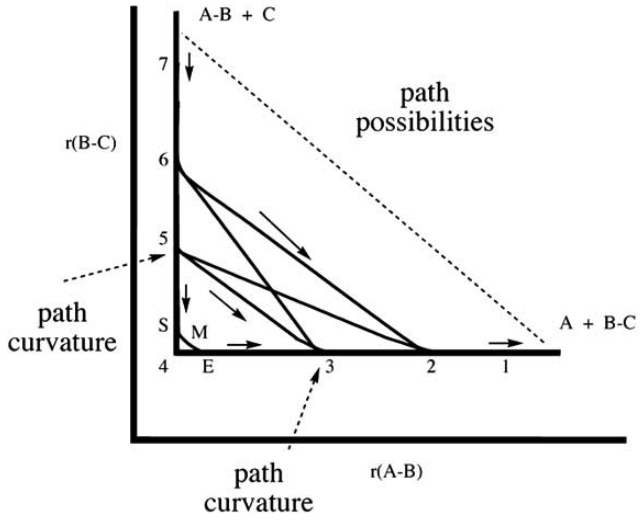

Fig. (10). Schematic representation of different reaction paths with different curvatures for the reaction $AB+C \rightarrow A+BC$ shown in the 2-dimensional space spanned by distances r(AB) and r(BC) (see text). Arrows indicate the direction of movement of the reaction complex.

3) Path 7-6-5-2-1 (path P3): In the general case of C being unequal to A and the bonds AB and BC being different with regard to both strength and polarizability, a path such as P3 may result. The reaction path curvature at point 5 will be larger than that at point 2 if bond AB is stronger and less well to polarize than bond BC and C has a lower polarizing power than A. Between points 5 and 2 the path curvature is likely to adopt smaller values or may vanish totally so that two rather than just one curvature peak result, the first for the cleavage of bond AB and the second for the formation of BC. The curvature of the reaction path will give more specific information on the nature of the reactants if it becomes possible to eliminate one or two of the contributing effects (bond strength, bond polarizability, polarizing power) by investigating a series of BX bonds for varying X and constant B all being attacked by the same atom A to form the bond AB and cleaving the bond BX (for example substitution reactions $A^- + CR_3X \rightarrow ACR_3 + X^-$). For path P3'(7-6-3-2-1), the situation of P3 is reverted and an equivalent description holds. - 4) Paths 7-6-5-3-2-1 and 7-6-2-1 (symmetric paths P4 and P5). These paths have equal curvature in the AB cleaving (points 5 or 6) and BC forming process (points 3 or 2). Although such cases cannot be excluded, identical curvatures are rare for bonds AB and BC (reaction partners C and A) being different. However, the space between the curvature areas, being for P5 larger than for P4, gives further insight into the chemical processes in so far as this also reflects lability (stability) of the bonds involved. In this connection, it must not be overlooked that the length of the IRC path depends on the number N of reaction complex atoms and their masses in the way that an increase in N and/or the atomic mass lengthen the path (because of mass-weighting) and thereby also the region between the locations of path curvature.

The region of the path curvature locations is the location of the chemical processes. This however does not imply that the curvature region is necessarily the region of the energy transition state. For P2 (path of a degenerate reaction), the transition state will be located on the diagonal r(AB) = r(BC), which will also be the position of the curvature maximum. For P3 or P3', however the location of the transition state can be anywhere between or at the curvature locations or even outside this range. There are possibilities to relate the position of the energy transition state to the shape and position of the curvature peaks [115, 117].

Physical Meaning of the Reaction Path Curvature

The observations made with regard to the reaction path curvature and schematically shown in Fig. (**10**) can be generalized: A chemical reaction that is a result of at least two chemical processes (bond cleavage and bond formation) requires a curving of the corresponding reaction path. An exclusively straight reaction path with zero curvature indicates a physical rather than chemical process. All vibrational motions of the reaction complex in a physical system are conserved and consequently both Coriolis and curvature couplings are nil. Only slight variations in the electronic structure of the reaction complex may take place because of van der Waals interactions or interactions with an electromagnetic field. A chemical reaction requires that at least one bond stretching motion vanishes and a new one appears. For the reaction AB+C→A+BC, the force constant k_a(AB)(s) (alternatively $[\omega_a(AB)(s)]^2$ decreases to zero whereas the force constant k_a(BC)(s) (alternatively $[\omega_a(BC)(s)]^2$ increases from zero to its equilibrium value. Hence, one might conclude that curvature reflects the change in the sum of the force constants, which however is not the case. In Fig. (**11**), the vibrational frequencies of the reaction $CH_3+H_2 \rightarrow CH_4+H$ are given in dependence of s. The bond AB corresponds here to the HH bond, which is broken to form the new bond CH (corresponding to bond BC). The vibrational modes change their character along the reaction path, especially at the avoided crossing AC1, AC2, and AC3 (Fig. **11**). For example, mode 11 corresponds in the entrance channel to the HH stretching vibration. At point AC1, this role is taken over by mode 8 and finally at point AC2, HH stretching becomes a translational motion. From AC2 on, mode 8 adopts the character of a CH stretching mode, which switches at AC3 to mode 11. Fig. (**11**) indicates that close to the positions of curvature peaks K2 and K3 (indicated by the vertical lines, top half of figure), there are inflection points of frequency functions ω(HH)(s) and ω(CH)(s), which means that ω'(HH)(s) and ω'(CH)(s) adopt maximal values. Hence, the largest changes in the stretching

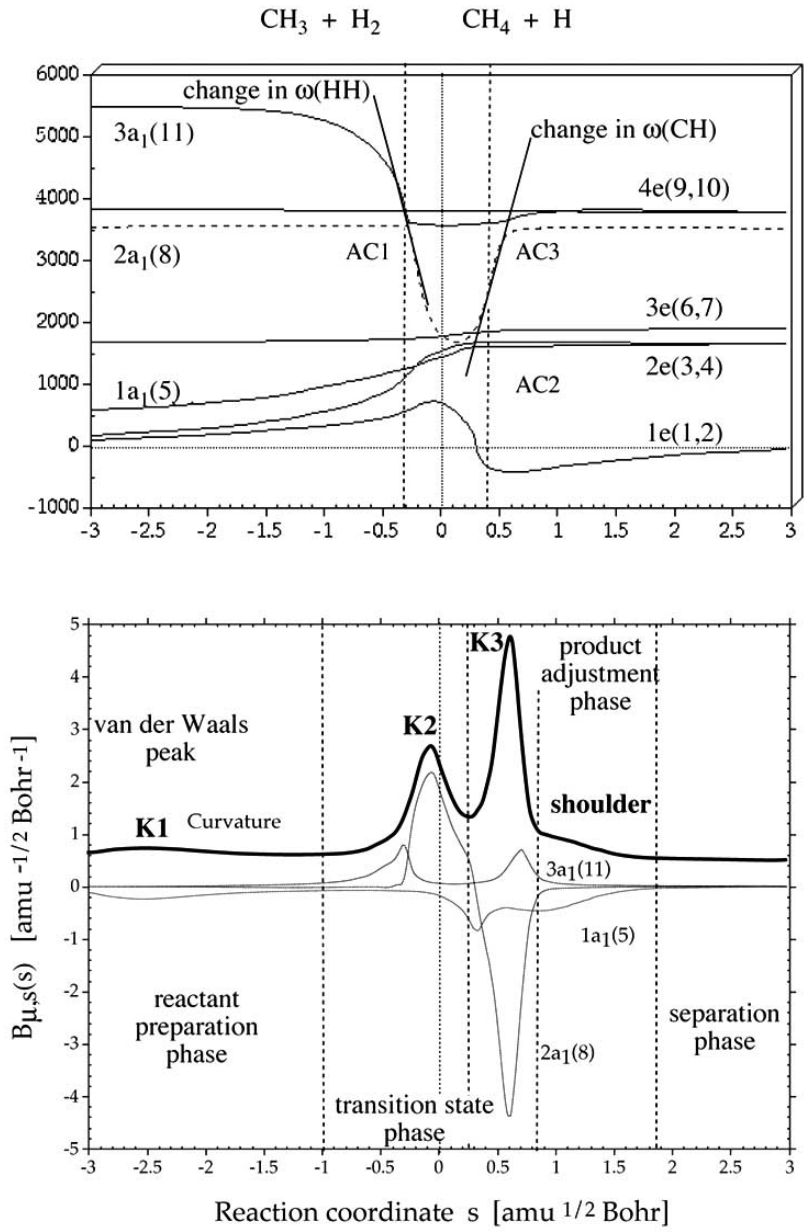

Fig. (11). Top: Variation of the HH (first mode 11; at AC1 mode 8) and CH stretching frequency (from AC2 on mode 8; at AC3 mode 11) in the reaction $CH_3+H_2 \rightarrow CH_4+H$. The slope of $\omega(HH)(s)$ and $\omega(CH)(s)$ is given at the inflection points close to s = -0.3 and 0.4 amu$^{1/2}$ Bohr. Bottom: Curvature diagram (bold line) with curvature peaks K1, K2, and K3. Curvature coupling coefficients are indicated by dashed lines. Reaction phases are separated by vertical dashed lines. Symmetry of vibrational modes are given. The energy transition state is located at s = 0 amu$^{1/2}$ Bohr [117].

vibrations of breaking and forming bond are responsible for the curvature maxima.

As is shown in Fig. (**11**) for the reaction $CH_3+H_2 \rightarrow CH_4+H$, the curvature is related to the change in the vibrational frequencies rather than their magnitude or the difference of the magnitudes. Frequency $\omega(HH)$ decreases slower than $\omega(CH)$ increases and this can be directly related to the fact that curvature peak K2 associated with the breaking of the HH bond is smaller and broader than curvature peak K3 associated with the formation of the CH bond. Since the force constant is directly related to the frequency and has the advantage of being mass independent, it is advantageous to use AICoM stretching force constants of cleaving bond AB and forming bond BC to describe the path curvature. Again, the change in the force constant in dependence of the path parameter s, i.e. the first derivatives $dk_a(AB)(s)/ds=k_a'(AB)(s)$ and $dk_a(BC)(s)/ds=k_a'(BC)(s)$ determines any path curving. Exact relationships can be obtained by starting from the definition of the curvature in terms of first and send derivatives of the energy with regard to internal coordinates and then solving for the force constants. In this way, it can be shown that there is a direct relationship between scalar curvature and the sum of the first derivatives, k'(AB)(s) + k'(BC)(s).

In the general case of a reaction $AB+C \rightarrow A+BC$, the maximal changes in the stretching force constants for cleaving bond AB and forming bond BC are most likely to occur at different positions of the reaction path, which means that two rather than just one curvature peak are found (see also Fig. **10**). For the purpose of

understanding this situation, its is important to provide further reasoning why the change in rather than the magnitude of the force constant determine the curving of the reaction path. The derivative k'(s) reflects the polarizability of a bond, which itself depends on the polarizing power of the attacking reactant. This confirms the essence of the discussion in connection with the path situations shown in Fig. (**10**): The shape of the curvature peaks (see bottom of Fig. **11**) reflects the ease by which the bond is broken by an agent: A broader smaller peak indicates a smooth cleaving of the bond starting early whereas a large narrow curvature peak has to be associated with a rapid bond cleavage starting after some sudden short-range polarization of the bond. Clearly, the magnitude of the curvature peaks does not exclusively relate to the strength of the bond. It is important to note in this connection that in the case of a polyatomic reaction complex bond cleavage may lead to geometry relaxation effects in other parts of the reaction complex and these changes may add to the path curvature. These contributions can become large when electronic effects such as bond conjugation causing strong geometry adjustments play a role. In turn, there are situations where just partial bond breakage, for example in the course of π-bond cleavage leaving at the same time the σ-bond intact, leads to smaller curvature enhancements. These details can be unraveled with the help of the curvature-coupling coefficients also shown in Fig. (**11**).

The CH bond in CH_4 possesses a bond dissociation energy D_e of 110.9 kcal/mol, which is of similar magnitude as that of H_2 (D_e = 109.2 kcal/mol) [207,208]. Since bond dissociation energies include also the stabilization energies of the dissociation products, it is better to refer to the adiabatic stretching force constants, which are 5.75 and 4.90 mdyne/Å for H_2 and CH stretching in CH_4, respectively. These values reflect the fact that the bond energy of the CH bond in methane is just 99 kcal/mol compared to the bond dissociation enthalpy of H_2 being 104.8 kcal/mol. The longitudinal static dipole polarizability α of the HH bond is 0.80 $Å^3$ and by this larger as the corresponding value of the somewhat polar CH bond in methane (α = 0.65 $Å^3$ [209]. Apart from this, the methyl radical with its anisotropic charge distribution at the C atom has a much stronger polarizing power than the H atom does. Accordingly, the polarization of the HH bond by $\dot{C}H_3$ starts earlier (at a larger distance between the reactants) and proceeds easier than the polarization of a CH bond in methane by a H atom. The H atom has to approach the CH bond much closer before polarization starts and the latter is followed directly by bond rupture so that these two electronic events take place in a relatively short part of the reaction path. Hence, the curvature is larger and the scalar curvature maximum K3 clearly exceeds that of K2 by 80% (Fig. **11**) Despite the fact that the HH bond is stronger (as clearly reflected by the AICoM force constants), the change in k(HH) close to curvature peak K2 is slower than that of k(CH) at K3, which is confirmed by Fig (**11**) (see tangent of the curve $\omega(HH)(s)$ as compared to that of curve $\omega(CH)(s)$. This confirms that the bond strength is not the decisive factor for bond cleavage. Bond polarizability and polarizing power of attacking agents have a strong impact on k'(AB)(s), which in turn determines (together with k'(BC)(s)) the path curvature.

Since each curvature peak is associated with a specific chemical process, it is useful to partition the reaction path in different phases using the curvature peaks (or other important features of K(s)). The minimum of the curvature between two peaks (corresponding to minimal chemical activity) indicates the transition from one reaction phase to the next. Each phase is characterized by one curvature peak or curvature enhancements. In this way, 6 phases can be recognized for the reaction $CH_3+H_2 \rightarrow CH_4+H$ as will be discussed in Section 5.6

5.3. Energy and Force Analysis

Changes of the energy of the reaction complex in dependence of the path parameter s determine the energetics of the reaction. The maximum of E(s) at the transition state (corresponding to a first order saddle point on the PES), is usually taken as distinct point that provides information of the reaction mechanism. Despite of common chemical thinking, in most cases the chemical processes do not take place at the transition state. If the preparation of the reaction complex requires much energy, the energy transition state is positioned on the reaction path before the location of the actual chemical processes. For example, in the case of the Diels-Alder reaction, equalization of single and double bonds and the associated distortion of the reaction complex requires about 23 kcal/mol and thereby determines the reaction barrier [125]. The formation of the new CC bonds leading to the cyclic structure of cyclohexene happens 56 kcal/mol downhill from the transition state, far out in the exit channel, shortly before the product is formed.

Use of the Term Transition State

It is appropriate to point out the various uses of the term "transition state." According to transition state theory and general chemical understanding, [210] a transition state corresponds to the highest energy point of the reaction path, which connects reactant and product minimum. Alternatively, one can consider enthalpy or Gibbs energy changes along the reaction path and define the transition state location as that corresponding to the highest enthalpy or Gibbs energy along the path. In view of the fact that neither energy nor enthalpy reveal mechanistic details, it has become customary to speak in connection with the reaction mechanism of a transition state region as that reaction phase in which the chemical processes of bond breaking and forming take place [115,117,119-124]. This is in line with the use of the term in *transition state spectroscopy*, which is a part of femtosecond spectroscopy [211-213]. Laser spectroscopists define the transition state as the full set of transient configurations which are traversed by the reaction complex in entrance and exit channel between reactants and products. Transition state spectroscopy exploits the fact that the electronic processes, which accompany bond breaking and bond formation are parallel to substantial changes in the internuclear separation. If one assumes that the atoms move during a chemical reaction by about 10 Å and if one further assumes that they move with a speed of 10^4 - 10^5 cm/s, then a period of about 10 ps will be sufficient to observe transition state configurations. Hence, femtosecond spectroscopy can detect transient reaction complex configurations along the reaction path and observe even path bifurcations. There are different approaches to obtain information about transition state configurations. Since the transition state is spectroscopically seen an unbound state, its absorption spectrum will be most meaningful if an electronic transition takes place into a bound state. An alternative way of getting information is the 'clocking' of transition states. Utilizing ultrashort laser pulses one is able to define a zero of time and follow the elementary dynamics of a chemical reaction [214]. Laser spectroscopy may even invoke vibrationally driven reactions, which includes both enhancement of reaction rates (see Section 5.6), manipulation of energy disposal and promotion of a certain product channel by mode selective excitation [214]. All the information gained by these approaches refer to a loose definition of the transition state region somewhere between reactants and products.

This use of the term is different from what is meant by *energy transition state* in transition state theory (first order saddle point of E) and *transition state region or phase* in mechanistic theory (region, in which the chemical processes of bond formation and cleavage take place as indicated by the corresponding curvature peaks).

Analysis of the Reaction Force

Terms such as *transition state zone* (zone between the IFPs before and after the energy transition state [157,158]) are based on the trends in the reaction force $F(s) = -dE(s)/ds$ and the changes in the reaction force along the path as reflected by the curvature of $E(s)$, $d^2E(s)/ds^2$. At the IFP of E(s) before (after) the transition state, the reaction force F(s) adopts a minimum (maximum) and its changes vanish (curvature of E(s) is zero). In the case of an elementary reaction with transition state, Toro-Labbe [157,158] partitions the reaction path in four zones (Fig. **12**) where these zones have no obvious connection with the reaction phases based on the path curvature. (It has to be noted that more than two IFPs appear along the reaction path of an elementary reaction with

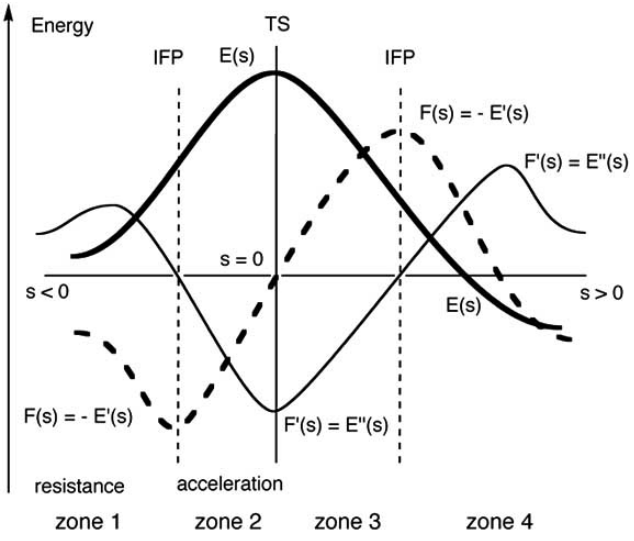

Fig. (12). Partitioning of the energy profile along the path of an elementary reaction with transition state (TS) into zones utilizing the reaction force F(s) = - E'(s). The reaction path parameter s (arc length) is set to zero at the transition state; s ≤0: entrance channel; s ≥0: exit channel; IFP: inflection point of E(s) with F(s) being extremal and F'(s) = E''(s) = 0. Reaction zones according to Ref. [157] (see text). Functions E(s), F(s), and F'(s) are not drawn to scale.

barrier when E(s) possesses shoulders). In zone 1 (reactant zone), the reaction complex "resists" any deformation caused by the chemical reaction. The retarding force (F(s) <0) becomes increasingly negative toward the IFP and then increases until it reaches a zero value at the transition state. This is reflected by the fact that in the reactant zone more energy as predicted from the reaction force is needed to move the reaction complex from path point s to path point $s+ds$: $\Delta E(s)=E(s+ds)- E(s)>E(s)+F(s)ds$. The additional energy is related to the curvature $d^2E(s)/ds^2$ which, increasing from a minimum value, achieves a maximum before the IFP and is exactly zero at the IFP (Fig. **12**). After the IFP, deformations of the reaction complex are "accelerated" because less energy, as predicted from the reaction force F(s), is needed to move the reaction complex from s to s+ds: $\Delta E(s)=E(s+ds)-E(s)<E(s)+F(s)ds$. The retarding force decreases and becomes zero at the transition state. Tentatively, one might relate the IFP with the position of spin decoupling in a simple bond dissociation reaction (Section 4.2) since the required force for driving the reaction becomes smaller after the spin decoupling occurs. However, this assumption does not hold in most reactions since the transition state region is not necessarily the region where the chemical processes take place. In the reactions investigated so far, the chemical processes often start before the energy IFP is reached and in the exit channel they end after zone 4 (product zone, Fig. **12**) has been entered, i.e. the relevant curvature regions (chemical processes) can be located before and after the two IFPs. We conclude that an E-based dissection of the mechanism into reaction zones misses mechanistic details. The energy is a cumulative quantity that absorbs all energy changes caused by geometry deformations and electronic structure adjustment of the reaction complex and accordingly, often disguises mechanistically relevant features such as bond breaking or forming.

Internal Coordinate Forces

It is more useful to monitor internal coordinate forces exerted on parts of the reaction complex such as bonds or functional groups along the reaction path rather than analyzing a collective reaction force F(s). The internal coordinate forces can be repulsive or attractive thus indicating whether the reaction complex resists or accepts a given structural change. Those forces, which are associated with internal coordinates dominating the path direction are especially interesting because they reveal which structural changes are responsible for what energy increase (decrease) along the reaction path [115,117,119-121]. There is also the possibility of relating changes in the forces to changes in the electron density distribution of the reaction complex (see Section 5.5).

5.4. Geometry Analysis

The most direct and detailed description of the reaction should be provided by the changes of the internal coordinates of the reaction complex. In Fig. (**13**) this is shown for the reaction $CH_3+H_2 \rightarrow CH_4+H$. In general, there are N_{vib} internal coordinates $q(s)$, i.e. in the case of the CH_3+H_2 reaction 12 coordinates that because of C_{3v}-symmetry of the reaction complex reduce to just 4: the HH distance R1, the CH distance R2, the bond length R3 of the CH spectator bonds (not involved in the reaction), and the $H_sC\ldots H$ angle β (alternatively, the H_sCH_s angle γ can be taken). The bond length R3 does not substantially change along the path and can be ignored because it is associated with the three CH spectator bonds of the methyl group. The changes in the geometry of the reaction complex caused by the chemical processes are described by just three parameters: R1, R2, and angle β (Fig. **13**). These internal coordinates reveal characteristic changes along the reaction path as indicated by arrows and associated with features of the scalar curvature shown in Fig. (**11**). There is an obvious relationship between the path curvature K(s) and changes in the q(s) functions, which can also be determined via the curvature $d^2q(s)/ds^2$. There are large curvature values for R1 at s = - 0.1 amu$^{1/2}$ Bohr and for R2 at s = 0.6 amu$^{1/2}$ Bohr, which are exactly the positions of the curvature peaks K2 and K3 (Fig. **11**). Therefore, one could argue that a mechanistic analysis of a chemical reaction is best carried out by studying the changes of all q(s) along the reaction path. Several problems prevent this possibility: i) The number of internal coordinates q(s) becomes prohibitively large for larger N. For example, in the case of the Diels-Alder reaction, N = 16 and N_{vib} = 42 [119]. ii) With increasing N, it is no longer possible to predict which internal coordinates are most important at what s-values for

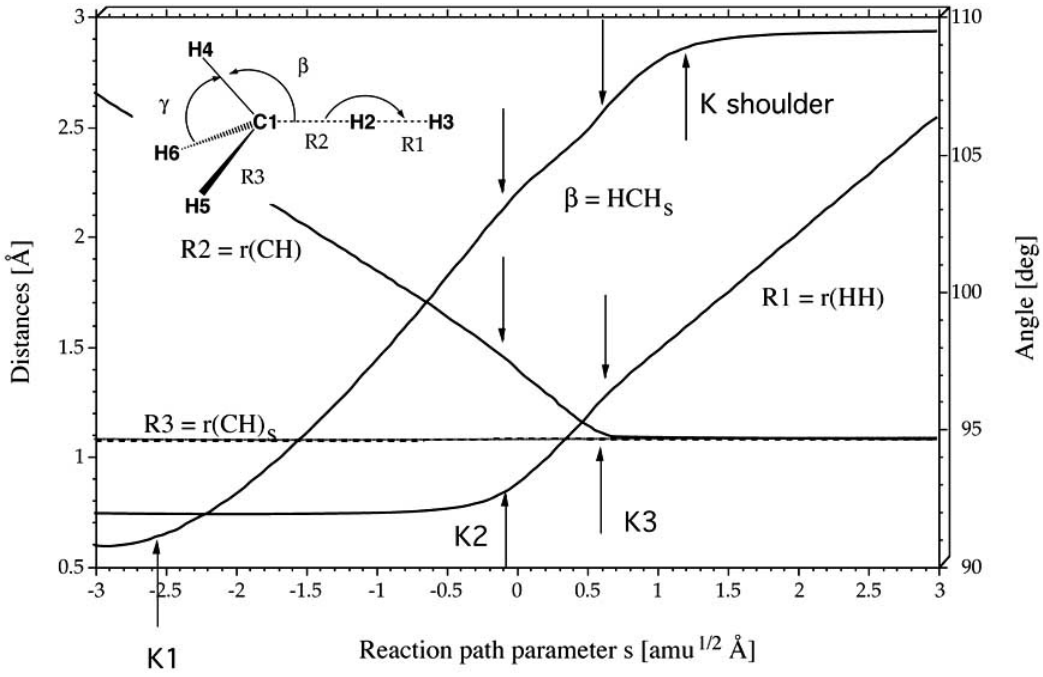

Fig. (13). Changes in the internal coordinates q(s) of the reaction complex of the reaction $CH_3+H_2 \rightarrow CH_4+H$ as a function of the path parameter *s* [117]. Curvature in the function q(s) is indicated by an arrow and relates to the curvature peaks K1, K2, and K3 as well as the shoulder behind K3 (see Fig. 11). Subscript s denotes a spectator atom or bond.

the description of the chemical processes. iii) Which changes in the internal coordinates are significant? For example there is a significant change in the curvature of R2(s) at s = - 0.1 amu$^{1/2}$ Bohr (upper arrow in Fig. **13**) that is difficult to see and to analyze because of its small magnitude. - In view of i) - iii), it is difficult to assess the importance of the changes in all q(n) along the path and to relate them to electronic structure changes and mechanistic detail. Also, there are different sets of $\{q_n(s)\}$ possible for the description of the reaction complex. A priori, it is not clear, which of those sets is the most suitable one. Also, different coordinate sets may be needed to appropriately describe entrance and the exit channel. For the purpose of avoiding all these difficulties, a procedure has been worked out that identifies those internal coordinates, which describe the chemical processes and thereby the reaction mechanism in a meaningful way (see section 5.7).

5.5. Electron Density Analysis

A direct insight into the changes in the electronic structure of the reaction complex during the reaction is provided by the electron density distribution. This can be obtained by analyzing the total electron density distribution $\rho(\mathbf{r})$ with the help of the topological or viral analysis, [131,150] difference density distributions $\Delta\rho(\mathbf{r})$, [115,117] Laplace concentrations of the electron density distribution, $-\nabla^2\rho(\mathbf{r})$ [120] population densities such as the Natural Bond Orbital (NBO) populations and Natural Atomic Orbital (NAO) populations [123,215], electron localization functions [216-218], or pair population densities [219,220]. The density analysis can be supplemented by pictorial representations of density changes along the reaction path [117,120]. Since the MED paths provide images of the bond paths within an electron density model of the chemical bond (Section 3.3) they can be used to follow the breaking of a chemical bond [132]. Cremer and Kraka have established necessary and sufficient conditions for covalent bonding by referring to the existence of a bond critical point (first order saddle point of the $\rho(\mathbf{r})$ of the MED path and a negative (stabilizing) energy density $H(\mathbf{r})$ at this point. Bond path and bond critical point vanish in the course of a bond cleavage process catastrophically (infinitesimally small change in bond length leads to vanishing of bond critical point) [132]. In most cases, the location of the density catastrophe along the reaction path does not coincide with that of the energy transition state but with the region of large path curvature caused by the bond cleavage. Future work has to show how the topological and virial analysis of the reaction complex can complement, detail, or confirm results of the URVA analysis.

Analysis of Difference Electron Density Distributions

Difference electron density distributions taken for the reaction complex along the reaction path and represented in form of contour line diagrams provide a sensitive visual tool of assessing the degree of reactant density or, more specifically, bond density polarization preceding bond cleavage. The difference density distribution is defined by

$$\Delta\rho(\mathbf{r},s) = \rho(\mathbf{r},s)[reaction\ complex] - \rho(\mathbf{r},s)[reference\ complex] \quad (5.6)$$

where the choice of an appropriate reference density distribution of a reference complex is difficult to make. In case of the $CH_3 + H_2$ reaction, the reference density was chosen as the average $0.5*\{\rho(\mathbf{r},s)[CH_3] + \rho(\mathbf{r},s)[H_2] + \rho(\mathbf{r},s)[CH_4] + \rho(\mathbf{r},s)[H]\}$ calculated for the noninteracting molecular subunits at the geometries they adopt within the reaction complex at point *s*. Taking snapshots of the difference density distribution in entrance and exit channel, the gradual polarization of the electron density distribution of the reaction complex could by demonstrated [117]. Clearly, such an approach cannot be generalized because the reference complex is not uniquely defined in this way. It suffers from the disadvantage that the reaction complex and the parts of the reference complex have to be calculated with different methods, which makes

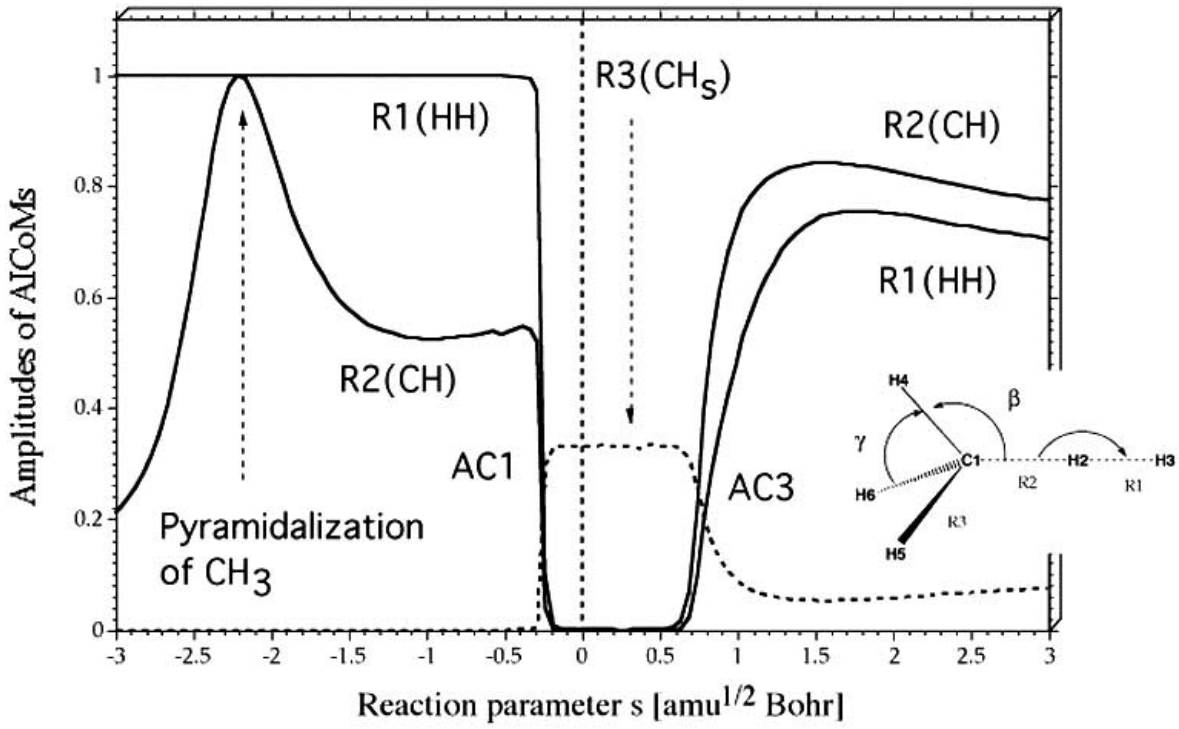

Fig. (14). Decomposition of vibrational mode 11($3a_1$) of the reaction complex of CH_3+H_2→CH_4+H in terms of AICoMs given as a function of the path parameter *s* [117]. AC: avoided crossing points; see Fig. (**11**). CH_s denotes the spectator bonds.

calculated difference densities method-dependent and contaminated by incompatible contributions. Also, if the same reaction complex geometry is used for molecular situations with little distortions (e.g., early in the entrance channel for CH_3···H_2) and at the same time for molecular situations with strong distortion (H_4C···H), calculational problems aggravate or even prevent the determination of a difference density. However, Cremer and co-workers [45] have offered an alternative approach of calculating difference densities in the case of an adiabatic mode, which can be easily generalized for the motion along the reaction path.

Analysis of Orbital Populations

Orbital population analyses have been used to study chemical reactions since decades, however their usefulness has to be questioned in view of the arbitrary nature of most of the original population analysis methods. NAO and NBO analyses are nowadays widely accepted since they are based on mature quantum chemical concepts (with the limitation that they favor Lewis structures where non-classical structures are more appropriate [15]). Therefore, NBO values have been calculated to document the electronic structure of the reaction complex in different reaction phases. For example, Cremer and co-workers [123] showed that in case of the methylene addition to ethene calculated NBO charges help to visualize the different phases of the reaction. - *Electron Localization functions (ELF)* basins [216] have also been utilized to distinguish between reaction domains as domains with different numbers or types of ELF basins. For example, Santos and co-workers [217] showed that the ELF analysis of the acetylene trimerization leads to five different domains describing 1) closed-shell repulsion between acetylene moieties, 2) deformation of the reactants under the impact of increasing repulsion, 3) preparation of the reaction complex for CC bond formation 4) simultaneous (concerted) formation of the CC σ-bonds, and finally 5) development of π-aromaticity. There has also been a successful attempt to combine the ELF analysis with Bader's virial partitioning of the electron density into atomic basins in the case of transition metal complexes [218] with the far-reaching goal of getting more detailed density descriptions for chemical reactions. - Ponec [219,220] has applied a pair population analysis to study electron reorganisation in the course of pericyclic reactions. Symmetry-allowed reactions could be described as a simple cyclic shift of electron pair bonds whereas symmetry-forbidden reactions imply complex changes in electron structure.

5.6. Analysis of Vibrational Motions

Monitoring the vibrational frequencies of the reaction complex along the reaction path (Fig. **11**, top) provides already insight into essential features of the reaction mechanism. In the case of the CH_3+H_2 reaction, the path regions where the chemical processes take place can be identified. Also, the splitting of the reaction valley is indicated by the fact that the frequencies of the 1e vibrational mode becomes imaginary (indicated in Fig. (**11**) by a negative value of ω (1*e*)). More details of the form and the partitioning of the reaction valley into phases are difficult to assess directly from the vibrational modes and their frequencies. Additional information however can be obtained by a more advanced analysis involving 4 steps: i) Decomposition of normal modes into AICoMs; ii) Analysis of curvature in terms of normal mode curvature couplings; iii) Analysis of mode-mode coupling; iv) Analysis of curvature in terms of adiabatic mode curvature couplings.

Decomposition of Normal Modes into Adiabatic Modes

Each vibrational mode is decomposed into AICoMs driven by the internal coordinates q(n) of the reaction complex. This is done in Fig. (**14**) where vibrational mode 11($3a_1$) is decomposed into the 4 AICoMs of the reaction complex {CH_3…H_2}, of which only R1(HH), R2(CH), and R3(CH_s) contribute. Mode 11 abruptly

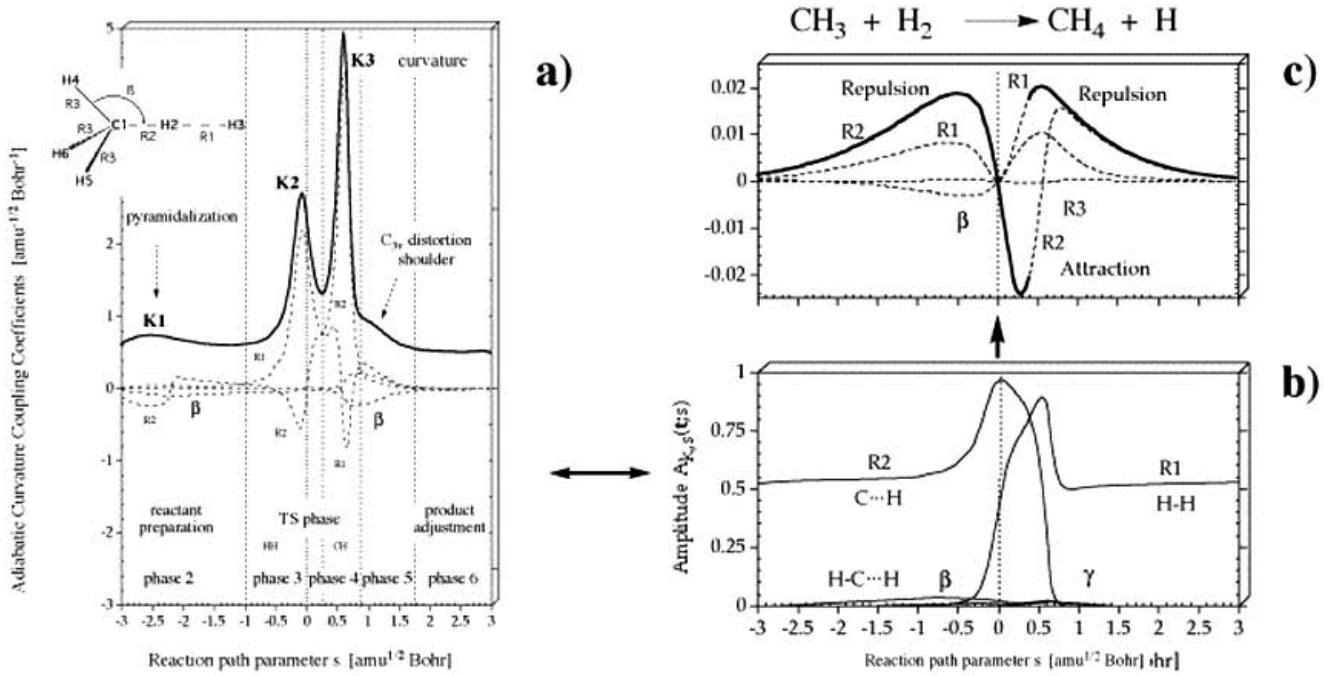

Fig. (15). a) Decomposition of the scalar curvature (bold line) into adiabatic curvature coupling coefficients (dashed lines) for the reaction $CH_3+H_2 \rightarrow CH_4+H$. Vertical lines indicate the borders of 5 of the 6 reaction phases. The vertical dashed line at s = 0 amu$^{1/2}$ Bohr denotes the position of the energy transition state. - b) Decomposition of the reaction path direction given by vector **t**(s) into adiabatic internal coordinate contributions. - c) Repulsive and attractive internal coordinate forces exerted on the atoms of the reaction complex. Bold lines indicate forces for which the associated internal coordinate dominates the direction of the reaction path.

changes its character at the avoided crossing points AC1 and AC3 (see Fig. **11**). It starts as a HH stretching vibration, becomes at AC1 the CH stretching vibration of the three CH spectator bonds, and then changes again at AC3 to become the CH stretching mode of the new CH bond of CH_4 mixed with HH stretching of the dissociating van der Waals complex $CH_4 \cdots H$. The CH/HH stretching admixture in mode 11 is a direct consequence of the linear C_{3v}-symmetrical $H_3C \cdots H \cdots H$ arrangement. Any movement of the central H triggers a CH and HH stretching motion. Interesting is the admixture of CH stretching to the HH stretching mode at s = -2.5 amu$^{1/2}$ Bohr. This is the position of curvature peak K1 and without analyzing the curvature at this path position it is difficult to rationalize this CH-AICoM admixture on common chemical understanding (see below).

Analysis of the Path Curvature in terms of Normal Mode Curvature Couplings

Each curvature peak or enhancement is decomposed into curvature coupling coefficients $B_{\mu,s}(s)$ given in terms of normal vibrational modes of the reaction complex. This is shown in Fig. (**11**) (bottom) and is the basis of the Laser-spectroscopic technique of *mode-selective rate enhancement* [221]. It exploits the fact that energy can be pumped at the beginning of a reaction into vibrational modes that couple with the translational motion of the reaction complex along the reaction path. A priori it is difficult to predict which of the vibrational modes are suitable for this purpose. Symmetry arguments can be used to exclude all those vibrational modes that do not comply with the symmetry of the translational mode vector, i.e. that of the reaction complex. Common chemical sense can also help to identify those modes that should influence the rate of a chemical reaction. However, all common chemical sense will not help if Coriolis coupling leads to a dissipation of vibrational energy before an energy transfer into the translational motion and thereby rate enhancement can take place. Accordingly, it is appropriate to combine analysis ii) with analysis iii), i.e. the analysis of the coupling between different vibrational modes in terms of the Coriolis coupling coefficients $B_{\mu,\nu}(s)$.

Analysis of Coriolis Couplings

The calculation of curvature and Coriolis coupling constants provides the only predictive analytical approach to the question of mode selective rate enhancement. A number of combined computational and spectroscopic investigations have gone this way: In the reaction of CH_3 with H_2 it has been demonstrated (Fig. **11**, bottom) that the a_1-symmetrical CH stretching mode of CH_3 (mode 8) couples strongly with the translational mode shortly before the energy transition state [117]. Despite of this fact it is advantageous to pump energy into mode 11, which undergoes an efficient Coriolis coupling with mode 8 at AC1 so that via curvature coupling the Laser energy is selectively channeled into the translational motion thereby enhancing the rate of reaction [117]. - Riedel and co-workers [222] reported on a reactive scattering experiment of Cl atoms with mode-selected, vibrationally selected dideutero-methane. They found that the vibrational excitation of either the symmetric or antisymmetric CH_2 stretching mode leads to a nearly identical enhancement factor in total reactivity, which again is a result of Coriolis coupling and energy dissipation. Throughout the reaction $Cl+CH_2D_2 \rightarrow HCl+CHD_2$ the reaction complex should conserve C_s-symmetry (collinear $Cl \cdots H-C$ configuration). Ab initio calculations reveal that there is a strong curvature coupling involving the symmetric C-H stretching mode whereas the asymmetric C-H stretching mode is of *b* symmetry and therefore cannot couple directly to the translational motion of the reaction complex. However, energy which is pumped into the

asymmetric stretching mode can wind up in the symmetric stretching mode and by this in the translational motion via an effective Coriolis coupling between the two modes, which is possible due to the twisting of the vibrational mode vectors around the path direction according to Eq. 5.4 (scalar product between mode vector and derivative of another mode vector) and the resulting mutual overlap despite of different starting symmetries. - Similar observations were made by Duncan and co-workers [223] who discussed ab initio dynamics studies of thermal and vibrational-state selected rates of the H abstraction reaction $CH_4+Cl\rightarrow CH_3+HCl$. - Liu and co-workers [224] showed in a dynamics study of the reaction $CH+H_2\rightarrow CH_2+H$ that vibrational excitation of the HH stretching mode leads to notable enhancement of reaction rates whereas excitation of the CH stretching mode is insignificant. This is reflected by a large HH stretching curvature coupling coefficient in the entrance channel of the reaction. - Formic acid decomposes via competing reactions to either H_2O+CO (1) or H_2+CO_2 (2). The measured reaction rate for path (2) is smaller by a factor of 40 than that for path (1) despite the fact that the calculated activation energies are comparable for both paths. Takahashi and co-workers used calculated curvature and Coriolis coupling coefficients to derive a rationale for these findings [225]. Both paths possess a comparable curvature pattern in the entrance channel. However, the Coriolis couplings are more pronounced in case of path (2), thus supporting energy dissipation rather than energy transfer into the translational motion, which consequently reduces the reaction rate of (2) compared to that of (1). It seems that mode selective enhancement of reaction rates does not only take place in the gas phase but also in surface chemistry as the HCD_3 decomposition to HCD_2+D on bulk nickel in heterolytic catalysis indicates [226]. - Analyses ii) and iii) lead to an understanding of the energy flow along the reaction path as it is reflected by processes of energy transfer and energy dissipation. They also provide the basis to determine the translational energies left with the products of a reaction.

Analysis of the Path Curvature in Terms of Adiabatic Mode Curvature Couplings

The decomposition of the curvature peaks (enhancements) in terms of curvature coupling coefficients is repeated, but now in terms of localized AICoMs rather than delocalized normal vibrational modes ($A_{m,s}(s)$ rather than $B_{\mu,s}(s)$ is analyzed). In Fig. (**15**), the scalar curvature K(s) is decomposed in terms of AICoM-curvature coupling coefficients. Curvature peaks K2 and K3 are associated with the HH stretching and the CH stretching modes, respectively where positive coefficients indicate that the local vibrational motion in question supports the curving of the reaction path and in this way the chemical reaction whereas negative coupling coefficients indicate that the corresponding vibrational motion resists the curving of the path. The maxima and minima of the AICoM coupling coefficients are located where the functions q(s) possess their maximal curving as reflected by the extremal values of $d^2q(s)/ds^2$ (Fig. **13**). For example, angle $\beta(HCH_s)$ determines the position of curvature peak K1 because at this point van der Waals interactions between methyl radical and hydrogen molecule cause the former to change from a planar to a pyramidal form (increase of β from 90° to larger values; alternatively changes in the angle $\gamma=H_sCH_s$ can be connected with K1). Pyramidalization couples with the R2 approach motion and therefore K1 is also effected by a R2 curvature coupling. This finally explains the R2 contribution to mode 11 at the position of K1 (see Fig. **14**). The HH vibration is at a certain contact distance R2 no longer free and starts involving th CH_3 radical so that a CH vibration mixes in with the HH vibration (Fig. **13**).

Curvature peak K2 is a consequence of the change in parameter R1(HH) (Fig. **13**) that via adiabatic curvature coupling $A_{R1,s}$ is responsible for the strong curving of the path. Local mode R2(CH) resists the curving of the path ($A_{R2,s}<0$, Fig. **15**, see also Fig. **13**)), which results from the exchange repulsion between the methyl radical and the hydrogen molecule. For curvature peak K3, the situation is reversed: Now the AICoM associated with R2(CH) couples with the path motion because a curving of the function R2(s) (Fig. **13**) dominates the path curvature. The AICoM driven by R1 resists this path curving, which has to do with exchange repulsion between CH_4 and H atom in the reverse reaction. When the process of CH bond formation is finalized, the C_{3v}-symmetrical reaction complex with angles $\beta<109.47^\circ$ adjusts to the tetrahedral angle of CH_4, which leads to the shoulder in the curvature diagram (Fig. **15**, see also Fig. **13**).

The adiabatic curvature coupling coefficients relate any change in the path curvature K(s) to a structural change of the reaction complex and by this to the electronic events driving the reaction. In this way, they provide the physical background to the partitioning of the reaction mechanism into reaction phases. It becomes possible to identify the positions of minimal path curving with structures of the reaction complex that are chemically meaningful. In the case of the reaction CH_3+H_2, there are six phases (Fig. **15**: phase 1: contact phase, not shown in Fig. (**15**); phase 2: reactant preparation phase; specifically pyramidalization and HH bond polarization phase; phase 3 + phase 4: transition state phase with the chemical processes (phase 3: HH bond loosening and initialization of CH bonding; phase 4: finalization of CH bond formation and HH bond cleavage); phase 5: product adjustment phase, especially adjustment from C_{3v}- to T_d-symmetry; phase 6: separation phase. Between the phases, at positions of low curvature (not necessarily a curvature minimum; see transition from phase 4 to phase 5), three chemically relevant transient structures can be identified: 1) van der Waals complex between pyramidal CH_3 and polarized H_2; 2) nonclassical $\bullet CH_5$ radical with 3-center 3-electron $C\cdots H\cdots H$ interaction; 3) van der Waals complex between CH_4 and H atom. By identifying the 6 reaction phases and the 3 transient structures, the reaction mechanism is established.

5.7. From Reaction Complex to Reaction Path: Strategy of an URVA Analysis

The analysis of the reaction mechanism based on URVA utilizes the close relationship between reaction complex and reaction path to overcome dimensionality problems and the problem of quantitatively identifying among the multitude of geometrical parameters the few that drive important structural or electronic changes of the reaction complex [115-124]. The analysis of 3N-L geometry parameters q(s) in the way indicated in Fig. (**13**) and the identification of those changes in q(s), which are relevant for the reaction mechanism, becomes tedious and ambiguous. URVA solves these problems by a shift in the analysis from reaction complex to reaction path as indicated in Fig. (**16**). The changes in the geometry of the reaction complex during the reaction are manifested in the form of the reaction path, which is also defined in 3N-6 dimensional space and on first sight does not seem to offer any advantages for the mechanistic analysis. However, the reaction path can be considered as a smooth, curved line, which is fully characterized by just three rather than 3N-L quantities at each path point s. These are the path direction given by the tangent

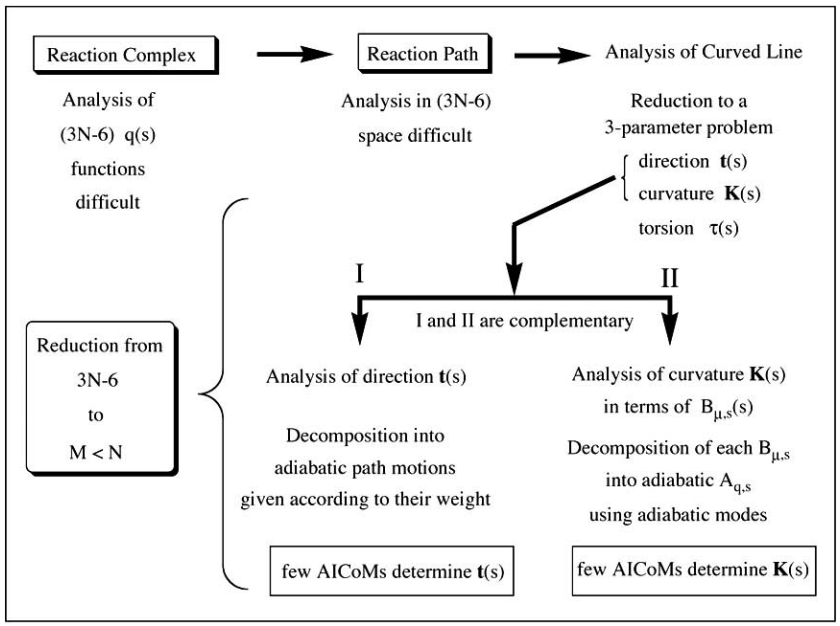

Fig. (16). Analysis scheme of URVA. The reaction path is analyzed in terms of path direction and path curvature to reduce the N_{vib}-dimensional problem of analyzing the reaction complex to a M-dimensional problem (M < N) with the help of adiabatic vibrational modes and adiabatic curvature coupling coefficients.

vector **t**(s), the path curvature given by the curvature vector **k**(s), and the path torsion given by τ(*s*). The latter parameter is of little relevance because helical or loop-type paths have not been observed. Hence, it is sufficient to analyze just path direction and path curvature as a function of *s* (Fig. **16**).

In Figs. (**9** and **16**), it is schematically shown that tangent vector and curvature vector describe complementary properties of the reaction path. URVA decomposes the translational motion in path direction and the vibrational motions orthogonal to the path direction into adiabatic modes driven by internal coordinates that are used to describe the reaction complex. Accordingly, if there is an internal coordinate *q* that dominates the path direction it will provide only a small or no contribution to the transverse vibrational modes of the reaction complex and vice versa. Therefore, there are two ways of analyzing the reaction mechanism: i) via the path direction; ii) via the path curvature. Since the latter is much more sensitive and physically related to the changes in the adiabatic force constants (i.e. the first derivative of k_a(s) with regard to *s*), which in turn measures the polarizability of a bond, URVA is primarily based on the analysis of the path curvature and uses the path direction only to obtain complementary information. By analyzing the curvature in terms of adiabatic curvature coupling coefficients a connection to the changes in the geometry of the reaction complex is made because the internal coordinates q(s) that drive the adiabatic modes with large curvature coupling coefficients determine in this way also the curvature. Use of the adiabatic curvature coupling coefficients has the advantage of i) singling out those few internal coordinates q(s) that reflect important structure changes of the reaction complex and ii) also identifying q(s) changes that are not detectable in a diagram such as that of Fig. (**13**). Normal mode curvature and Coriolis coupling coefficient are used to determine energy transfer and energy dissipation whereas adiabatic curvature coupling coefficients provide the basis to elucidate the reaction mechanism.

Fig. (**15b**) contains a diagram with the amplitudes of the adiabatic modes dominating the direction of the reaction path. In phase 2, where AICoM R1 dominates the curvature, AICoM R2 does the same with regard to the path direction whereas in phase 3 the situation is reverted. Once it is clear which internal coordinates dominate the path direction, one can calculate the corresponding internal coordinate forces (Fig. (**15c**): bold lines). They can be interpreted using changes in the electron density distribution and atomic population values. The sum of all forces leads to the reaction force discussed in connection with Fig. (**12**).

6. CONCLUSIONS AND OUTLOOK

Vibrational spectroscopy provides a wealth of data that helps to describe bonding, structure, and stability of molecules in their equilibrium as well as in the situation of a chemical reaction. Utilizing the Vib-Cal-X method as one of the Cal-X methods one can use measured vibrational frequencies and derive from them a complete set of normal mode force constants and their normal mode eigenvectors. With the help of the adiabatic mode concept it is possible to derive from the normal modes local modes that are associated with the internal coordinates describing the molecule in question. The AICoMs are based on a dynamic principle and possess properties such as frequency, mass, and force constant. It is the advantage of the Vib-Cal-X approach that in this way experimental frequencies can be directly used for the determination of AICoM bond stretching frequencies and force constants. Contrary to bond length, bond density, and bond dissociation energy, which all depend on two or more molecular quantities, the bond stretching force constant is the only quantity that directly relates to the intrinsic strength of a bond and therefore provides a useful starting point for defining bond order or intrinsic bond dissociation energies.

The information contents of the molecular vibrations can be also exploited when studying a reacting molecule. The vibrations of a reaction complex span the reaction valley, determine its shape, the

curving of the floor line of the valley, bi- or trifurcations of the valley, and the conversion of a local vibrational movement into a translational motion along the reaction path. Any reaction if properly triggered starts with a vibration of increasing amplitude. Since normal mode vibrations are delocalized, the analysis and understanding of their properties require also for the reaction complex a decomposition into local AICoMs. It has been shown in this article that chemical reactions that involve at least two chemical processes imply a curving of the reaction path. Paths without curvature describe physical rather than chemical processes. The path curvature is related to the change in the force constants of the cleaving and forming bonds as reflected by the derivatives $k_a'(s)$. The derivative of the force constant reflects both the polarizability of the changing bond and the polarizing power of the reaction partner. Since the peaks of the scalar curvature K(s) correspond to the chemical processes, their number and sequence determines the number and sequence of chemical events. From the magnitude and shape of a curvature peak, one can draw conclusions with regard to bond strength, polarizability, and reaction partner. Due to the chemical importance of the path curvature, the curvature diagram K(s) can be used for the partitioning of a reaction into reaction phases. For an elementary reaction with transition state, van der Waals or contact phase, reactant preparation phase, transition state phase, product adjustment phase, and separation phase can be distinguished. Attempts to obtain a similar mechanistic partitioning with the help of the reaction force are limited by the fact that the energy is a cumulative quantity that does not enable one to distinguish between individual chemical events. This is possible in the case of the scalar curvature because the latter can be expressed with the help of the curvature coupling coefficients, which in turn can be related to AICoMs and adiabatic curvature coupling coefficients driven by the internal coordinates used to describe the geometry of the reaction complex. Hence, by shifting the analysis from the reaction complex to the reaction path, describing the latter by path direction and path curvature, and decomposing them into adiabatic contributions, each of which is driven by an internal coordinate, a complicated N_{vib}-dimensional problem is reduced to a much simpler M-dimensional problem (M < N). This is the essence of the URVA mechanistic analysis (Fig. **16**).

A number of reaction systems have been studied so far utilizing URVA and the insight provided by the vibrations of the reaction complex [115-124]. Important outcomes of these studies concern the dynamic definition of a chemical bond, the partitioning of the reactions into reaction phases, and many other aspects of chemical reactions. Noteworthy are the following findings.

1) In a study of HX and XX (X: halogen) cycloaddition reactions to CC double bonds [120] the role of van der Waals complexes was illuminated: They determine via exchange, dispersion, inductive, and electrostatic forces the first electronic structure changes in the reaction complex. Especially, van der Waals interactions can determine the steric arrangement of the reaction partners which is often kept throughout the reaction. In these cases, it is justified to say that the van der Waals complex determines the fate of the reaction complex for the whole reaction. The URVA analysis reveals furthermore that even without the formation of a stable van der Waals complex any van der Waals interactions can be detected and their consequences for the chemical changes of the reaction complex determined. - 2) In larger reaction systems, the breaking of a bond can involve several individual steps such as charge transfer or bond polarization, rehybridization at the atomic centers involved, conformational changes, π-bond shifts, etc. All these changes can be identified with the help of the local vibrational modes and their coupling with the curvature vector. Especially, it is possible to determine the degree of (a)synchronicity of coupled bond breaking and forming processes [117,121,123]. - 3) Energy transition state and transition state region, i.e. the region where the chemical processes take place are not necessarily related. The preparation of a reaction complex for the actual chemical processes can require so much energy that it leads to the highest point of energy along the reaction path. The chemical processes take place in such a situation down hill long after the energy transition state. An example for such a discrepancy between energy transition state and transition state region is the Diels-Alder reaction [119]. - 4) The partitioning of the reaction mechanism into reaction phases unravels similarities between seemingly different reaction types that were so far not known. For example, the cycloaddition of HX (X = halogen) to CC multiple bonds resembles in the first part of the mechanism a substitution reaction and in the second part a simple ion combination reaction. This can be used for an advanced classification of elementary chemical reactions [120]. - 5) The shape and magnitude of the calculated curvature peaks provide direct insight into the ease of breaking or forming a chemical bond. It is possible to determine the interplay between the strength of a bond being changed and the bond polarizing ability of a reaction partner. Future work is aimed at setting up quantitative relationships so that the outcome of chemical reactions becomes predictable and controllable. - 6) By studying the avoided vibrational crossings of the reaction complex along the reaction path it becomes possible to make qualitative predictions with regard to energy dissipation (between vibrational modes) and energy transfer (between vibrational and translational motions). In this way, mechanistic predictions with regard to mode-selective rate enhancement can be made even in non-trivial cases [117]. In many cases, the possibility of rate enhancement is lost as a consequence of energy dissipation between vibrational modes. A detailed understanding of the reaction mechanism makes it possible to change the reaction complex in such a way (isotope substitution, substituent variation, etc.) that energy transfer is suppressed because of extended energy dissipation.

Previous work with URVA has focused on two major mechanistic topics: i) To understand the dynamic reality of the Woodward-Hoffmann rules and to unravel the mechanistic differences between symmetry-allowed and symmetry-forbidden reactions [119-121]. Results obtained so far clearly show that forbidden reactions involve the drastic change of just a few bonds of a reaction complex leaving all other structural parameters largely unaffected. Symmetry-allowed reactions mostly possess a preparation phase in which many structural parameters collectively and smoothly change to some degree. This requires some energy, however not as much as would be required for the drastic change of just a few parameters in a symmetry-forbidden reaction. In the latter case, there are additional reaction phases that develop into distinct reaction steps as soon as environmental factors lead to the generation of an intermediate and a second transition state. ii) These observations have led to the *concept of hidden transition states and intermediates* [120,123]. By partitioning the reaction mechanism into reaction phases with the help of the path curvature one can identify transient structures of the reaction complex in regions of minimal curvature that relate to real structures in form of radicals or

biradicals, carbenes or ions, nonclassical structures with 3-center bonds, transition state similar structures, etc. It has been shown that by changing the reaction environment (temperature, pressure, solvent) or by introducing stabilizing factors such as substituents, rings, hetero atoms or units with electron-delocalization possibilities the transient structures can become real intermediates and real transition states. Therefore the terms hidden intermediates and hidden transition states have been coined. It was shown for the strongly exothermic barrierless chelotropic cycloaddition of methylene to ethene yielding cyclopropane that its mechanism comprises four reaction phases, two hidden intermediates and one hidden transition state, which by variation of the methylene (either by substituent variation or by exchange of the central atom) can be converted into real intermediates and real transition state. The investigation further suggested that by the mechanistic description of a prototypical reaction the mechanism of other chelotropic carbene (silylene, etc.) additions can be reliably predicted [123]. Clearly, the identification of hidden intermediates and hidden transition states is a step forward to both the understanding and controlling of chemical reaction mechanism.

There is a broad spectrum of possible applications for both the Vib-Cal-X approach and URVA analysis of chemical reactions. A systematic application of the former approach will lead to a more comprehensive understanding of chemical bonding that will provide detailed scales of bond strength as reflected by adiabatic force constants and bond orders and intrinsic bond dissociation energies derived therefrom. It will be possible to assess the various facets of weak bonding reaching from 3-electron situations to H-bonding, agostic bonds, and noncovalent interactions in general. It will be challenging to establish bond order relationships that can be applied throughout a chemical reaction thus offering simple parameters that measure the degree to which a chemical process has been developed and that help to compare transient structures of different or the same reaction. With such a tool at hand, it will be also possible to design bonds of extreme strength where especially transition metal combinations are suitable candidates for high bond energies. It will be another challenge to determine intrinsic bond dissociation energies and fragment stabilisation energies to complement the description of chemical bonding. - So far the URVA analysis has provided advanced insight into chemical reaction mechanism. However, there is still a long way to go to detail all factors that influence the sequence of reaction steps, mutations of the reaction complex, energetics, stereochemistry, and the environmental dependence of a chemical reaction. Primary goal of the current work is i) to exploit the informational content of vibrational spectra using Vib-Cal-X and ii) the understanding of enzymatic reactions and chemical catalysis in general. By fulfilling these goals it will be possible to control chemical reactions and to design effective chemical catalysts.

ACKNOWLEDGMENT

This work was financially supported by the National Science Foundation, Grant CHE 071893. We thank SMU for providing computational resources. Proofreading and useful comments by Robert Kalescky are acknowledged.

REFERENCES

[1] Schleyer, P. v. R.; Allinger, N. L.; Clark, T.; Gasteiger, J.; Kollman, P. A.; Schaefer III, H. F.; Schreiner, P. R.; Eds. *Encyclopedia of Computational Chemistry*; Wiley: Chichester, UK, **1998**.

[2] Hehre, W.J.; Radom, L.; Schleyer, P.v.R.; Pople, J.A. *Ab Initio Molecular Orbital Theory*, Wiley: New York, **1986**.

[3] Comparison of Ab Initio Quantum Chemistry with Experiment for Small Molecules. The State of the Art, Bartlett, R. J. Ed.; D. Reidel Publishing Company: Dordrecht, **1985**.

[4] Cremer, D.; Reichel, F.; Kraka, E. Homotropenylium cation: structure, stability, and magnetic properties. *J. Am. Chem. Soc.*, **1991**, *113*, 9459-9466.

[5] Cremer, D.; Olsson, L.; Reichel, F.; Kraka, E. Calculation of NMR chemical shifts - the third dimension of quantum chemistry. *Israel J. Chem.*, **1993**, *33*, 369-385.

[6] Ottosson, C.-H.; Kraka, E.; Cremer, D. Theory as a Viable Partner for Experiment - the Quest for Trivalent Silylium Ions in Solution; in Theoretical and Computational Chemistry, *Pauling's Legacy - Modern Modelling of the Chemical Bonding*; Maksic, Z., Ed., Elsevier, Amsterdam, **1999**, Vol. *6*, pp. 231-301.

[7] Childs, R.F. The homotropylium ion and homoaromaticity. *Acc. Chem. Res.*, **1984**, *17*, 347-352.

[8] Childs, R.F.; Faggiani, R.; Lock, C.J.L.; Mahendran, M. Structure of 1-ethoxyhomotropylium hexachloroantimonate: a nonaromatic homotropylium cation. *J. Am. Chem. Soc.*, **1986**, *108*, 3613-3617.

[9] Childs, R. F.; Varadarajan, A.; Lock, C.J.L.; Faggiani, R.; Fyfe, C. A.; Wasylishen, R.E. Structure of the 2-hydroxyhomotropylium cation. unequivocal evidence for homoaromatic delocalization. *J. Am. Chem. Soc.*, **1982**, 2452-2456.

[10] Haddon, R.C. Regioselectivity of the (ethoxycarbonyl)nitrene insertion reaction on monochloro- and dichloroalkanes and cycloalkanes. *J. Org. Chem.*, **1979**, *44*, 3608-3616.

[11] Haddon, R.C. Homotropenylium cation revisited: POAV and 3D-HMO analysis. *J. Am. Chem. Soc.*, **1988**, *110*, 1108-1112.

[12] Kutzelnigg, W. Theories of magnetic susceptibilities and NMR chemical shifts in terms of localized quantities. *Israel J. Chem.*, **1980**, *19*, 193-201.

[13] Schindler, M.; Kutzelnigg, W. Theory of magnetic susceptibilities and NMR chemical shifts in terms of localized quantities. II. Application to some simple molecules. *J. Chem. Phys.*, **1982**, *76*, 1919-1934.

[14] Kutzelnigg, W.; Schindler, M.; Fleicher, U. in *NMR, Basic Principles and Progress*, Diehl. P. Ed.; Springer, Berlin: **1991**, Vol. *23*, pp. 165-181.

[15] Cremer, D.; Childs, R.F.; Kraka, E. Cyclopropyl Homoconjugation, Homoaromaticity And Homoantiaromaticity - Theoretical Aspects and Analysis; in *The Chemistry of Functional Groups, the Chemistry of the Cyclopropyl Group.*, Rappaport, Z., Ed., John Wiley: New York, **1995**, Vol. *2*, pp. 339-410.

[16] Mitzel, N.W.; Losehand, U.; Wu, A.; Cremer, D.; Rankin, D.W.H. (N,N-dimethylaminoxy)trifluorosilane: Strong, dipole moment driven changes in the molecular geometry studied by experiment and theory in solid, gas, and solution phases. *J. Am. Chem. Soc.*, **2000**, *122*, 4471-4482.

[17] Olsson, L.; Cremer, D. Evidence for the existence of silylium cations in condensed phases. *Chem. Phys. Lett.*, **1993**, *215*, 413-443.

[18] Arshadi, M.; Johnels, D.; Edlund, U.; Ottosson, C.-H.; Cremer, D. Solvated silylium cations: structure determination by nmr spectroscopy and the nmr/ab initio/iglo method. *J. Am. Chem. Soc.*, **1996**, *118*, 5120-5131.

[19] Ottosson, C.-H.; Cremer, D. Nature of the $Si(SiMe_3)^{3+}$ cation in aromatic solvents. *Organometallics*, **1996**, *15*, 5495-5501.

[20] Ottosson, C.-H.; Szabo, K.; Cremer, D. The tris(9-borabicyclo[3.3.1] nonyl-silylium cation: A suggestion for a weakly coordinated silylium cation in solution. *Organometallics*, **1997**, *16*, 2377-2385.

[21] Olsson, L.; Ottosson, C.-H.; Cremer, D. Properties of R_3SiX compounds and R_3Si^+ ions: do silylium ions exist in solution? *J. Am. Chem. Soc.*, **1995**, *117*, 7460-7479.

[22] Bühl, M.; Schleyer, P. v. R. in *Electron Deficient Boron and Carbon Clusters*., Olah, G.A.; Wade, K.; Williams, R.E., Eds., Wiley: New York, **1991**.

[23] Bühl, M.; Hommes, N.J.R.; Schleyer, P.v.R.; Fleicher, U.; Kutzelnigg, W. Applications and evaluations of IGLO (individual gauge for localized orbitals) chemical shift calculations for organolithium compounds. *J. Am. Chem. Soc.*, **1991**, *113*, 2459-2465.

[24] Bühl, M.; Steinke, T.; Schleyer. P.v.R.; Boese, R. Solvation effects on geometry and chemical shifts. an ab initio/iglo reconciliation of apparent experimental inconsistencies on H_3BNH_3. *Angew. Chem. Int. Ed. Eng.*, **1991**, *30*, 1160-1161.

[25] Kraka, E.; Sosa, C.; Gräfenstein, J.; Ottosson, C.-H.; Cremer, D. Dimesitylketone O-oxide: verification of an unusually stable carbonyl oxide by nmr chemical shift calculations. *Chem. Phys. Lett.*, **1996**, *260*, 43-50.

[26] Pople, J.A.; Raghavachari, K; Trucks, G.W.; Pople, J.A.; Head-Gordon, M. A fifth-order perturbation comparison of electron correlation theories. *Chem. Phys. Lett.*, **1989**, *157*, 479-483.

[27] Wilson, E. B.; Decius, J. C.; Cross. P. C. *Molecular Vibrations: The Theory of Infrared and Raman Spectra*. McGraw-Hill: New York, **1980**.

[28] Califano, S. *Vibrating States,* Wiley: New York, **1976**.

[29] Chalmers, J. M.; Griffiths, P. R., Ed.; *Handbook of Vibrational Spectroscopy*, Wiley: New York, **2002**.

[30] Meier, R. J. Vibrational spectroscopy: a vanishing discipline? *Chem. Soc. Rev.*, **2005**, *34*, 743-752.

[31] Andrew, L.; Moskovits, M.; Ed.; *Chemistry and Physics of Matrix-Isolated Species*; North-Holland: Amsterdam, **1989**.

[32] Sander, W.; Exner, M.; Winkler, M.; Balster, A.; Hjerpe, A.; Kraka, E.; Cremer, D. Vibrational spectrum of m-benzyne: A matrix isolation and computational study. *J. Am. Chem. Soc.*, **2002**, *124*, 13072-13079.

[33] Marquardt, R.; Sander, W.; Kraka, E. 1,3-Didehydrobenzene (meta-benzyne). *Angew. Chem.*, **1996**, *108*, 825-828.

[34] Bucher, G.; Sander, W.; Kraka, E.; Cremer, D. 2,4-Didehydrophenol - first proof of a meta-Aryne by IR spectroscopy. *Angew. Chem. Int. Ed. Engl.*, **1992**, *31*, 1230-1233.

[35] Sander, W.; Bucher, G.; Wandel, H.; Kraka, E.; Cremer, D.; Sheldrick, W. S. Photochemistry of p-Benzoquinone diazide carboxylic acids: formation of 2,4- didehydrophenols. *J. Am. Chem. Soc.*, **1997**, *119*, 10660-10672.

[36] Kraka, E.; Cremer, D.; Bucher, G.; Wandel, H.; Sander, W. A CCSD(T) and DFT investigation of m-benzyne and 4-hydroxy-m-benzyne. *Chem. Phys. Lett.*, **1997**, *268*, 313-320.

[37] Marquardt, R.; Balster, A.; Sander, W.; Kraka, E.; Cremer, D.; Radziszewski, J. G. 1,4-Didehydrobenzol. *Angew. Chem.*, **1998**, *110* , 1001-1005.

[38] Sander, W.; Wandel, H.; Bucher, G.; Gräfenstein, J.; Kraka, E.; Cremer. D. Alpha,3-didehydro-5-methyl-6-hydroxytoluene - matrix isolation of a biradical related to the neocarzinostatin chromophore. *J. Am. Chem. Soc.*, **1998**, *120*, 8480-8485.

[39] Wrobel, R.; Sander, W.; Cremer, D.; Kraka, E. Photochemistry of butatriene – spectroscopic evidence for the existence of allenylcarbene. *J. Phys. Chem. A*, **2000**, *104*, 3819-3815.

[40] Trommer, M.; Sander, W.; Ottosson, C.-H.; Cremer, Reaction of 1,1-dimethylsilene with formaldehyde. *Angew. Chem. Int. Ed. Engl.*, **1995**, *34*, 929-931.

[41] Sander, W.; Block, K.; Kappert, W.; Kirschfeld, A.; Muthusamy, S.; Schroeder, K.; Sosa, C. P.; Kraka, E.; Cremer, D. Dimesitylketone O-oxide: spectroscopic characterization, conformation, and reaction modes: OH formation and OH capture. *J. Am. Chem. Soc.*, **2001**, *123*, 2618.

[42] Sander, W.; Schroeder, K.; Muthusamy, S.; Kirschfeld, A.; Kappert, W.; Boese, R.; Kraka, E.; Sosa, C. P.; Cremer, D. Dimesityldioxirane. *J. Am. Chem. Soc.*, **1997**, *119*, 7265-7270.

[43] Wierlacher, S.; Sander, W.; Marquardt, C.; Kraka, E.; Cremer, D. Propinal O-Oxide. *Chem. Phys. Lett.*, **1994**, *222*, 319-324.

[44] Larsson J. A.; Cremer. D.; Theoretical verification and extension of the McKean relationship between bond lengths and stretching frequencies. *J. Mol. Struct.*, **1999**, *485*, 385-407.

[45] Cremer, D.; Wu, A.; Larsson, J. A.; Kraka. E. Some thoughts about bond energies, bond lengths, and force constants. *J. Mol. Model.*, **2000**, *6*, 396-412.

[46] Christen, D.; Coudert, L. H.; Larsson, J. A.; Cremer, D. The rotational-torsional spectrum of the g'Gg conformer of ethylene glycol: elucidation of an unusual tunneling path. *J. Mol. Spectrosc.*, **2001**, *205*, 185-196.

[47] Oomens, J.; Kraka, E.; Nguyen, M. K.; Morton, T. H. Structure, vibrational spectra, and unimolecular dissociation of gaseous 1-fluoro-1-phenethyl cations. *J. Phys. Chem.*, **2008**, *112*, 10774-10783.

[48] Kraka. E.; Cremer, D. Characterization of CF bonds with multiple-bond character: bond lengths, stretching force constants, and bond dissociation energies. *Chem. Phys. Chem.*, **2009**, *10*, 686-698.

[49] Kraka, E.; Larsson, J. A.; Cremer, D. Generalization of the Badger Rule Based on the Use of Adiabatic Vibrational Modes. in *Computational IR Spectroscopy*, Grunenberg, J., Ed.; Wiley: New York, **2010**, in press.

[50] Konkoli Z.; Cremer D. A new way of analyzing vibrational spectra i. derivation of adiabatic internal modes. *Int. J. Quant*, bf **1998**, *11*, 1-9.

[51] Konkoli Z.; Larsson, J. A.; Cremer D. A new way of analyzing vibrational spectra ii. comparison of internal mode frequencies. *Int. J. Quant.*, **1998**, *11*, 11-27.

[52] Konkoli Z.; Cremer D. A new way of analyzing vibrational spectra iii. characterization of normal vibrational modes in terms of internal vibrational modes. *Int. J. Quant.*, **1998**, *11*, 29-40.

[53] Konkoli Z.; Larsson, J. A.; Cremer D. A new way of analyzing vibrational spectra iv. application and testing of adiabatic modes within the concept of the characterization of normal modes. *Int. J. Quant.*, **1998**, *11*, 41-55.

[54] Cremer, D.; Larsson, J. A.; Kraka, E. New Developments in the Analysis of Vibrational Spectra: on the Use of Adiabatic Internal, Vibrational Modes, in *Theoretical and Computational Chemistry, Theoretical Organic Chemistry*; Parkanyi, C., Ed; Elsevier: Amsterdam, **1998**, Vol. *5*, pp. 259-327.

[55] As expressed in Zerbi, G.; Siesler H. W.; Noda, I.; Tasumi, M; Krimm, S. *Modern Polymer Spectroscopy*, Wiley: New York, **1999**, "For unfortunate reasons the success of vibrational infrared and Raman spectroscopy in industrial and university laboratories seems to fade quickly in favor of other physical techniques which aim at chemical and structural diagnosis of unknown samples".

[56] Carbonniere, P.; Barone, V. Performances of different density functionals in the computation of vibrational spectra beyond the harmonic approximation. *Chem. Phys. Lett.*, **2004**, *399*, 226-229.

[57] Barone, V. Vibrational spectra of large molecules by density functional computations beyond the harmonic approximation: the case of pyrrole and furan. *Chem. Phys. Lett.*, **2004**, *383*, 528-532.

[58] Barone, V.; Festa, G.; Grandi, A.; Rega, N.; Sanna, N. Accurate vibrational spectra of large molecules by density functional computations beyond the harmonic approximation: the case of uracil and 2-thiouracil. *Chem. Phys. Lett.*, **2004**, *388*, 279-283.

[59] Wathelet, V.; Champagne, B.; Moseley, D. H.; Andre, J.-M.; Massida, S. Vibrational frequencies of diatomic molecules from Car and Parrinello molecular dynamics. *Chem. Phys. Lett.*, **1997**, *275*, 506-512.

[60] Margi, P.; Schwarz, K.; Blöchl, P. E. Finite-temperature characterization of ferrocene from first-principles molecular dynamics simulations. *J. Chem. Phys.*, **1994**, *100*, 8194-8203.

[61] Fontaine-Vive, F.; Johnson, M. R.; Kearly, G. J.; Howard, J. A. K.; Parker, S. F. How phonons govern the behavior of short, strong hydrogen bonds in urea phosphoric acid. *J. Am. Chem. Soc.*, **2006**, *128*, 2963-2969.

[62] Meier R.J. Calculating the vibrational spectra of molecules: An introduction for experimentalists with contemporary examples. *Vib. Spectrosc.*, **2007**, *43*, 26-37.

[63] Larsson, J.A.A. *Direct Assessment of Properties of the Chemical Bond Utilizing Vibrational Spectroscopy - a Quantum Mechanical Investigation*. Doctor Thesis, Department of Chemistry, University of Göteborg, Sweden, **1999**.

[64] Vijay, A.; Sathyanarayana, D.N. Structures of 4-phenylcyclohexa[e] [1,3]oxazine-4H-2(3H)-thione and 2-chlorophenyl-4H-4-phenylcyclopenta[e][1,3] oxazine: an X-ray study. *J. Mol. Struct.*, **1994**, it 328, 269-276.

[65] Pulay, P.; Fogarasi, G.; Pongor, G.; Boggs, J.E.; Vargha, A. Combination of theoretical ab initio and experimental information to obtain reliable harmonic force constants. Scaled quantum mechanical (SQM) force fields for glyoxal, acrolein, butadiene, formaldehyde, and ethylene. *J. Am. Chem. Soc.*, **1983**, *105*, 7037-7047.

[66] Baker, J.; Jarzecki, A.A.; Pulay, P. Direct scaling of primitive valence force constants: An alternative approach to scaled quantum mechanical force fields. *J. Phys. Chem. A*, **1998**, *102*, 1412-1421.

[67] Scott, A.P.; Radom, L. Harmonic vibrational frequencies: An evaluation of hartree-fock, moller-plesset, quadratic configuration interaction, density functional theory, and semiempirical factors. *J. Phys. Chem.*, **1996**, *100*, 16502-16513.

[68] Borowski, P.; Gömez-Fernändez, M.; Fernändez-Liencres, M.-P.; Ruiz, T.P. An effective scaling frequency factor method for scaling of harmonic vibrational frequencies: theory and preliminary application to toluene. *Chem. Phys. Lett.*, **2007**, *446*, 191-198.

[69] Borowski, P.; Gomez-Fernandez, M.; Fernandez-Liencres, M.-P.; Ruiz, T.P.; Rincön, M.Q. An effective scaling frequency factor method for scaling of harmonic vibrational frequencies: Application to toluene, styrene, and its 4-methyl derivative. *J. Mol. Struct.*, **2009**, *924-926*, 493-503.

[70] Yoshida, H.; Ehara, A.; Matsuura, H. Density functional vibrational analysis using wavenumber-linear scale factors. *Chem. Phys, Lett.*, **2000**, *325*, 477-483.

[71] Yoshida, H.; Takeda, K.; Okamura, J.; Ehara, A.; Matsuura, H. A new approach to vibrational analysis of large molecules by density functional theory: Wavenumber-linear scaling method. *J. Phys. Chem. A*, **2002**, *106*, 3580-3586.

[72] Kochikov, I.V.; Kuramshina, G.M.; Stepanova, A.V. New approach for the correction of ab initio molecular force fields in Cartesian Coordinates. *Int. J. Quant. Chem.*, **2009**, *109*, 28-33.

[73] Andersson, M. P. ; Uvdal, P. New scale factors for harmonic vibrational frequencies using the b3lyp density functional method with the triple ζ basis set 6-311+G(d,p). *J. Phys. Chem. A*, **2005**, *109*, 2937-2941.

[74] Dennison, D.M. The infrared spectrum of carbon dioxide, I. *Phys. Rev.*, **1940**, *43*, 716-23.

[75] Darling, B.T.; Dennison, D.M. The water vapor molecule. *Phys. Rev*, **1940**, *7*, 128-139.

[76] Tennyson, J.; Zobov, N.F.; Williamson, R.; Polyanski, O.L.; Bernath, P.F. Experimental energy levels of the water molecule. *J. Phys. Chem. Ref. Data*, **2001**, *30*, 735-831.

[77] Boatz, J.A.; Gordon, M.S. Decomposition of normal-coordinate vibrational frequencies. *J. Phys. Chem.*, **1989**, *93*, 1819-1826.

[78] Jacob, C. R. ; Reiher, M. Localizing normal modes in large molecules. *J. Chem. Phys.*, **2009**, *130*, 084106-084106.

[79] Choi, J.-H.; Cho, M. Calculations of intermode coupling constants and simulations of amide I, II, and III vibrational spectra of dipeptides. *Chem. Phys.*, **2009**, *361*, 168-175.

[80] Jeon, J.; Yang, S.; Choi, J.-H.; Cho, M. Computational vibrational spectroscopy of peptides and proteins in one and two dimensions. *Acc. Chem. Res.*, **2009**, *42*, 1280-1289.

[81] See for example discussion in Bell, R. J.; Deans, P.; Hibbins-Butler, D. C. Localization of normal modes in vitreous silica, germania and beryllium fluoride. *J. Phys. C: Solid St. Phys.,* **1970**, *3*, 2111-2118.

[82] McCluskey, M. D. Local vibrational modes of impurities in semiconductors. *J. Appl. Phys. Appl. Phys. Rev.*, **2000**, *87*, 3594-3615; and references therein.

[83] McCluskey, M.D. Resonant interaction between hydrogen vibrational modes in AlSb:Se. *Phys. Rev. Lett.*, **2009**, 102, 135502-1-135502-6.

[84] Estreicher, S.K.; 1, Backlund, D.; Gibbons, T. M.; Docaj, A. Vibrational properties of impurities in semiconductors. *Model. Simul. Mater. Sci. Eng.*, **2009**, *17*, 084006-1-084006-14.

[85] Leu, B. M.; Silvernail, M. J.; Zgierski, M. Z.; Wyllie, G. R.A.; Ellison, M. K.; Scheidt, R. W.; Zhao, J.; Sturhahn, W.; Alp, E. E.; Sage, J. T. Quantitative vibrational dynamics of iron in carbonyl porphyrins. *Biophys. J.*, **2007**, *92*, 3764-3783.

[86] Scheidt, W. R.; Durbin, S. M.; Sage, J.T. Nuclear Resonance Vibrational Spectroscopy-Nrvs; in *The Smallest Biomolecules: Diatomics and their Interactions with Heme Proteins*, Ghosh A., Ed. Elsevier: Amsterdam, **2008**, chapter 5, pp. 124-146.

[87] W. Robert Scheidt, W.R.; Durbin, S.M.; Sage, J.T. Nuclear resonance vibrational spectroscopy - NRVS. *J. Inorg. Biochem.*, **2005**, *99*, 60-71.

[88] Bergmann, U.; Sturhahn, W.; Linn, D.E.; Jenney Jr., F.E.; Adams, M.W.W.; Rupnik, K.; Hales, B.J.; Alp, E.E.; Mayse, A.; Cramer, S.P. Observation of Fe H/D modes by nuclear resonant vibrational spectroscopy. *J. Am. Chem. Soc.*, **2003**, *125*, 4016-4017.

[89] McKean, D. C. Individual CH bond strengths in simple organic compounds: effects of conformation and substitution. *Chem. Soc. Rev.*, **1978**, *7*, 399-422.

[90] McKean, D. C. CH stretching frequencies, bond lengths and strengths in halogenated ethylenes. *Spectrochim. Acta A*, **1975**, **31**, 1167-1186.

[91] McKean, D. C. CH bond dissociation energies, isolated stretching frequencies, and radical stabilization energy. *Int. J. Chem. Kinet.*, **(1989)**, *21*, 445-464.

[92] McKean, D. C.; Torto, I. CH Stretching frequencies and bond strengths, and methyl-group geometry in CH_3CXO compounds (X = H, Me, F, Cl, Br, CN, OMe) and CH_3CH_2CN. *J. Mol. Struct.*, **1982**, *81*, 51-60.

[93] Duncan, J. L.; Harvie, J. L.; McKean, D. C.; Cradock, S. The ground-state structures of disilane, methyl silane and the silyl halides, and an sih bond length correlation with stretching frequency. *J. Mol. Struct.*, **1986**, *145*, 225-242.

[94] McKean, D.C. CH Bond-dissociation energies, isolated stretching frequencies, and radical stabilization energy. *Int. J. Chem. Kinet.*, **1989**, *21*, 445-464.

[95] Murphy, W. F.; Zerbetto, F.; Duncan, J. L.; McKean, D. C. Vibrational-spectrum and harmonic force-field of trimethylamine. *J. Phys. Chem.*, **1993**, *97*, 581-595.

[96] Caillod, J.; Saur, O.; Lavalley J.-C. Etude par spectroscopie infrarouge des vibrations □(CH) de composes cycliques: Dioxanne-1,4, dithianne-1,4, oxathianne-1,4 et cyclohexane. *Spectrochim. Acta A*, **1980**, *36*, 185-191.

[97] Snyder, R. G.; Aljibury, A. L.; Strauss, H. L.; Casal, H. L.; Gough, K. M.; Murphy, W. J. Isolated C-H stretching vibrations of n-alkanes - assignments and relation to structure. *J. Chem. Phys.*, **1984**, *81*, 5352-5361.

[98] Henry, B. R. The local mode model and overtone spectra - a probe of molecular-structure and conformation. *Acc. Chem. Res.*, **1987**, *20*, 429-435; and references therein.

[99] Mizugai, Y.; Katayama, M. The 5th overtone of the c-h stretching vibrations and the bond lengths in some heterocyclic-compounds. *Chem. Phys. Lett.*, **1980**, *73*, 240-243.

[100] Wong, J. S.; Moore, C. B. Inequivalent C-H oscillators of gaseous alkanes and alkenes in laser photo-acoustic overtone spectroscopy. *J. Chem. Phys.*, **1982** , *77*, 603-615.

[101] Sbrana, G.; Muniz-Miranda, M. High overtones of c-h stretching vibrations in isoxazole, thiazole, and related methyl and dimethyl derivatives. *J. Phys. Chem. A*, **1998**, *102*, 7603-7608.

[102] Halonen, L. Local Mode Vibrations in Polyatomic Molecules in *Advances in Chemical Physcis,* Prigogine, I.; Rice, S.A., Eds, Wiley: New York, **2007**, Vol, *104*.

[103] Hollensteun, H.; Luckhaus, D.; Quack, M. Dynamics of the CH chromophore in chx_3 - a combined treatment for a set of isotopic-species. *J. Mol. Struct.*, **1993**, *294*, 65-70.

[104] Decius, J. C. Compliance matrix and molecular vibrations. *J. Chem. Phys.*, **1963**, *38*, 241-248.

[105] Brandhorst, K.; Grunenberg, J. How strong is a bond? The interpretation of force and compliance constants s bond strength descriptors. *Chem. Soc. Rev,*, **2008**, *37*, 1558-1567.

[106] Grunenberg, J.; Goldberg, N. How strong is the gallium gallium triple bond? theoretical compliance matrices as a probe for intrinsic bond strengths. *J. Am. Chem. Soc.*, **2000**, *122*, 6046-6047.

[107] Grunenberg, J.; Streubel, R.; V Frantzius, G.; Marten, W. The strongest bond in the universe? Accurate calculation of compliance matrices for the ions N_2H^+, HCO^+, and HOC^+. *J. Chem. Phys.*, **2003** , *119*, 165-169.

[108] Grunenberg, J. Direct assessment of interresidue force in watson-crick base pairs using theoretical compliance constants. *J. Am. Chem. Soc.*, **2004**, *126*, 16310-16311.

[109] Madhav, M. Y.; Manogara, S. A relook at the compliance constants in redundant internal coordinates and some new insights. *J. Chem. Phys.*, **2009**, *131*, 174112-1-174112-6.

[110] Peter R. Schreiner, P. R.; Reisenauer, H. P.; Romanski, J.; Mloston, G. A formal carbon sulfur triple bond HCSOH. *Angew. Chem. Int. Ed. Engl*, **2009**, *121*, 8277-8280.

[111] Torkington, P. The general solution of the secular equation of second degree, with application to the class-a1 vibrations of the symmetrical triatomic molecule. *J. Chem. Phys.*, ***1949***, *17*, 357-369.

[112] Morino, Y.; Kuchitsu, K. A note on the classification of normal vibrations of molecules. *J. Chem. Phys.*, **1952**, *20*, 1809-1810.

[113] Pulay, P.; Török, F. On parameter form of matrix f. 2. investigation of assignment with aid of parameter form. *Acta Chim. Hung.*, **1966**, *47*, 273-279.

[114] Keresztury, G.; Jalsovszky, G. Alternative calculation of vibrational potential energy distribution. *J. Mol Struct.*, **1971** *10*, 304-319.

[115] Kraka, E. Reaction Path Hamiltonian and its Use for Investigating Reaction Mechanism, in *Encyclopedia of Computational Chemistry*, Schleyer, P. v. R.; Allinger, N. L.; Clark, T.; Gasteiger, J.; Kollman, P. A.; Schaefer III, H. F.; Schreiner, P. R.; Eds.; Wiley: Chichester, UK, **1998**, pp. 2437-2463.

[116] Kraka, E.; Dunning, Jr, T. H. Characterization of molecular potential energy surfaces: critical points, reaction paths and reaction valleys., in *advances in Molecular Electronic Structure Theory: the Calculation and Characterization of Molecular Potential Energy Surfaces*, dunning. Jr., T. H. Ed, JAI Press, Inc.: Greenwich, **1990**, pp.129-173.

[117] Konkoli, Z.; Kraka, E.; Cremer, D., Unified reaction valley approach: mechanism of the reaction $CH_3+H_2 \rightarrow CH_4+H$, *J. Phys. Chem. A*, **1997**, *101*, 1742-1757.

[118] Konkoli, Z.; Cremer, D.; Kraka, E. Diabatic ordering of vibrational normal modes in reaction valley studies. *J. Comp. Chem.*, **1997**, *18*, 1282-1289.

[119] Kraka, E.; Wu, A.; Cremer, D. The mechanism of the Diels-Alder reaction studied with the united reaction valley approach: mechanistic differences between symmetry-allowed and symmetry-forbidden reactions. *J. Phys. Chem. A* , **2003**, *107*, 9008-9021.

[120] Cremer D.; Wu, A.; Kraka, E.. The mechanism of the reaction $FH+H_2C=CH_2 \rightarrow H_3C-CFH_2$ Investigation of hidden intermediates with the unified reaction valley approach. *Phys. Chem. Chem. Phys.*, **2000**, *3*, 674-687.

[121] Kraka, E.; Cremer, D., Mechanism and dynamics of organic reactions: 1,2-h shift in methylchlorocarbene. *J. Phys. Org. Chem.*, **2002**, *15*, 431-447.

[122] Quapp, W.; Kraka, E.; Cremer, D. Finding the transition state of quasi-barrierless reactions by a growing string method for newton trajectories: application to the dissociation of methylenecyclopropene and cyclopropane. *J. Phys. Chem. A*, **2007**, *111*, 11287-11293.

[123] Joo, H.; Kraka, E.; Quapp. W.; Cremer, D. The mechanism of a barrierless reaction: hidden transition state and hidden intermediates in the reaction of methylene with ethene. *Mol. Phys.*, **2007**, *105*, 2697-2717.

[124] Kraka, E.; Cremer, D. Computational analysis of the mechanism of chemical reactions in terms of reaction phases: hidden intermediates and hidden transition states. *Acc. Chem. Res.*, **2010**, *43*, 591-601.

[125] Wu, A.; Cremer, D. Correlation of the vibrational spectra of isotopomers: Theory and application. *J. Phys. Chem. A*, **2003**, *107*, 10272.

[126] Pauling, L. *Nature of the Chemical Bond*, 3rd ed. Cornell University Press: Ithaca, New York, **1960**.

[127] McWeeny, R. Coulson's Valence. Oxford University Press: London, **1979**,

[128] Gimarc, B. M. *Molecular Structure and Bonding*. Academic Press: New York, **1979**.

[129] Brooks, C.L.; Frenking, G.; Sakaki, S. Eds. *Journal of Computational Chemistry, Special Issue: 90 Years of Chemical Bonding*, **2006**, *28*, and references therein.

[130] Coppens, P.; Hall, M.B., Eds., *Electron Distributions and the Chemical Bond*. Plenum Press: New York, **1982**.

[131] Bader, R. F. W. Atoms in Molecules: A Quantum Theory. International Series of Monographs on Chemistry, 22. Oxford University Press: Oxford, **1995**.

[132] Kraka, E.; Cremer, D. Chemical Implication of Local Features of the Electron Density, in *Theoretical Models of Chemical Bonding, Part 2, the Concept of the Chemical Bond*, maksics, Z. B., Ed., Springer: Heidelberg, **1990**, pp.453-542

[133] Lide, D. R., Ed.; Handbook of Chemistry and Physics, 90. ed., CRC: Boca Raton, **2009**.

[134] Cremer, D.; Kraka, E. Theoretical determination of molecular structure and conformation. 15. three-membered rings: bent bonds, ring strain, and surface delocalization. *J. Am. Chem. Soc.*, **1985**, *107*, 3800-3810.

[135] Cremer, D.; Kraka, E. Scope and Limitations of the Concept of Strain, in *Molecular Structure and Energetics, Structure and Reactivity*, Liebman, J.F.; Greenberg, A., Eds; VCH: Deerfield Beach, **1988**, Vol. *7*, pp. 65-92.

[136] Badger, R.M.A. Relation between internuclear distances and bond force constants. *J. Chem. Phys.*, **1934**, *2*, 128-132.

[137] Badger, R.M. The relation between the internuclear distances and force constants of molecules and its application to polyatomic molecules *J. Chem. Phys.*, **1935**, *3*, 710-715.

[138] Hershbach, D.R.; Laurie, V.W. Anharmonic potential constants and their dependence upon bond length. *J. Chem. Phys.*, **1961**, *35*, 458-463.

[139] Kurita, E.; Matsuura, H.; Ohno, K. Relationship between force constants and bond lengths for CX (X = C, Si, Ge, N, P, As, O, S, Se, F, Cl, and Br) single and multiple bonds: formulation of Badger's rule for universal use. *Spectrochim. Acta Part A*, **2004**, *60*, 3013-3023.

[140] Mack, H.G.; Christen, D.; Oberhammer, H. J. Theoretical study of fluorinated amines. *Mol. Struct.*, **1988**, *190*, 215-226.

[141] Christen, D.; Gupta, O.D.; Kadel, J.; Kirchmeier, R. L.; Mack, H.G.; Oberhammer, H.; Shreeve. An unusual relationship between the n-f bond lengths and force constants in n-fluoroamines. *J.M. J. Am. Chem. Soc.*, **1991**, *113*, 9131-9135.

[142] Politzer. P.; Habibollahzadeh, D. Relationship between dissociation energies, force constants, and bond lengths for some N-F and O-F bonds. *J. Chem. Phys.*, **1993**, *98*, 7659-7660.

[143] Hagen. K.; Hedberg, K.; Obed, E.; Robert, J.; Kirchmeier, L.; Shreeve, J. M. Structure and vibrational force field of methyldifluoroamine, $ch-3nf-2$. an electron-diffraction investigation augmented by microwave and infrared spectroscopic data and by ab initio molecular orbital calculations. *J. Phys. Chem. A*, **1998**, *102*, 5106-5110.

[144] Pierce, L.; DiCianni, N.; Jackson, R.H.J. Centrifugal distortion effects in asymmetric rotor molecules. i. quadratic potential constants and average structure of oxygen difluoride from the ground-state rotational spectrum. *Chem. Phys.*, **1963**, *38*, 730-739.

[145] Kim, H.; Pearson, E.F.; Appelman, E. H. J. Millimeter-wave spectrum and structure of hypofluorous acid: HOF and DOF. *Chem. Phys.*, **1972**, *56*, 1-3.

[146] Murrell, J.N.; Carter, S.; Mills, I. M.; Guest, M. F. Analytical potentials for triatomic molecules from spectroscopic data V. Application to HOX (X=F, Cl, Br, I). *Mol. Phys.*, **1979**, *37*, 1199-1222.

[147] Filatov, M.; Cremer, D. Revision of the dissociation energies of mercury chalcogendies - Unusual types of mercury bonding. *ChemPhysChem*, **2004**, *5*, 1547-1556.

[148] Cremer, D.; Kraka, E.; Filatov, M. Bonding in mercury molecules described by the normalized elimination of the small component and coupled cluster theory. *ChemPhysChem*, **2008**, *9*, 2510-2521.

[149] Kaka, E.; Filatov, M.; Cremer, D. Comparison of gold bonding with mercury bonding. *Croat. Chim. Acta*, **2009**, *82*, 233 - 243; *in honor of Prof. Z. Maksic.*

[150] Bader, R. F. W.; Slee, T. S.; Cremer, D.; Kraka, E. Description of conjugation and hyperconjugation in terms of electron distributions. *J. Am. Chem. Soc.*, **1983**, *105*, 5061-5068.

[151] Cremer, D.; Gauss, J. Theoretical determination of molecular structure and conformation. 20. re-evaluation of the strain energies of cyclopropane and cyclobutane-CC and CH bond enegies, 1,3-interactions, and σ - aromaticity. *J. Am. Chem. Soc.*, **1986**, *108*, 7467-7477.

[152] Cremer, D; Kraka, E. A description of the chemical bond in terms of local properties of electron density and energy. *Croat. Chim. Acta*, **1984**, *57*, 1259-1281.

[153] Cremer D.; Kraka, E. Chemical bonds without bonding electron density - does the difference electron density analysis suffice for a description of the chemical bond? *Angew. Chem. Int. Ed. Engl.*, **1984**, *23*, 627-628.

[154] Kamienska-Trela, K. Correlation of the $^{13}C–^{13}C$ spin-spin coupling constants with the stretching force constants of single and double carbon-carbon bonds. *Spectrochim. Acta, Part A: Mol. Spectrosc.*, **1980**, *36*, 239-244.

[155] Cremer, D.; Gräfenstein, J. Calculation and analysis of NMR spin-spin coupling constants. *Phys. Chem. Chem. Phys., Feature Article*, **2007**, *9* , 2791-2816.

[156] Cremer, D.; Kraka, E.; Wu, A.; and Lüttke, W. Can one assess the π character of a C-C bond with the help of the NMR spin-spin coupling constants? *ChemPhysChem*, **2004**, *5*, 349-366.

[157] Gutierrez-Oliva, S.; Herrera, B.; Toro-Labbe, A; Chermette, H. On the mechanism of hydrogen transfer in the HSCH(=O) → (S)CHOH and HSNO → SNOH reactions, *J. Phys. Chem. A*, **2005**, *109*, 1748-1751.

[158] Toro-Labbe, A; Gutierrez-Oliva, S.; Murray, J. S.; Politzer, P. A new perspective on chemical and physical processes: The reaction force, *Mol. Phys.*, **2007**, *105*, 2619-2625.

[159] Murray, J. S.; Lane, P.; Göbel, P. Klapötke, T. M.; Politzer, P. Reaction force analyses of nitro-aci tautomerizations of trinitromethane, the elusive trinitromethanol, picric acid and 2,4-dinitro-1H-imidazole. *Theo.r Chem. Acc.*, **2009**, *124*, 355-363.

[160] Holbrook, K. A.; Pilling, M. J.; Robertson, S. H. Unimolecular reactions, 2nd ed. Wiley: New York, **1996**.

[161] Carter. S.; Handy, N. C. Rovibrational energy levels of hydrogen peroxide, studied by MULTIMODE with a reaction path Hamiltonian. *Spectrochim. Acta Part A: Mol. Biomol. Spectrosc.*, **2004**, *60*, 2107-2111.

[162] Kato, S.; Morokuma, K. Potential energy characteristics and energy partitioning in chemical reactions: Ab initio MO study of $H_2CCH_2F→H_2CCHF+H$ reaction. *J. Chem. Phys.*, **1980**, *73*, 3900-3915.

[163] Secrest, D. Theory of rotational and vibrational energy transfer in molecules. *Ann. Rev. Phys. Chem.*, **1973**, *24*, 379-406.

[164] See for example Quapp, W. Chemical reaction paths and calculus of variations. *Theor. Chem. Acc.*, **2008**, *121*, 227-237, and references cited therein.

[165] Heidrich, D., Ed. *The Reaction Path in Chemistry: Current Approaches and Perspectives*, Kluever Academic Publishers, Dordrecht, **1995**.

[166] Fukui, K. The path of chemical reactions - the IRC approach. *Acc. Cem. Res.*, **1981**, *14*, 363-368.

[167] Hratchian, H.P.; Schegel, H. Accurate reaction paths using a Hessian based predictor-corrector integrator. *J. Chem. Phys.*, **2004**, *120*, 9918-9924.

[168] Quapp, W.; Heidrich, D. Analysis of the concept of minimum energy path on the potential energy surface of chemically reacting systems. *Theor. Chim. Acta*, **1984**, *66*, 245-260.

[169] Quapp, W. Gradient extremals and valley floor bifurcations on potential energy surfaces. *Theor. Chim. Acta*, **1989**, *75*, 447-460.

[170] Hirsch, M; Quapp, W. The reaction path way of a potential energy surface as curve with induced tangent. *Chem Phys. Lett.*, **2004**, *395*, 150-156.

[171] Pancrir, S. Calculation of least energy path on energy hypersurface. *Coll. Czech. Chem. Commun.*, **1975**, 1112-1118.

[172] Hoffmann, D.K.; Nord, R.S.; Ruedenberg, K. Bifurcations and transition states. *Theor. Chim. Acta*, **1986**, *69*, 265-279.

[173] Quapp, W. A valley following method. *Optimization*, **2003**, *52*, 317-331.

[174] Quapp W.; , Hirsch, M.; Heidrich, D. Searching for saddle points of potential energy surfaces by following a reduced gradient. *J. Comp. Chem.*, **1998**, *19*, 1087-1100.

[175] See, e.g. Williams, J.H.; Maggiora, G.M. Use and abuse of the distinguished-coordinate method for transition-state structure searching. It. *J. Mol. Struct., Theochem.,* **1982**, *6*, 365-378.

[176] Gonzales, J.; Gimienez, X.; Bofill J.M., Generalized reaction path hamiltonian dynamics. *Theor. Chem. Acc.*, **2004**, *112*, 75-83.

[177] Gimenez, X.; Bofill, J.M., The canonical transformation theory and its application to the reaction path hamiltonian. *J. Mol. Struct. Theochem.*, **2005**, *727*, 21-27.

[178] Ess, D. H.; Wheeler, S. E.; Lafe, R. G.; Xu, L.; Celebi-Ölüm; Houk, K. N. Bifurcatins on potential energy surfaces of organic reactions. *Angew. Chem. Int. Ed. Engl.*, **2008**, *47*, 7592-7601.

[179] Quapp, W.; Hirsch, M.; Heidrich, D. An approach to reaction path branching using valley-ridge inflection points of potential energy surfaces. *Theor. Chem. Acc.*, **2004**, *112*, 40-51.

[180] Singleton, D. A.; Hang, C.; Szymanski, M. J.; Meyer, M. P.; Leach, A. G.; Kuwata, K. T.; Chen, J. S.; Greer, A.; Foote, C. S.; Houk, K. N. Mechanism of ene reactions of singlet oxygen. a two-step no-intermediate mechanism. *J. Am. Chem. Soc.*, **2003**, *125*, 1319-1326.

[181] Valtazanos, P.; Ruedenberg, K. Bifurcations and transition states. *Theor. Chim. Acta* , **1986**, *69*, 281-307.

[182] Schlegel, H. B. Some thoughts on reaction-path following. *J. Chem. Soc. Faraday Trans.*, **1994**, *90*, 1569-1574.

[183] Stanton, R. E.; McIver Jr., J. W. Group theoretical selection rules for the transition states of chemical reactions. *J. Am. Chem. Soc.*, **1975**, *97*, 3632-3646.

[184] Toma, L.; Romano, S.; Quadrellia, P.; Caramella, P. Merging of 4+2 and 2+4 cycloaddition paths in the regiospecific dimerization of methacrolein. A case of concerted crypto-biradical cycloaddition. *Tetrahedron Lett.*, **2001**, *42*, 5077-5080.

[185] Caramella, P.: Quadrelli, P.: Toma, L. Unexpected bispericyclic transition structure leading to 4+2 and 2+4 cycloadducts in the endo dimerization of cyclopentadiene. *J. Am. Chem. Soc.*, **2002**, *124*, 1120-1131.

[186] Quadrelli,P.; Romano, S.; Toma, L.; Caramella, P. Merging and bifurcation of 4+2 and 2+4 cycloaddition modes in the archetypal dimerization of butadiene. A case of competing bispericyclic, pericyclic and biradical paths. *Tetrahedron Lett.*, **2002**, *43*, 8785-8789.

[187] Quadrelli,P.; Romano, S.; Toma, L.; Caramella, P. Bispericyclic transition structure allows for efficient relief of antiaromaticity enhancing reactivity and endo stereoselectivity in the dimerization of the fleeting cyclopentadienone. *J. Org. Chem.*, **2003**, *68*, 6035-6038.

[188] Hrovat, D. A.; Borden, W. T. CASSCF calculations find that a D8h geometry is the transition state for double bond shifting in cyclooctatetraene. *J. Am. Chem. Soc.*, **1992**, *114*, 5879-5881.

[189] Kumeda, T.; Taketsuga, T. Isotope effect on bifurcating reaction path: Valley-ridge inflection point in totally symmetric coordinate. *J. Chem. Phys.*, 113 *J. Chem. Phys.*, **2000**, *113*, 477-484.

[190] Lasorne, B.; Dive, G.; Desouter-Lecomte, M. Wave packet dynamics along bifurcating reaction paths. *J. Chem. Phys.*, **2003**, *118*, 5831-5840.

[191] Yanai, T.; Taketsugu, T.; Hirao K. Theoretical study of bifurcating reaction paths. *J. Chem. Phys.*, **1997**, *107*, 1137-1146.

[192] Castano, O.; Palmeiro, R.; Frutos, L. M. ; Luisandres, J. Role of bifurcation in the bond shifting of cyclooctatetraene. *J. Comput. Chem.*, **2002**, *23*, 732-736.

[193] Castano, O.; Frutos, L. M. ; Palmeiro, R.; Notario, R.; Andres, J.-L.; Gomperts, R.; Blancfort, L.; Robb, M. A. The valence isomerization of cyclooctatetraene to semibullvalene. *Angew. Chem. Int. Ed. Engl.*, **2000**, *39*, 2095-2097.

[194] Hoffman, D. K.; Nord, R.S.; Ruedenberg, K. Gradient extremals. *Theor. Chim. Acta*, **1986**, *69*, 265-280.

[195] Özkan, L.; Zora, M. Transition structures, energetics, and secondary kinetic isotope effects for cope rearrangements of cis-1,2-divinylcyclobutane and cis-1,2-divinylcyclopropane: A DFT Study. *J. Org. Chem.*, **2003**, *68*, 9635-9642.

[196] Suhrada, C. P.; Selcuki, C.; Nendel, M.; Cannizzaro, C.; Houk, K. N.; Rissing P.-J.; Baumann, D.; Hasselmann, D. *Angew. Chem. Int. Ed. Engl.*, **2005**, *44*, 3548.

[197] Bekele, T.; Christian, C.F; Lipton, M.A.; Singleton, D.A. "Concerted" transition state, stepwise mechanism. dynamics effects in $C^2–C^6$ enyne Allene cyclizations. *J. Am. Chem. Soc.*, **2005**, *127*, 9216-9223.

[198] Ussing, B. R.; Hang, C.; Singleton, D. A. Dynamic effects on the periselectivity, rate, isotope effects, and mechanism of cycloadditions of ketenes with cyclopentadiene. *J. Am. Chem. Soc.*, **2006**, *128*, 7594-7607.

[199] Cremer, D.; Crehuet, R.; Anglada, J., The ozonolysis of acetylene - a quantum chemical investigation. *J. Am. Chem. Soc.*, **2001**, *123*, 6127-6141.

[200] Cremer, D.; Kraka, E. Joo, H.; Stearns, J.A.; Zwier, J.A. Exploration of the potential energy surface of C4H4 for rearrangement and decomposition reactions of vinylacetylene: A computational study. *Phys. Chem. Chem. Phys.*, **2006**, *8*, 5304 -5316.

[201] Stearns, J.A.; Zwier, T.S.; Kraka, E.; Cremer, D. Experimental and computational study of the ultraviolet photolysis of vinylacetylene *Phys. Chem. Chem. Phys.*, **2006**, *8*, 5317 -5327.

[202] Miller, W.H.; Handy, N.C.; Adams, J.E. Reaction path hamiltonian for polyatomic molecules. *It. J. Chem. Phys*., **1980**, *72*, 99-112.

[203] Hofacker, G. L. Theory of intramolecular relaxation processes. *It. J. Chem. Phys.,* **1965**, *43*, 208-215.

[204] Marcus, R. On the analytical mechanics of chemical reactions. quantum mechanics of linear collisions. *J. Chem. Phys.*, **1966**, *45*, 4493 - 4499.
[205] Page, M.; McIver, Jr. J.W. On evaluating the reaction path hamiltonian. *J. Chem. Phys.*, **1988**, *88*, 922-935.
[206] Miller, W. H.; Ruf, B. A.; Chang, Y.-T. A diabatic reaction path hamiltonian. *J. Chem. Phys.*, **1988**, *89*, 6298-6304.
[207] Luo, Y.-R., *Handbook of Bond Dissociation Energies in Organic Compounds*. CRC Press: Boca Raton, **2003**.
[208] Huber, K.P.; Herzberg, G. *Molecular Spectra and Molecular Structure iv. Constants of Diatomic Molecules, Van Nostrand Rheinhold*: London, **1979**.
[209] Truhlar, D.; Garrett, B. Variational transition state theory. *Ann. Rev. Phys. Chem.*, **1984**, *35*, 159-189.
[210] Neumark, D. M.; Transition state spectroscopy. *Science, New Series*, **1996**, *272*, 1446-1447.
[211] Zewail, A. Femtochemistry: Ultrafast dynamics of the chemical bond, World Scientific Publishing: Singapuore, **1994**, Vol. *1*, *2*.
[212] Spencer, J.; Zewail, A. H. Freezing atoms in motion: principles of femtochemistry and demonstration by laser stroboscopy. *J. Chem. Ed.*, **2001**, 737-751.
[213] Polani, J,C.; Zewail, A.H. Direct observation of the transition state. *Acc. Chem. Res.,* **1995**, *28*, 119-132.
[214] Crim, F.F. Vibrational state control of bimolecular reactions: Discovering and directing the chemistry. *Acc. Chem. Res.,* **1999**, *32*, 877-884.
[215] Reed, A.E.; Curtiss, L.A.; Weinhold, E. Intermolecular interactions from a natural bond orbital, donor-acceptor viewpoint. *Chem. Rev.*, **1988**, *88*, 899-926.
[216] Becke, A. D.; Edgecombe, K.E. A simple measure of electron localization in atomic and molecular systems. *J. Chem. Phys.*, **1990**, *92*, 5397-5403.
[217] Santos, J. C.; Polo, V.; Andres, J. An electron localization function study of the trimerizationof acetylene: Reaction mechanism and development of aromaticity.electron density. *Che. Phys. Lett.*, **2005**, *406*, 393-397.
[218] Matito, E.; Sola, M. The role of electronic delocalization in transition metal complexes from the electron localization function and the quantum theory of atoms in molecules viewpoints. *Coord. Chem. Rev.*, **2009**, *253*, 647-665.
[219] Ponec, R. Topological aspects of chemical-reactivity - simple alternative method for determining parity of kekule structures. *Coll. Czech. Chem. Commun.*, **1985**, *50*, 2639-2646.
[220] Ponec, R. Electron reorganization in chemical reactions: pair population analysis along concerted reaction path of allowed and forbidden pericyclic reactions. *Int. J. Quant. Chem.*, **1997**, *62*, 171-176.
[221] Yan, S,; Wu, Y.-Y., Liu, K. Tracking the energy flow along the reaction path. *Proc. Natl. Acad. Sci. USA*, **2008**, *105*, 12667-12672.
[222] Riedel, J.; Yan, S.; Liu, K. Mode specificity in reactions of CL with CH_2 stretch-excited CH_2D_2 ν1,ν6=1) *J. Phys. Chem. A*, **2009**, DOI: 10.1021/jp902629h.
[223] Duncan, W.T.; Truong, T.N. Thermal and vibrational-state selected rates of the $CH_4+Cl\rightarrow HCL+CH_3$ reaction. *J. Chem. Phys.*, **1995**, *103*, 9642-9652.
[224] Liu, R.; Ma, S; Li, Z. Theoretical study on the dynamic properties and state-selected rate constants of the reaction $CH(^4\Sigma^-)+H_2\rightarrow CH_2(^3B_1)+H$. *Chem. Phys. Lett.*, **1994**, *219*, 143-150.
[225] Takahashi, O.; Itoh, K.; Kawano, A.; Saito, K. A theoretical study of the bifurcation reaction of formic acid: dynamics around the intrinsic reaction coordinate. *J. Mol. Struct. Theochem.*, **2001**, *545*, 197-205.
[226] Killelea, D.; Campbell, V.L.; Shuman, N.S.; Utz, A.L. Bond-selective control of a heterogeneously catalyzed reaction. *Science*, **2008**, *319*, 790-793.

Received: 26 December, 2009 Revised: 11 February, 2010 Accepted: 11 February, 2010